INVESTIGATION OF AIRCRAFT LATERAL MOTION PERFORMANCE FUNCTION BY PULSE TECHNIQUE

BY

JOHN B. DAIN
FREDERICK H. MICHAELIS
JOHN C. WOOTTON

M.I.T. 1949

COPY #8

sis

Thesis
B14

INVESTIGATION OF AIRCRAFT LATERAL MOTION PERFORMANCE FUNCTION BY PULSE TECHNIQUE

by

JOHN B. BAIN
S.B. MILLSAPS COLLEGE
1940

FREDERICK H. MICHAELIS
S.B. U.S. NAVAL ACADEMY
1940

JAMES C. WOOTTON

SUBMITTED IN PARTIAL FULFILLMENT OF THE

REQUIREMENTS FOR THE DEGREE OF

MASTER OF SCIENCE

at

MASSACHUSETTS INSTITUTE OF TECHNOLOGY

1949

Library
U. S. Naval Postgraduate School

September 9, 1949

Prof. Joseph S. Newell
Secretary of the Faculty
Massachusetts Institute of Technology
Cambridge 39, Massachusetts

Dear Professor Newell:

In accordance with the regulations of the faculty, we respectfully submit a thesis entitled, "Investigation of Aircraft Lateral Motion Performance Function by Pulse Technique", in partial fulfillment of the requirements for the degree of Master of Science.

ABSTRACT

This thesis presents the results of an investigation of the lateral performance functions of an airplane by the analysis of the transient response of the airplane to finite pulse of control surface deflection.

The method is an extension of pulse technique used by Clementson, Ref.(2), to measure the longitudinal performance functions of an airplane and further described by Seamans, Blasingame, and Clementson, Ref.(3), for more general cases. In this thesis the successful extension to highly oscillatory lightly damped responses is shown. Also a possible technique of analyzing divergent responses is indicated.

The instrumentation and calibration necessary to measure inputs of aileron and rudder deflection and outputs of time-rate of geometric yaw and roll are described in detail. The separate deflections of each aileron were added electrically to give the total differential aileron deflection thus obviating the necessity for adding these deflections during analysis. Microsyn signal generators were used to measure aileron and rudder deflections. Rate gyros were used to measure the angular velocities in roll and yaw. These were the only outputs measured due to the limited time available.

Determination of the performance functions from the transient response was accomplished by approximating the Fourier Integral of the time responses of the inputs and outputs using the method of summing approximating triangles.

The technique of measuring the transient response to finite pulse inputs is shown to be accurate, reliable and reproducible with a low level of uncertainties.

Special methods of analyzing lightly damped oscillatory modes are developed and compared. The recommended method will vary somewhat with the form of the response curve but generally speaking the most satisfactory

method consists of approximating the Fourier Transform of the output over the early portion of the time response to a point beyond which the response is, within the accuracy of measurement, only a damped sinusoid. At this value of time the Fourier Transform of the oscillatory mode obtained analytically is added vectorially to the Fourier Transform of the initial portion of the response.

Comparison with computed performance functions based on calculated derivatives shows qualitative agreement but clearly shows that these computed performance functions may differ considerably from the actual performance functions of the full scale airplane in flight.

The saving in instrumentation and flight time effected by the pulse technique over that required by the sinusoidal technique is a major factor in recommending the former. Changes in the mass and moment of inertia due to fuel consumption are negligible for the short duration of test flights made possible by using the pulse technique.

ACKNOWLEDGEMENT

The authors wish to express their gratitude and appreciation to the following persons who rendered assistance in the development of this thesis:

To Professor R. C. Seamans, Jr. for the opportunity of performing this investigation and for his helpful and constructive supervision.

To the staff of the Tracking Control Project of the Instrumentation Laboratory for invaluable technical support and for many helpful and practical suggestions.

To the personnel of the Bedford Flight Facility of the Instrumentation Laboratory, M.I.T. for splendid and cheerful cooperation with the flight test phases of this investigation.

To Mr. L. E. Payne and his associates of Jackson and Moreland for reproducing the manuscript.

The graduate work, for which this thesis is a partial requirement, was performed while the authors were assigned to Naval Training School, Massachusetts Institute of Technology.

This thesis was prepared under the auspices of D.I.C. Project 6445, sponsored by the Office of Air Research and the Armament Laboratory, Engineering Division, Air Materiel Command, through Contract W33-038-ac-13969, Project MX755.

TABLE OF CONTENTS

OBJECT

To instrument a B-25J airplane and measure the lateral transient responses in rate of roll and rate of geometric yaw to pulses of aileron and rudder deflection.

To determine the lateral performance functions of the airplane from these responses by approximating the Fourier Integrals of the input and output.

To evaluate this method of obtaining these performance functions.

INTRODUCTION

Recent demands for high-performance automatic control of aircraft for both military and commercial uses have focused attention on the airplane as the dynamic system being controlled. It is fundamental that the synthesis of a controlling system starts with the best possible evaluation of the dynamical system to be controlled. Additional interest in the dynamics of the airplane arises from the problems of stabilizing some of the auxiliary equipment utilized in modern airplanes, such as navigating and fire control equipment.

The frequency response of an airplane can be calculated from computed derivatives based on wind tunnel tests. However, the comparison of these calculated responses with those measured on the actual airplane has shown appreciable discrepancies, due in part to the difference in stability derivatives obtained in the wind tunnel from those of the airplane, and in part to ignorance of the moments of inertia about the axes of motion.

The most generally used methods of synthesis and design of automatic control systems requires the dynamic characteristics of the airplane to be presented as a frequency response. A measured frequency response is most often obtained by the direct method of applying sinusoidal inputs and measuring the amplitude and phase angle of the outputs. This is done for enough frequencies to define the complete frequency response.

Pioneer work using the sinusoidal oscillation technique was carried out by the Cornell Aeronautical Laboratories with outstanding results.(Ref.1.) These tests required an auto-pilot, a sinusoidal input generator and measuring equipment. Extensive flight time, with its consequent expense, is associated with this technique.

An alternative technique, that of measuring the transient response to a step function input, has the drawback that such an input to the elevators

or ailerons will in a very short time cause the airplane to rotate through a large angle and hence will have displaced it so far from the original position of equilibrium that the motion is non-linear. Such motion at the present time can be analyzed only by extremely tedious and lengthy methods of numerical computations.

A technique which obviates a large part of the instrumentation and saves a great deal of flight time is that of measuring the transient response to a finite pulse of control surface deflection. This method was successfully used by Clementson (Ref.2.) in determining frequency response in the case of longitudinal motion. The mathematical background and the technique of application are presented in a paper by Seamans, Blasingame, and Clementson. (Ref.3.)

In extending the pulse technique to the measurement of the lateral modes of motion of the airplane, the characteristic of spiral divergence, which exists in many airplanes, must be taken into account. The Fourier Transformation method and its approximation (Ref.3.) are valid only for stable systems. Therefore, it becomes necessary to identify and remove the unstable mode prior to transformining the pulse response. Furthermore, the oscillation that occurs in lateral motion is lightly damped. This oscillatory mode must be given special treatment, or the analysis will become exceedingly tedious, in the regions of resonance.

Methods of analyzing the oscillatory mode were successfully used in this investigation to find the lateral performance functions of the B-25J airplane. However, this airplane did not have any measurable characteristic of spiral divergence, therefore, to illustrate a method of analysis when such a characteristic is involved, a simple system was analyzed.

or ailerons will in a very short time cause the airplane to rotate through a large angle and hence will have displaced it so far from the original position of equilibrium that the motion is non-linear. Such motion at the present time can be analyzed only by extremely tedious and lengthy methods of numerical computations.

A technique which obviates a large part of the instrumentation and saves a great deal of flight time is that of measuring the transient response to a finite pulse of control surface deflection. This method was successfully used by Clementson (Ref.2.) in determining frequency response in the case of longitudinal motion. The mathematical background and the technique of application are presented in a paper by Seamans, Blasingame, and Clementson. (Ref.3.)

In extending the pulse technique to the measurement of the lateral modes of motion of the airplane, the characteristic of spiral divergence, which exists in many airplanes, must be taken into account. The Fourier Transformation method and its approximation (Ref.3.) are valid only for stable systems. Therefore, it becomes necessary to identify and remove the unstable mode prior to transformining the pulse response. Furthermore, the oscillation that occurs in lateral motion is lightly damped. This oscillatory mode must be given special treatment, or the analysis will become exceedingly tedious, in the regions of resonance.

Methods of analyzing the oscillatory mode were successfully used in this investigation to find the lateral performance functions of the B-25J airplane. However, this airplane did not have any measurable characteristic of spiral divergence, therefore, to illustrate a method of analysis when such a characteristic is involved, a simple system was analyzed.

CHAPTER 1

DETERMINATION OF AIRPLANE LATERAL MOTION PERFORMANCE FUNCTIONS BY PULSE TECHNIQUES

The airplane in flight may be considered as an operating component which operates on specified inputs to produce certain outputs. More than one output may result from a given input. The operation on an input to produce a specified output is expressed mathematically by a concept of wide generality called a Performance Operator.

By restricting the airplane and its controls to small excursions from an equilibrium condition, its motion may be defined by a system of linear differential equations. Then the response can be related to the input by means of a Performance Function. The concept of Performance Operator and Performance Function were both developed by Dr. C. S. Draper and his associates of the Instrumentation Laboratory of the Massachusetts Institute of Technology. A complete discussion of their application to airplane dynamics is contained in Refs. (1) and (10). The relation between the two may be summarized by the following equation:

$$\{P\}_{[q_{in},q_{out}]}\, e^{+jwt} = e^{+jwt}\, (PF)_{[q_{in},q_{out}]}$$

When the output of an operating component can be related to the input by a set of linear differential equations, and the input is described by a complex exponential, the output is described by

$$q_{(out)} = q_{(out)a}\, e^{j(w_f t + PA)}$$

The ratio of the output to the input then defines the performance function of the operating component relating the two. In equation form

$$(PF)_{(\ )(q_{in},q_{out})} = \frac{q_{(out)a}\, e^{j[w_f t + (PA)_{out}]}}{q_{(in)a}\, e^{j[w_f t + (PA)_{in}]}}$$

The term $e^{jw_f t}$ factors out, and it is seen that the performance function is independent of time. For use in the synthesis of control or stabilizing systems, the performance function is usually presented graphically, either as a locus on the complex plane or as an amplitude ratio and phase angle plotted versus forcing angular frequency on the real plane. (1)(2)(3)(10)

It is the need for the frequency spectrum of the airplane's dynamics that has extended the study of these dynamics beyond the classical approach which, until the last few years, has been concerned with only the characteristics equation of the dynamic response and sensitivities. This approach does not give sufficient information to permit the design of a high-performance closed-loop system with the airplane as the controlled member. On the other hand, performance functions provide this necessary information in a form readily adapted to the problems of closed-loop design.

This investigation is concerned only with some of the performance functions which describe the lateral motion of the airplane.

Specifically, they are:

$(PF)_{A[\delta_a, W_X]}$

$(PF)_{A[\delta_a, W_Z]}$

$(PF)_{A[\delta_r, W_X]}$

$(PF)_{A[\delta_r, W_Z]}$

The limitation in time available precluded the investigation of four more lateral motion performance functions of importance, e.g.

$(PF)_{A[\delta_a, \ddot{Y}]}$

$(PF)_{A[\delta_a,\beta]}$

$(PF)_{A[\delta_r,\ddot{Y}]}$

$(PF)_{A[\delta_r,\beta]}$

Analytical expressions for these performance functions can be obtained from the differential equations for lateral motion.

The Laplace Transformations of the analytical equations are:

$$(s - Y_v)v + Ur - g\phi = 0$$

$$-vL_v + (-\frac{I_{XZ}}{I_{XX}} s - L_r)r + (s - L_p)p = L_{\delta_a} \delta_a(s)$$

$$vN_v + (s - N_r)r + (-\frac{I_{XZ}}{I_{ZZ}} s - N_p)p = N_{\delta_a} \delta_a(s) + N_{\delta_r} \delta_r(s) \qquad (1\text{-}1)$$

Side force and rolling moment due to rudder deflection and side forces due to rolling and yawing velocities are considered negligible. The axes and symbols conform to NACA notation. Fig. 1-1 pictures the axes; the symbols are defined in the Glossary, Appendix E.

In order to measure the outputs due to a specific input, all other inputs must be zero. Letting δ_r equal zero and specifying δ_a as the forcing function, the solution of equation (1-1) yields the performance function,

$(PF)_{A[\delta_a,W_Z]}$

where W_Z is equal to r

This performance function for the B-25J is computed in Appendix D, using values for the aerodynamic derivatives based on wind tunnel tests. Plots of the amplitude ratio and phase angle of this calculated performance function are given in Figs. 3-3 and 3-4, respectively.

All of these lateral motion performance functions can be obtained

experimentally by sinusoidally oscillating the control surface and measuring the airplane's steady state response. This sinusoidal method requires a sine generator and an auto-pilot to supply the inputs, and requires as well, the usual measuring equipment. In addition, considerable flight time is needed to obtain results over a sufficient range of forcing frequencies.

In the case of rudder deflection inputs, a step-function input would yield a transient response from which the performance function could be determined. (See Ref.1) But a step-function of aileron deflection will produce a steady-state rolling velocity which in a short time will generate such a large angle of bank that the motion could no longer be considered linear.

The method of using a finite pulse of control deflection has the advantages associated with obtaining a transient response, and, since the control surface returns quickly to the trim position, the disadvantage of a step-function input is eliminated. Finite pulses of elevator deflection have been successfully used to determine the airplane's longitudinal performance functions.(See Ref.2) But, to the knowledge of the authors, this technique has not been applied to the lateral performance functions of an airplane.

The mathematical background for a method of obtaining the performance function from the transient response to a pulse is presented in Refs. (2) and (3). Briefly, the method consists of approximating the Fourier Transforms of the input and the response. The ratio of the latter to the former is the performance function, that is,

$$(PF)_{A[q_i, q_o]} = \frac{(FT)[q_o(t)]}{(FT)[q_i(t)]} \qquad (1\text{-}2)$$

or, more generally,

$$(PF)_{A[q_i,\ q_o]} = \left.\frac{(LT)[q_{out}(t)]}{(LT)[q_{in}(t)]}\right|_{s\ =\ jw} \qquad (1\text{-}3)$$

When the response is convergent, it is shown in (2) and (3) that

$$(FT)[q_o(t)] \cong (FT)[UT(t)]_o \sum_{n\ =\ 1,2,\ldots} q_o(\tau_n) e^{-jn\Delta\tau\ w_f} \qquad (1\text{-}4)$$

The lateral response of an airplane requires special treatment because of the lightly-damped oscillatory mode and because of the divergent mode found in many airplanes. The factored characteristic equation for the lateral motion of the B-25J, derived in Appendix D, shows both characteristics:

$$[s^2 + (2)(.141)(1.34)s + (1.34)^2][s + 2.9][(s - .0013)] = 0 \qquad (1\text{-}5)$$

The lateral response of an airplane having this characteristic equation would not be convergent. However, by resolving the response into components, the performance function can be determined.

For example,

$$(PF)_{(\ )(q_{in}q_{out})} = \left.\frac{(LT)[q_{(out)(div.)}(t)]}{(LT)[q_{in}(t)]}\right|_{s\ =\ jw}$$

$$+ \frac{(FT)[q_{(out)(osc)}(t)]}{(FT)[q_{in}(t)]} + \frac{(FT)[q_{(out)(rem)}(t)]}{(FT)[q_{in}(t)]} \qquad (1\text{-}6)$$

The Laplace Transform of $q_{(out)(div)}(t)$ is obtained by first determining the analytical expression for $q_{(out)(div)}(t)$; this is obtained by plotting (on semilog coordinates) the response, $q_{(out)}(t)$, for large values of time, where, for practical purposes, only the divergent mode remains. From this plot, the slope and intercept provide the necessary information to define the divergent mode analytically and the Laplace Transform of this analytical expression can be determined. (ref. 8) The Laplace Transform of the input is equal to the Fourier Transform, since the input has the value of zero for all values of time less than zero and its integral is convergent. Thus, the first term on the right side of equation (1-6) can be found from a time response.

No evidence of a divergent mode was found in this investigation for the

B-25J. Therefore, it was unnecessary to employ the technique described in the above paragraph. However, to illustrate the procedure the performance function of an idealized physical system with divergence was determined from a computed time response. This performance function was compared with the ideal performance function, thus showing the feasibility of the method. This analysis is contained in Appendix C.

The divergent component of the time response must be subtracted from the recorded response. The integral of the remaining function of time converges. However, because of the lightly-damped oscillatory mode, the approximation of the Fourier Transform by triangles becomes tediously long. This problem can be overcome by subtracting the oscillatory mode. The frequency, damping ratio, and amplitude of the oscillatory mode are determined as described in detail in Appendix D. This mode may be either subtracted over the region of time from zero to infinity, or it may be subtracted only in the region from any selected time, t_p, to infinity. In the first case, the performance function becomes:

$$PF_{(\ )}[q_i, q_o] = \frac{(FT)[q_{(out)(osc)}(t)] + [q_{(out)(rem)}(\tau_0)](FT)[(URT)(t)]_o}{(FT)[UT(t)]_i \sum_{n=1,2,3} q_{(in)}(\tau_n) e^{-jn\Delta\tau_i w}} + \left. \frac{(FT)[UT(t)]_o \Sigma[q_{(out)(rem)}(\tau_n)] e^{-jn\Delta\tau_o w}}{(FT)[UT(t)]_i \Sigma[q_{(in)}(\tau_n)] e^{-jn\Delta\tau_i w}} \right|_{n=1,2,\ldots}$$

The unit triangle of t is here defined as a triangle of unit height and with a base length of $2\Delta\tau$, as in Ref. 3. Similarly, the unit right triangle of t is defined as a right triangle of unit height with a base length of $\Delta\tau$. Note that $q_{(out)(rem)}(t)$ is not the same function as $q_{(out)(rem)}(t)$ in eq. (1-5).

In the second of these two methods, the performance function becomes:

$$(PF)_{(\ )}[q_{(in)}q_{(out)}] = \frac{(FT)[q_{(out)(osc)}(t_p)]_{(t_p \leq t \leq \infty)}}{(FT)[UT(t)]_i \sum_{n=1,2,3,\ldots} q_{in}(\tau_n)e^{-jn\Delta\tau_i w}} \qquad \frac{(FT)[UT(t)]_o \sum_{n=1,2,\ldots t_p} q_{(out)}(\tau_n)e^{-jn\Delta\tau_o w}}{(FT)[UT(t)]_i \sum_{n=1,2,\ldots} q_{in}(\tau_n)e^{-jn\Delta\tau_i w}} \qquad (1\text{-}7)$$

If the $\Delta\tau$ associated with $q_{(out)}$ equals that associated with q_{in}, only the summations remain in the second term on the right side of equation (1-7). However, if $\Delta\tau_o$ is not equal to $\Delta\tau_i$, a correction factor must be applied, since the Fourier Transform of a unit triangle of t is

$$(FT)(UT(t)) = \left[\frac{(\sin\frac{w\Delta\tau}{2})^2}{(\frac{w\Delta\tau}{2})^2}\right] \Delta\tau$$

The Fourier Transforms of both a unit triangle and a unit right triangle, as functions of $w\Delta\tau$, are plotted in Ref. (3). The Fourier Transforms of both a sine function and a cosine function over the region t_p to infinity are developed in Appendix D, and their application to the determination of the lateral motion performance functions measured in this investigation is discussed in detail.

Either of the above methods is considered acceptable. However, the results of this investigation indicate that adding of the oscillatory mode at t_p is a somewhat better method than including the oscillatory mode from time equal to zero.

The input pulse should have sufficient area to produce a desirable magnitude of response, but should not cause motion beyond the linear region of the airplane's aerodynamic characteristics. Also, to simplify the data reduction, it is desirable that the pulse be of short duration. The pulses used in this investigation were roughly estimated from previous data on static sensitivities, such as p b/2U, Ref. 4, together with the experience

gained from the longitudinal pulse tests on this airplane. The linearity ranges of the linkages for the control deflection pick-offs (microsyn signal generators) and the sensitivities of the rate gyros were determined on the basis of those estimates with a 100 percent safety factor. After flight trials, the rough estimate of the aileron pulse was increased by about 50 percent in magnitude, with the duration remaining as originally estimated. On the other hand, the estimated rudder pulse was reduced slightly after flight trials.

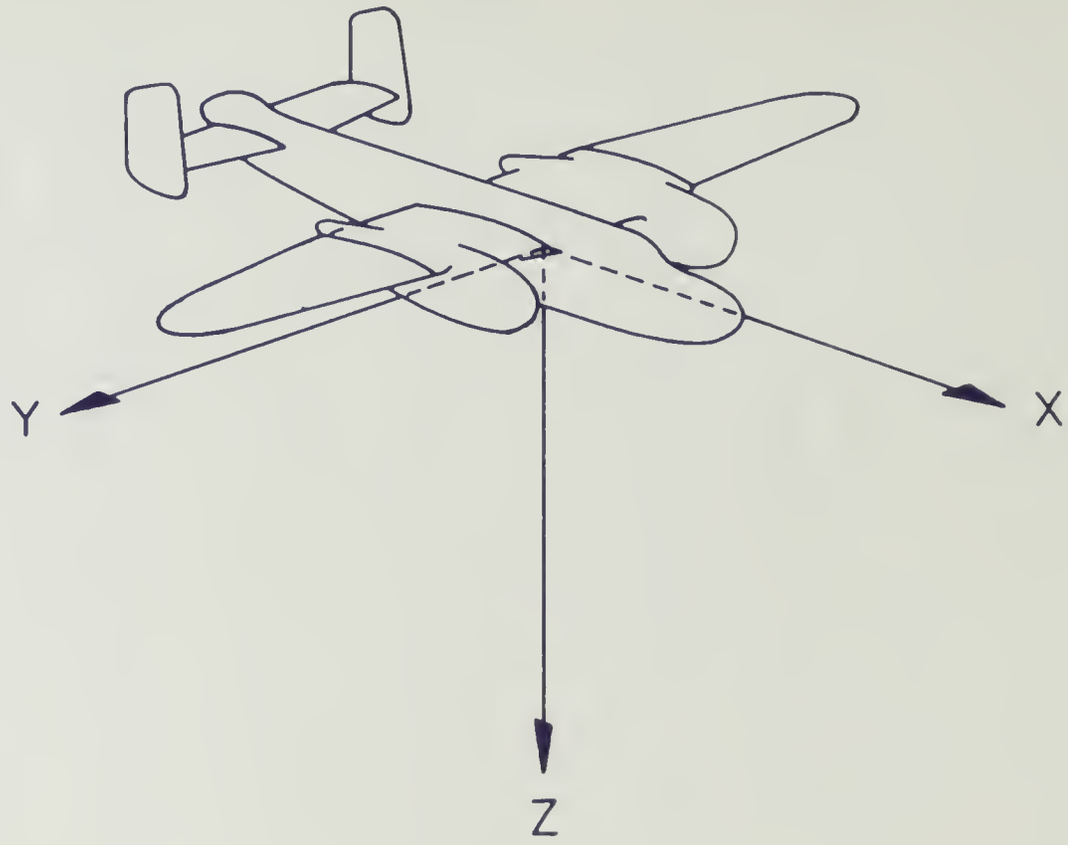

FIG. 1-1. AIRPLANE REFERENCE AXES

CHAPTER 2

INSTRUMENTATION AND FLIGHT TEST PROCEDURE

A. INSTRUMENTATION

The airplane employed as a test vehicle for this investigation was a USAF North American B-25J, Army Number 44-30328. The airplane had been stripped of all armament. A photograph, a three-view drawing and a table of general specifications and dimensions are presented in Appendix A. This airplane had previously been instrumented to record the normal acceleration and pitching velocity responses to a recorded pulse of elevator displacement. The amplifying and recording systems used in the earlier testing were retained for the present studies augmented by the following:

1. Adjustable rudder stop device (mounted on the co-pilot's right rudder pedal), fulfilling the dual purpose of providing rudder pulses of any desired fixed magnitude, and of locking the rudder while aileron pulses were being applied. See Figs. 4 and 5, Appendix B.

2. Adjustable aileron stop device (mounted on the co-pilot's control column), fulfilling the dual purpose of providing aileron pulses of any desired fixed magnitude, and of locking the ailerons while rudder pulses were being applied. See Figs. 1, 2 and 3, Appendix B.

3. Microsyn signal generator units, linked to each aileron for recording the magnitude of the aileron displacement. See Figs. 6 and 7, Appendix B.

4. Microsyn signal generator unit mounted at the rudder control bell crank (right rudder) for recording the magnitude of the rudder displacement. See Fig. 8, Appendix B.

5. Rate gyro, for measuring the angular velocity in yaw. See Fig. 15, Appendix B.

6. Rate gyro, for measuring the angular velocity in roll. See Fig. 15, Appendix B.

7. Electronic current regulator, used to regulate a set value of stiffness current applied to the elastic restraint generators of the roll and yaw gyros.

Four channels of amplification and four channels of a Consolidated recording oscillograph were utilized to record:

1. Aileron input pulses.

2. Rudder input pulses.

3. Roll angular velocity.

4. Yaw angular velocity.

The amplifiers and oscillograph are described in Appendix B.

Several ground calibrations were made before any flights were attempted, and a final ground calibration was performed prior to the final flight. The methods of calibration and the calibration curves are presented in Appendix B.

The center of gravity of the airplane was determined by means of a USAF electronic weighing kit. The center of gravity of the airplane was maintained near the center of gravity of the front main fuel tanks by shutting off the other tanks during flight. This caused the shift in the center of gravity during flight to be negligible.

An accurate determination of the moments of inertia of the B-25J airplane for use in the theoretical calculations of this thesis posed a difficult problem. Obviously, they could be determined most accurately by experimental means, but, because of the size and weight of the B-25J, such a procedure was beyond the scope of the present study. As a practical alternative, the moments of inertia were fixed by careful estimates from known data already established on similar aircraft.

Estimates were first based on the fairly complete data for a B-25J contained in Ref. 1. However, a subsequent comparison of the values for I_{YY} contained in the data with the value for I_{YY} determined for our test airplane by other investigators (Ref. 2) indicated that the test airplane and the reference airplane differed somewhat in configuration. Therefore, the final estimates were based on a comparison with similar data from the A-26 airplane discussed in Refs. 7 and 9. This comparison was expected to

increase the validity of the estimated figures because the test airplane and the A-26 had similar dimensions and differed only slightly in weight. This comparison yielded somewhat higher figures for I_{XX} and I_{ZZ} than those given in Ref. 1, in line with the higher value for I_{YY} determined experimentally for the test airplane, to which reference has already been made.

B. FLIGHT TEST METHODS

Thirty minutes prior to a flight, all equipment was turned on temporarily and the following items were checked to insure proper operation:

1. 300-volt d-c supply
2. 26-volt three-phase gyro wheel excitation
3. 150-volt d-c supply
4. Gyro stiffness current
5. Amplifier outputs
6. Paper supply in oscillograph
7. Frequency of the inverter output

Soon after take-off, all equipment was turned on again — this time for the duration of the flight — to insure sufficient warm up time, and the items mentioned above were rechecked. Then, with the airplane trimmed at 175 mph and 10,000 ft. altitude, test pulses were applied so that the zero position of the light traces of the oscillograph, the amplifier attenuation settings, and the input pulse amplitude could be adjusted. An effort was made to keep the attenuation settings constant so as to reduce the number of calibrations required.

After the preliminary adjustments had been made, the airplane was carefully trimmed, with all controls held firmly against the stops; the pilot then started the oscillograph, and three seconds later gave the signal for the impulse. The oscillograph was stopped by the oscillograph

operator when the oscillations had attenuated to a negligible amplitude.

The number of control stops used in these tests made it necessary for the pilot and co-pilot to follow a certain sequence of operations. This sequence was:

1. Prior to recorded run:

   a. Pilot trimmed airplane to maintain straight and level flight, holding the elevator control against the elevator stop.

   b. Co-pilot adjusted aileron and rudder stops to give desired pulse amplitudes. (This was done by applying pulses of various magnitudes, within the linear range, until the desired response was observed on the oscillograph.)

2. For a recorded run:

   a. Pilot trimmed airplane in straight and level flight, holding the elevator control against the elevator stop.

   b. Co-pilot moved adjustable trim screw for rudder until the proper stop was engaged, the rudder was then held firmly against this stop.

   c. Co-pilot moved the adjustable trim stop pin for the aileron until the proper stop was engaged, the aileron control was then held firmly against this stop.

   d. Pilot called oscillograph operator and, if the recording equipment was ready, pushed the button to start the oscillograph.

   e. Three seconds after starting the oscillograph, the pilot signalled the co-pilot to apply the pulse.

On each flight, two records were made for each of the following types of pulse:

1. Positive aileron (right aileron down)

2. Negative aileron

3. Right rudder

4. Left rudder

After the above records had been taken, the airplane was held on a straight course at 10,000 ft. for a sufficient time to make calibration records. The method of calibration is discussed in detail in Appendix B.

In addition to the oscillograph records, the following data were also recorded for each run:

1. Attenuation settings
2. Direction of control deflection
3. Altitude
4. Indicated airspeed
5. Outside air temperature
6. Fuel load
7. Engine rpm
8. Inverter frequency
9. Gyro elastic restraint current
10. Signal generator excitation current

CHAPTER 3

RESULTS AND DISCUSSION

A satisfactory instrumentation and calibration of the test vehicle was achieved. It is shown in Appendix B that the maximum uncertainty in calibration was 1.7 percent.

The flight test data was reduced by the methods outlined in Ref. 3 with the following results:

(a) The uncertainty in reproducing results, obtained by analyzing three independent records of rolling velocity response to input aileron pulses, was found to be 1.5 percent average deviation from the average measured performance function in amplitude ratio, and 2° average deviation in phase angle. (See Figures 3-1 and 3-2).

(b) The comparison of the experimentally determined performance function with the performance function calculated from wind tunnel stability derivatives for rolling velocity response to aileron input showed very close agreement in phase angle at all frequencies within the range investigated (0.5 to 6.0 rad/sec). The comparison in AR showed both curves following the same general pattern with the calculated performance function having a lower AR at all frequencies except the resonant frequency. The resonant frequencies were displaced both in amplitude ratio and in frequency in accordance with the respective differences in damping ratio and undamped natural frequency of the oscillatory modes. (See Figures 3-4 and 3-2).

(c) The sensitivities of the calculated and experimental performance functions for rolling velocity response to aileron input compared as follows:

$$S_{(A)(\delta_a W_X)(calc)} = -.992 \quad 1/sec$$

$$S_{(A)(\delta_a W_X)(exper)(aver)} = -1.00 \quad 1/sec$$

Utilizing $\frac{pb}{2U}$ vs δ_a data obtained from flight test data (Ref. 4) an additional sensitivity is available, i.e.,

$$S_{(A)(\delta_a W_X)_{(flt.\ test\ data)}} = -0.90 \quad 1/sec$$

(This sensitivity allows a rough check on overall calibration of the instrumentation system).

(d) Comparison of the experimental performance function for yawing rate out to aileron input with the calculated performance function shows good correlation in AR. The PA comparison is satisfactory for low frequencies (.5 to 3 rads/sec). However, at high frequency a wide scattering of points is produced using three different systems of analysis. (See Figures 3-3 and 3-4).

(e) Sensitivity comparison of the calculated and experimental performance functions for yawing velocity response to aileron input is as follows:

$$S_{(A)[\delta_a W_Z]_{calc}} = .209 \quad 1/sec$$

$$S_{(A)[\delta_a W_Z]_{exper}} = .17 \quad 1/sec$$

(f) From an investigation of three different methods of dividing the output into components, as discussed in Appendix D, it was found that the most accurate and fastest system of graphical analysis for use in the case of a lightly damped oscillatory response was method (2) of Table 2, Appendix D. In this method the usual triangular approximation is used until the time response is only a pure damped sinusoid. At this point, $t = t_p$, the Fourier Transform of a cosine or sine, whichever is appropriate, is added.

(g) Investigation of the scattering of points at high frequency in the performance function, $(PF)_{(A)(\delta_a W_Z)}$, showed that the uncertainty was a function of the following:

(1) The measurement uncertainty in determining vector magnitudes from the oscillograph record.

(2) Determination of the proper base line.

(3) The time response pattern — depends on whether the maximum ordinate occurs early or late in the time response, and on how large a proportion of the response is purely oscillatory.

(4) The ratio of magnitudes of the last plotted vector in the output summation to the resultant vector representing the response.

(5) The method of component breakdown.

(6) The frequency — uncertainty increases with frequency in the usual case.

(7) Size of $\Delta\tau$ used in the approximation of the input and output.

Instrumentation and the actual test flights for this project consumed a relatively large percentage of the time available. Consequently, the time remaining for analysis of the oscillograph records required that only those analyses most pertinent to the objectives of the project be undertaken. Since the main objective of the project was to investigate the practical aspects of the application of the pulse technique to dynamic systems in general, and since determination of the performance functions of the test vehicle were of secondary importance, the scope of data analysis was limited to the following investigation:

1. Determination of the uncertainty in repeating results by obtaining a performance function from each of three oscillograph records independently, using aileron pulse inputs and rolling velocity response.

2. Evaluation of several different graphical plotting methods as to accuracy, speed, and applicability to various response configurations.

3. Comparison of the experimental performance function with the calculated performance functions, using response in rolling velocity and

yawing velocity to aileron inputs as examples.

4. Seeking out of limitations imposed on the accuracy of the pulse technique due to the approximations involved in the process of converting from the time domain to the frequency domain.

Table 1 of Appendix D lists the oscillograph records analyzed, and the method of analysis used.

The uncertainty in reproducing results using the pulse technique is considered to be entirely satisfactory, and well within the demands of usual engineering requirements. In evaluation of the ability of the pulse technique to reproduce results two investigations were pertinent. They were: (1) the ability to produce the same performance function by analyzing different records, and (2) the ability of two different analysis methods to produce the same performance function when applied to the same oscillograph record. The results of the first investigation are shown in Figures 3-1 and 3-2. The three oscillograph records used to obtain the experimental results shown in Figures 3-1 and 3-2 are tabulated in Table 1, Appendix D. The experimental curve shown is the average of three performance functions determined independently. The maximum AR deviation from the mean curve is 5.9 percent at ω_f = 1.5 rad/sec., and the average AR deviation from the mean curve is 1.5 percent. For the phase angle, the maximum deviation is 6^o and the average deviation is 2^o.

The uncertainty in repeating results by utilizing the three graphical methods listed in Table 2 of Appendix D, was found to be a variable depending on the response pattern in the time domain, and the forcing frequency. In general, the method described as Method (2) in Table 2, Appendix D, offers the least uncertainty. This method utilizes the same degree of approximation in determining the Fourier Transform of the input and output from the records in the time domain out to $t = t_p$. Disregarding frequency effects, the

uncertainty of this method may be held fairly constant with variation in response pattern by selecting t_p at increasingly higher values as the response pattern becomes increasingly more oscillatory. Comparing the pattern of rolling velocity response with the pattern of yawing velocity response using aileron inputs for both, it was found that in the former a low proportion of the response was oscillatory while in the latter a high proportion of the response was oscillatory. Consequently, in the latter case, if t_p was not increased beyond the t_p used in the rolling response case, a higher proportion of the response was represented by a Fourier Transform which is exact, while the input remains an approximation to the exact Fourier Transform. The ultimate limit is to let t_p increase to a time beyond which the response is negligible, plotting all vectors directly from the record. This is listed in Table 2, Appendix D as method (1). This method offers the least error in the hypothetical case where instrumentation inaccuracies and noise are at such a low level that ordinates may be measured accurately at large values of time.

Increasing t_p as the percentage of oscillatory portion of the response increases is also important in nullifying errors occassioned by choosing t_p at a point which is not exactly a true peak or zero of the response curve. An error of this nature serves to shift the phase angle of the added vector for the oscillatory remainder ($t \geq t_p$) by an amount equal to $\omega_f \Delta\tau$. If the magnitude of the last vector plotted in the summation of triangles is only a small percentage of the added vector, the error in phase angle may be large. However, if the magnitude of the vector added is of exactly the same length as the last vector of the summation, an error in t_p as large as $t = \Delta\tau$ will yield no error in the PA of the response vector.

The method of dividing the output into components, described in Appendix D, Table 2, as method (3), appears to be subject to the greatest inaccuracies

any of the methods investigated in analyzing a lightly damped oscillatory response. Theoretically, this method of analysis is as sound as any of the methods investigated. However, the practical application of this method presents an additional source of error since the input and output are not represented with the same degree of approximation. In the lightly damped, highly oscillatory response, essentially the entire output is represented by the Fourier Transform of the oscillatory mode, which is the exact transform of an analytical expression. On the other hand, the input is approximated by a vector addition, the exactness of which depends on the accuracy of curve fitting achieved. At relatively high frequency, the small resultant vector of the remainder summation, although approximated with the same degree of exactness as the input resultant vector, is ineffectual in changing the total output phase angle which is dominated by the large vector representing the oscillatory mode. Consequently, the output phase angle becomes nearly static as the limiting phase angle of the oscillatory mode is approached, while the input phase angle continues to grow as the forcing frequency increases.

In performing the component breakdown necessary in this system, additional measurement errors may accumulate if more than one set of measurements are taken from the response. That is, in removing the oscillatory mode, the ordinates as determined by the analytic expression of the oscillatory mode should be subtracted algebraically rather than graphically from measured ordinates of the total response. Furthermore, since the oscillatory mode represents the major part of the response, great care must be exercised in determining W_n, DR, and $q_{(a)}$.

In Figures 3-3 and 3-4, the results of analyses by the various methods discussed are shown. The scatter of points at high frequency shows the inaccuracies of the several methods. Theoretically, the PA curve should level off in the vicinity of -90° phase angle. However, Fig. 3-4 shows the

experimentally determined PA lagging less at ω_f of 5 and 6 rad/sec than at 3 rad/sec. In investigating this discrepancy between theoretical and experimental results, the question of accuracy in approximating the Fourier Transform arose.

To determine how closely the approximation of input and output time response by summation of triangles fits the actual curves, frequency spectra of yaw response and aileron input were prepared by numerical means. The results are shown in Figures 3-5 and 3-6. The circled points show the results of the numerical analysis and the dotted curve shows the mean curve of the experimental points obtained in Figures 3-3 and 3-4. The phase angles determined by the numerical analysis show a variation of more than 30° from the average curve at many points. The explanation for such a discrepancy was found to lie in a difference in measurement of the ordinates, $[q(t_n)]$, between those used in the numerical analysis and those used in the graphical analysis. The measurements of the respective areas, for each analysis, are as follow:

	AREA Numerical Analysis	AREA Graphical Analysis
1st positive lobe	0.268 in sec	0.26 in sec
1st negative lobe	0.6170 in sec	0.5990 in sec
2nd positive lobe	0.1126 in sec	0.1096 in sec

In the two most important lobes, the deviation in measurement of area is approximately 3 percent, and in each case the graphical analysis is the smaller area. Thus it is noted in Figure 3-7 that a small uncertainty of 3 percent in area determination may cause as much as 30° difference in phase angle, provided, the vector plot of the output ''winds up'' near the origin. Since the numerical analysis gives only a check on how closely the triangular summation approximates the area of the curve, the performance

function was again determined at several forcing frequencies using the same ordinates as used in the numerical analysis. The triangles in Figure 3-6 show the points thus determined. It is seen that the uncertainty of reproducing results is satisfactory, indicating that the use of triangles in approximating the area yields approximately the same accuracy as the numerical approximation. It is now apparent that any inaccuracies in measuring the ordinates have a critical effect on the performance function when the end point of the vector summation is near the origin. However, the PA variations due to inaccuracies in measurement of ordinates is not constant, but is a function of frequency. Although the measuring error in this case gives an increase of ordinate magnitude in both the positive and negative lobes, the errors in a positive lobe do not nullify the errors in a negative lobe except at certain frequencies which are indeterminate unless the actual measurement errors are known. Figure 3-7 shows the results of measurement error at ω_f = 5 rad/sec. Due to the phase angle shift with each added vector ($\omega_f \Delta\tau$) the errors are apportioned in accordance with the sine and cosine of the vector phase angle multiplied by the magnitude of the error in that vector. If the sum of the imaginaries and reals of the measurement errors add up to give a vector which has an angle corresponding to that of the original resultant vector, no change in PA will result. However, this rarely happens, and at high frequencies a large phase angle change results. Note in Fig. 3-7 that the largest differences in the vectors of the first two lobes occur in measuring vectors which have phase angles close to $+90^{\circ}$, i.e., vector 10 in the first lobe and vectors 28 and 30 in the second lobe. All of these difference tend to increase the phase angle at ω_f = 5. Each frequency will have a different total PA error due to measurement uncertainties, since the phase angle of each vector changes with each different forcing frequency.

Again note that measurement errors have an insignificant effect unless the end point of the summation is near the origin. At ω_f = 1.75 rad/sec the PA is the same, whether determined graphically or numerically, and the effect of measurement differences on uncertainty in determining the performance function is negligible as shown by the superimposed points lying on the average experimental curve.

In general, it appears that any uncertainty, whether in measurement of ordinates or base line location, gives a magnified uncertainty in PA if the end point of the summation is near the origin.

The phase angle uncertainty is not due to a breakdown in the theory of the pulse technique, nor caused directly by the triangular approximation of the input and response. Rather it is a function of uncertainty in measurement of ordinates and in plotting which accumulate under the conditions of high frequency (rapid phase angle change of each added vector) and low amplitude ratio (requires end point to be near the origin). Furthermore, this uncertainty in phase angle is not restricted to the predominately oscillatory response. It merely appears at a lower frequency in this case due to the rapid attenuation in amplitude ratio (small vectors in the early portion of the response). The same phase angle uncertainty would occur in the rolling velocity reponse to aileron input if the performance function determination had been carried out to those high frequencies where the amplitude ratio was greatly attenuated.

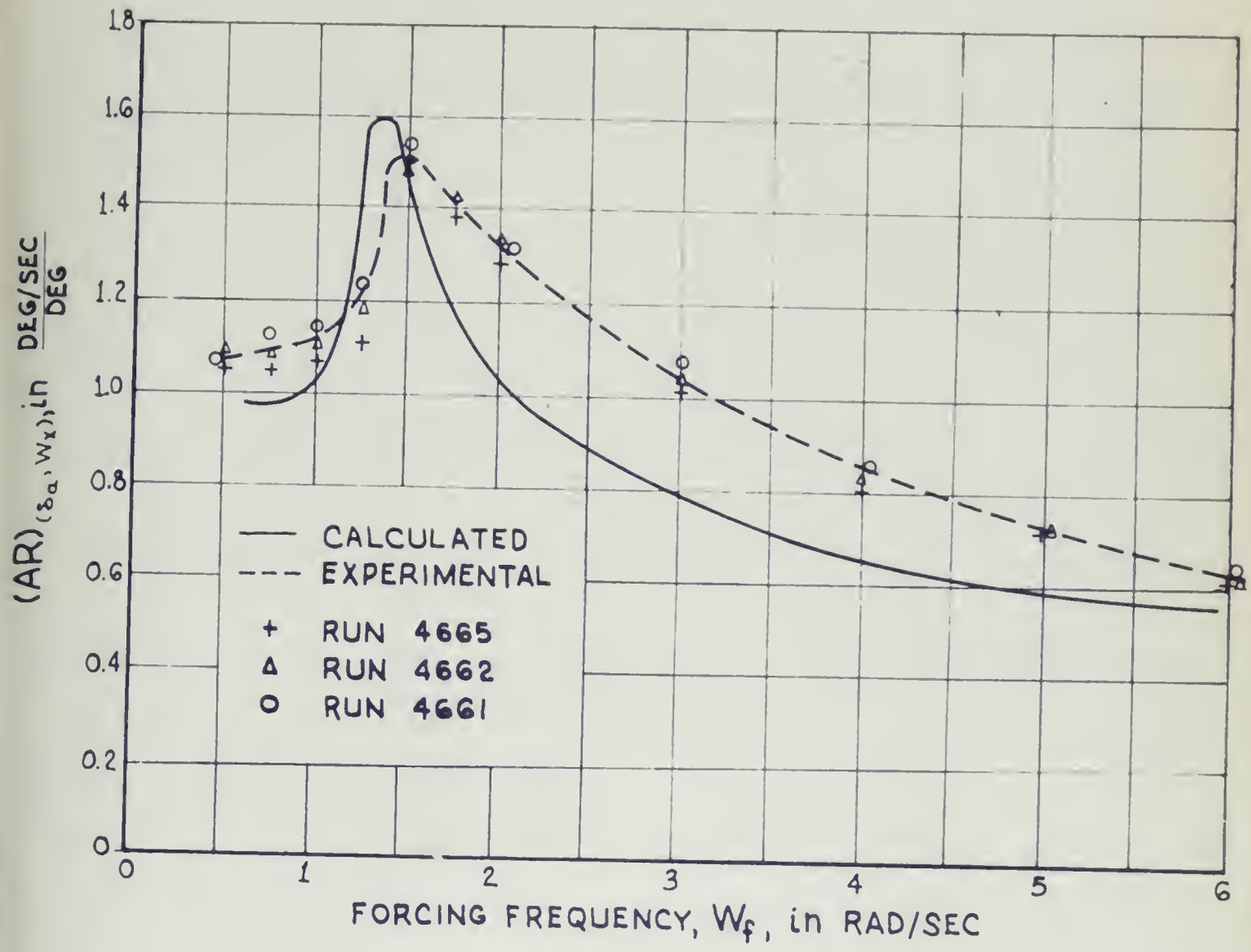

FIG. 3-1. AR OF AIRCRAFT PERFORMANCE FUNCTION FOR ROLLING VELOCITY RESPONSE TO AILERON INPUT $[PF]_{(A)(\delta_a, W_x)}$

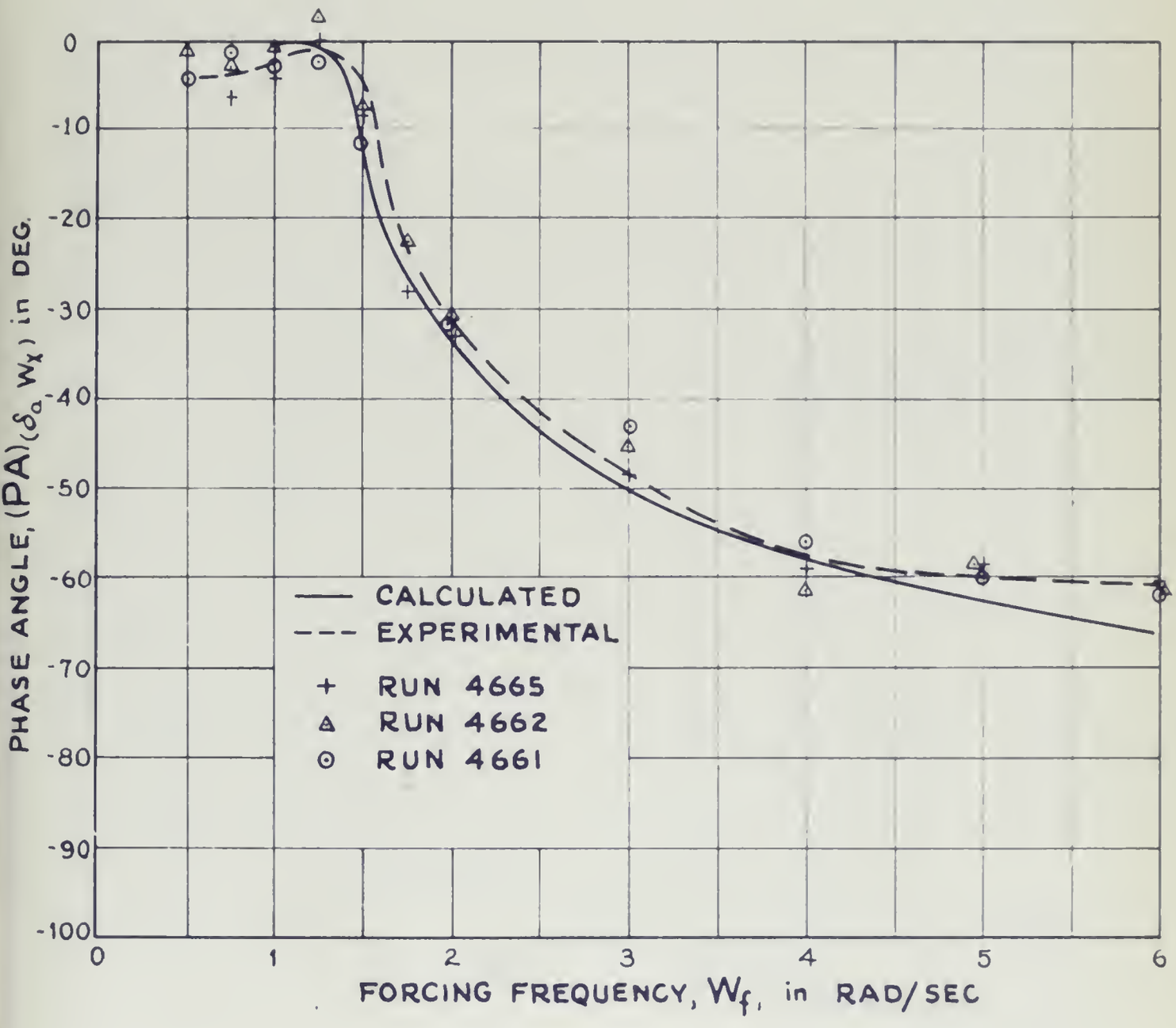

FIG. 3-2. PHASE ANGLE OF AIRCRAFT PERFORMANCE FUNCTION FOR ROLLING VELOCITY RESPONSE TO AILERON INPUT, $(PF)_{(\delta_a, W_x)}$.

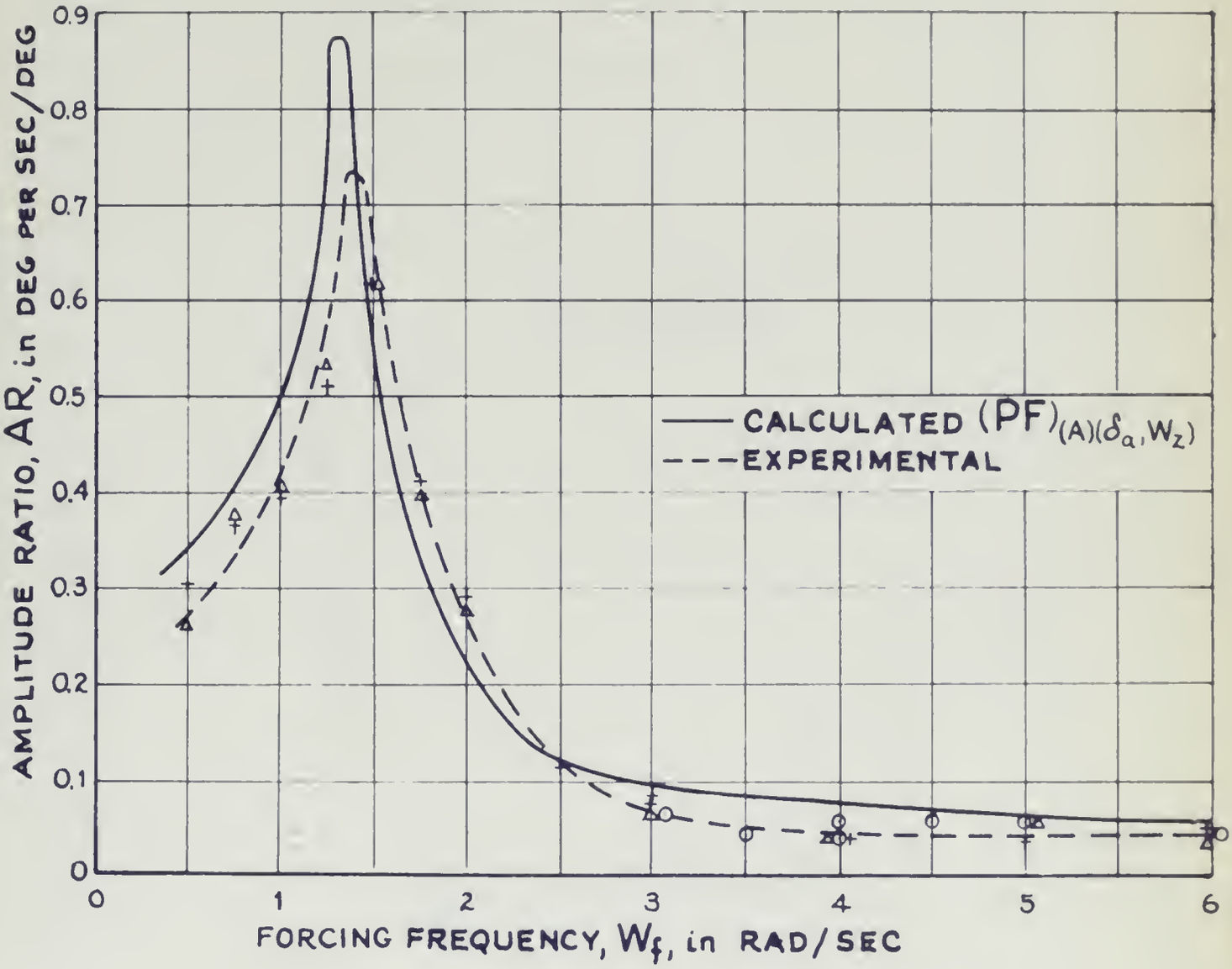

FIG. 3-3. AR OF AIRCRAFT PERFORMANCE FUNCTION FOR YAWING VELOCITY RESPONSE TO AILERON INPUT, $(PF)_{(A)(\delta_a, W_z)}$

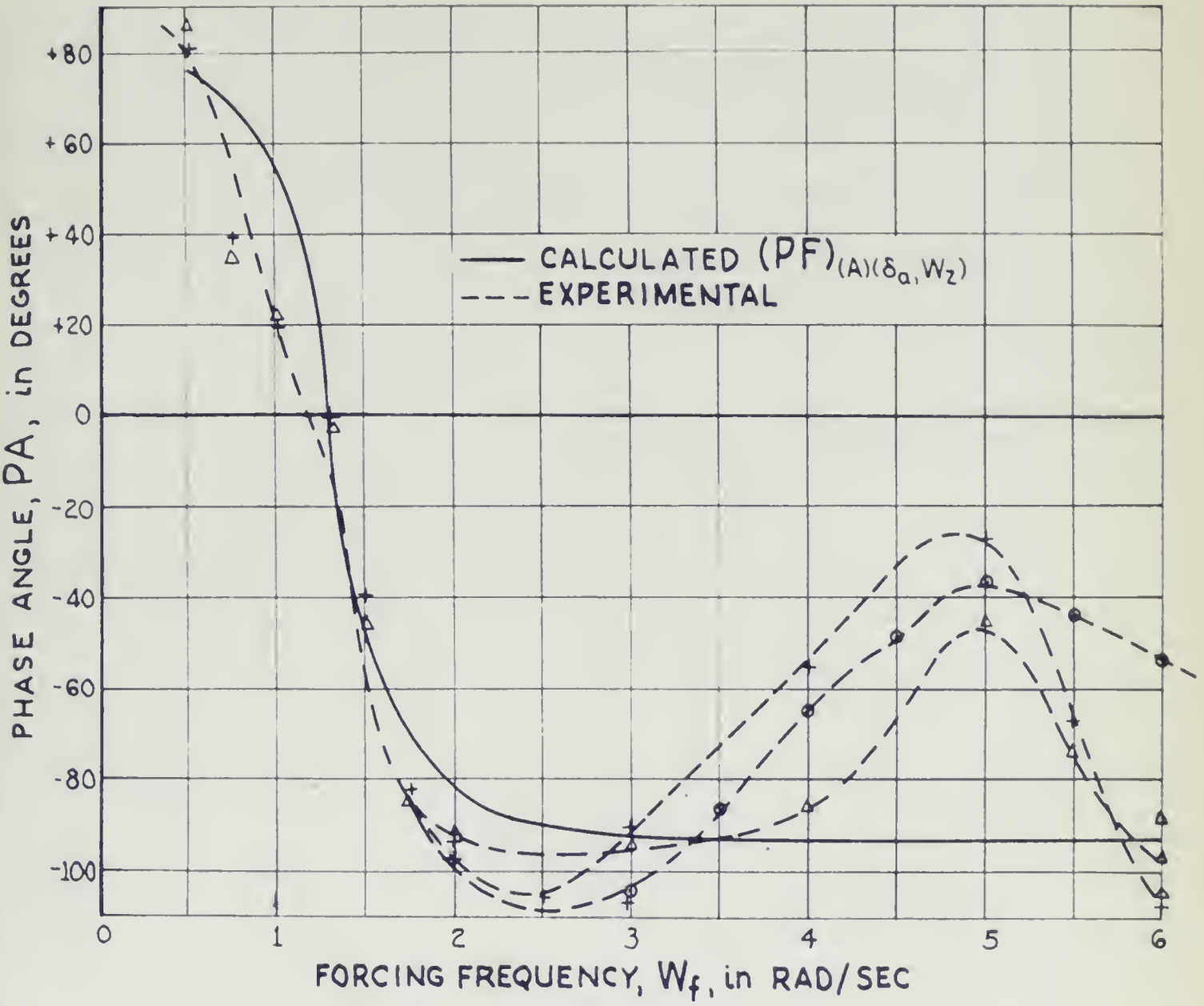

METHOD of ANALYSIS (App. D - Table 2)

Method	Symbol
2	+ Cosine added at t_p
	Δ Sine added at t_p
3	⊙ Rt. Tri. + Osc. + Rem.

FIG. 3-4. PA OF AIRCRAFT PERFORMANCE FUNCTION FOR YAWING VELOCITY RESPONSE TO AILERON INPUT, $[PF]_{(A)(\delta_a, W_z)}$

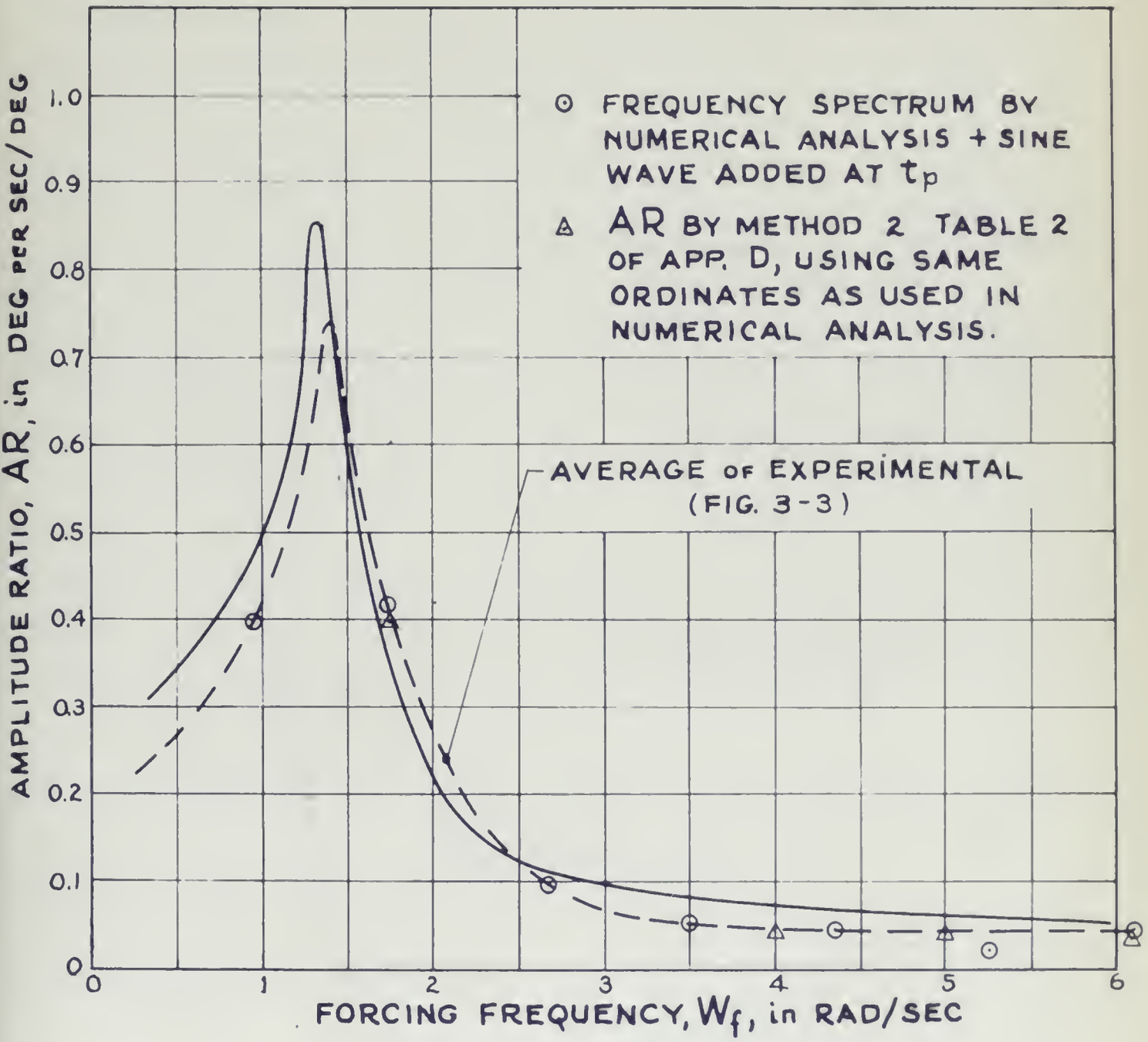

FIG. 3-5. AR OF AIRCRAFT PERFORMANCE FUNCTION, YAWING VELOCITY RESPONSE TO AILERON INPUT, $(PF)_{(A)(\delta_a, W_z)}$

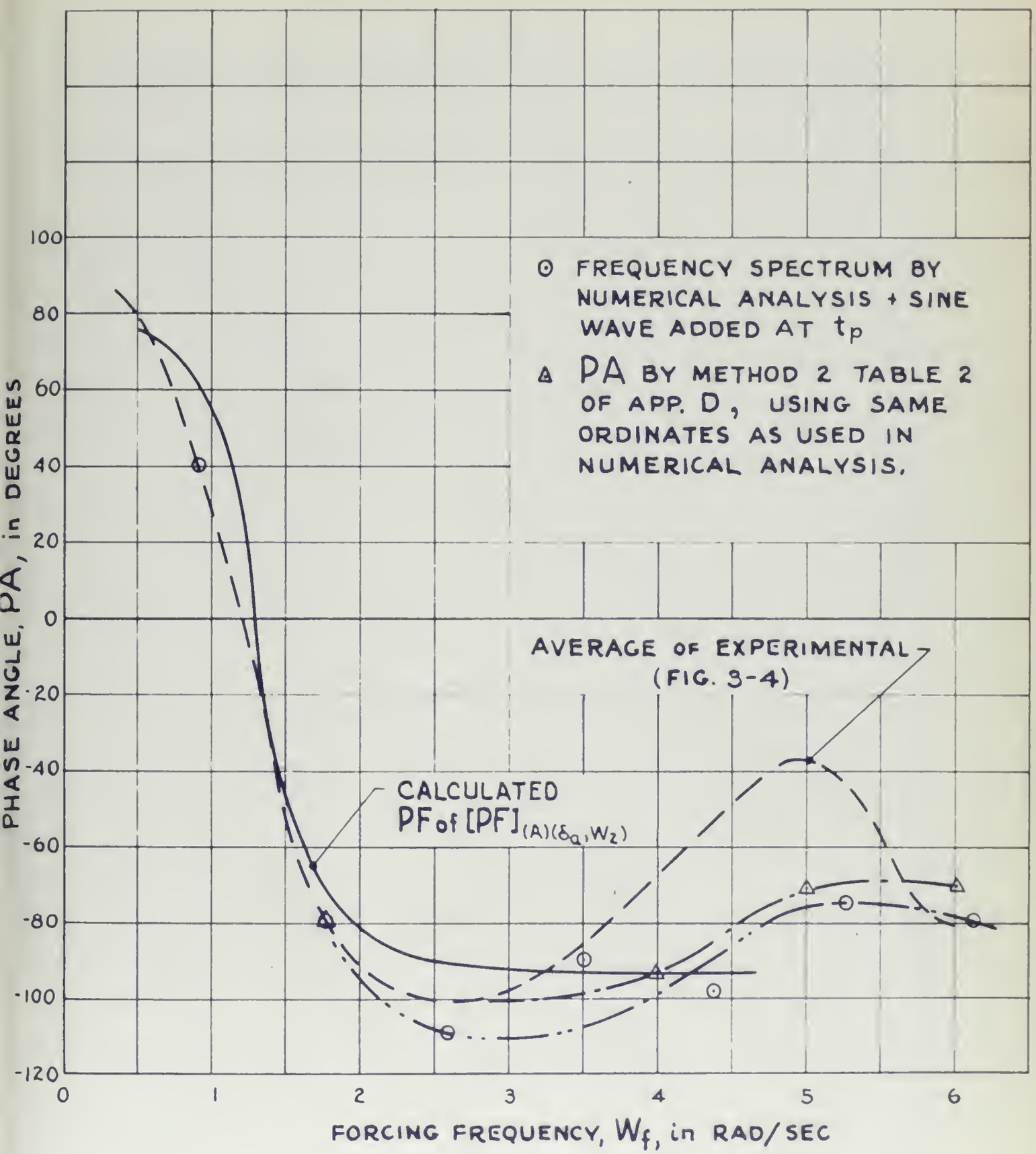

FIG. 3-6. PA OF AIRCRAFT PERFORMANCE FUNCTION - YAWING VELOCITY RESPONSE TO AILERON INPUT, $[PF]_{(A)(\delta_a, W_z)}$

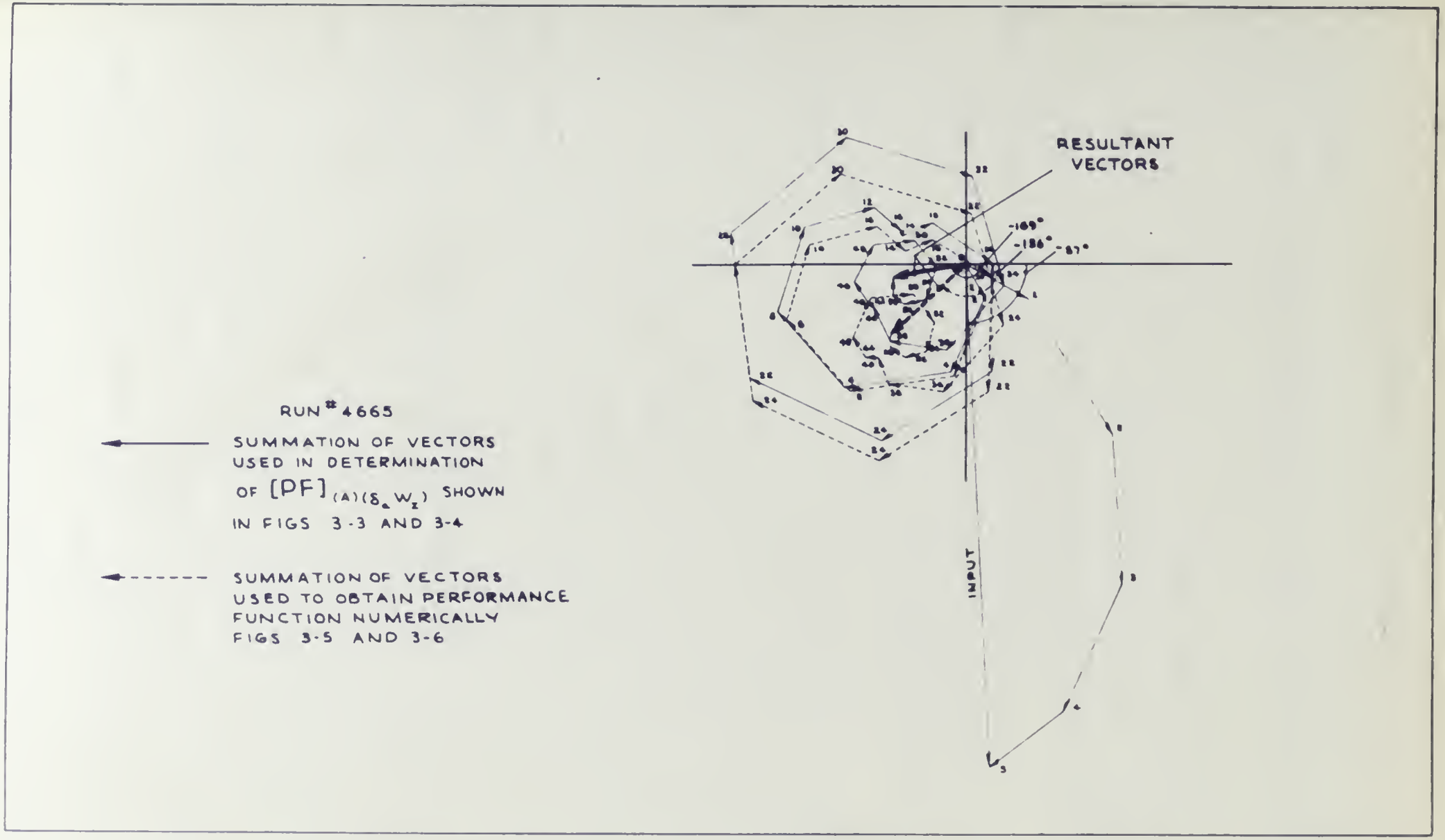

FIG 3-7 DETERMINATION OF PERFORMANCE FUNCTION $[PF]_{(A)(\delta_a W_z)}$, AT W_f = 6 RAD / SEC
(EXAMPLE OF MEASURING ERROR EFFECT ON PERFORMANCE FUNCTION)

CHAPTER 4

CONCLUSIONS AND RECOMMENDATIONS

A. CONCLUSIONS

As a result of this investigation the following conclusions are submitted:

1. The pulse technique is a practical and suitably accurate method for determining aircraft performance functions from flight tests.

2. Economy in flight time and instrumentation are gained by the pulse technique as compared to the sinusoidal method.

3. The accuracy of the results obtained is enhanced by the short duration of test flights in that the changes in mass and moments of inertia due to fuel consumption are negligible.

4. Erroneous performance function phase angles will in general be obtained at relatively high frequencies when the amplitude ratio has attenuated to a very small value (order of five percent). This is due to the fact that the errors in measurements of the ordinates of the recorded response accumulate at those frequencies where the series of vectors, representing the ordinates and their individual phase angles, encircle the origin.

5. Lightly damped oscillatory responses may be analyzed with reasonable simplicity and accuracy. However, in the case of a response which is almost wholly oscillatory, uncertainty in the data may cause anomalous phase effects to appear in the plots of the performance function at the higher forcing frequencies when the amplitude ratio is considerably attenuated. These phase effects are more pronounced in the performance functions which are highly dependent on coupling terms in the equations of motion rather than the forcing function itself, since high attenuation in AR occurs at a relatively low frequency. For example, $PF_{[\delta_a\ W_Z]}$ and $PF_{[\delta_r\ W_X]}$ are such performance functions.

6. A predominately oscillatory response is best approximated by use of isosceles triangles to a value of time beyond which only a damped sinusoid remains. The Fourier Transform of the sinusoid is then obtained by transforming the analytic expression which is then added vectorially to the approximate transform of the early portion of the response.

7. The most important sources of error in reduction of data are:

a. Choosing the base line on the oscillograph record.

b. Measurement of the ordinates from this base line.

8. The calculated and experimental performance functions are qualitatively comparable, but the quantitative differences indicate the requirement that the dynamic characteristics of all high speed and non-conventional aircraft be determined by flight tests.

B. RECOMMENDATIONS

To aid further research in the use of the pulse technique to determine aircraft performance functions the following recommendations are presented:

1. Obtain relatively long records of lightly damped oscillatory responses to facilitate the determination of W_n and DR of the oscillation.

2. Amplify low amplitude predominately oscillatory responses as much as is consistent with the noise level and linearity of the recording instruments, the friction torque level of the gyros, and the linearity of aircraft motion.

3. Limit the shock mounting of the gyros to landing and take-off only. During tests the gyros should be rigidly attached to the aircraft structure so that the input to the gyros is the true angular velocity of the airplane and is not modified by the flexibility of the shock mounts.

4. Superimpose a reference trace on each response to aid in the determination of the base line and in indicating any drift or divergence

of the response trace.

5. Investigate by flight test the lateral motion performance functions of an airplane having a relatively high degree of spiral divergence. Since the degree of spiral divergence increases with angle of attack, it may be necessary to perform these measurements at a high angle of attack in order to obtain suitable responses.

6. Investigate the performance functions of an airplane having dynamics quite different from those of the B-25J. Several modern fighter types exhibit an undamped oscillation about the Z axis. A study of this motion should prove most worthwhile and interesting.

APPENDIX A

DESCRIPTION OF AIRPLANE IN TEST CONFIGURATION

The airplane used in the tests was a USAF B-25J under bailment contract to the Instrumentation Laboratory, M.I.T. The airplane had previously been stripped of all guns and turrets, as shown in Fig. A-1.

Following is a listing of the specifications and dimensions of the airplane as it was used in the tests described in this thesis:

Manufacturer	North American Aviation Corporation, Inc.
Type	B-25J-25-N.C.
Serial Number	44-30328
Center-of-gravity range	
Forward limit	16.5 percent M.A.C.
Aft limit	34.0 percent M.A.C.
For tests	27.4 percent M.A.C.
Gear retraction moment/1000	59.7 in-lbs
Overall length	53 ft 5.75 in
Height	16 ft 4.19 in
Wing, airfoil section	
Root	NACA 23017
Tip	NACA 4409 R
Span	67 ft 6.704 in
Area (Total)	609.8 sq ft
Area (less ailerons)	577.67 sq ft
Aspect ratio	7.48
Taper ratio (tip chord/root chord)	0.415
Chord at root	12 ft 10.6 in
Chord near tip (380.75 from fuselage)	5 ft 10.14 in

Projected tip chord	5 ft 4.257 in
Mean aerodynamic chord	
Length	116.16 in
Distance of leading edge back of nose reference datum line	212.68 in
Incidence	
Root	3° 0' 30''
Tip	0° 21' 39''
Dihedral (25 percent line)	
Wing center section	4° 38' 23''
Wing outer section	0° 12' 39''
Sweepback (leading edge)	4° 12' 13''

Aileron

Type	Internal balance unsealed
Area	32.13 sq ft
Span	137.25 in
Chord	
Inboard	19.87 in
Outboard	12.45 in
Travel	
Up (from neutral)	28°
Down (from neutral)	15°
Tab area	3.86 sq ft
Tab span	57.911 in
Tab chord (mean)	5.375 in
Tab travel	
Up (from aileron trailing edge)	12°
Down (from aileron trailing edge)	12°

Wing flaps

Type	Variable-slot trailing edge
Area (total)	75.8 sq ft

Center section flaps	
Area	32.6 sq ft
Span (mean)	127.5 in
Travel (down)	43°
Outboard flap	
Area	43.2 sq ft
Span (mean)	214.5 in
Travel (down)	45°
Horizontal tail surface	
Area (including elevators)	132.4 sq ft
Span	22 ft 2 in
Maximum chord	7 ft 1.875 in
Incidence	2°
Dihedral	None
Elevator area (two, including tabs)	50.6 sq ft
Elevator span (two)	216.5 in
Elevator travel	
Up (from streamline with stabilizer)	25°
Down (from streamline with stabilizer)	10°
Elevator trim tab area (total)	4.22 sq ft
Elevator trim tab span (2)	57.2 in
Elevator trim tab mean chord	7.875 in
Elevator trim tab travel	
Up (from elevator trailing edge)	4°
Down (from elevator trailing edge)	20°
Vertical tail surfaces	
Area (total)	91 sq ft
Fin area (two)	47.8 sq ft
Span (maximum)	104.25 in

Rudder area (two including tabs)	43.2 sq ft
Rudder span (maximum)	101.1 in
Rudder travel	
Right (from streamline with fin)	20°
Left (from streamline with fin)	20°
Rudder trim tab area (total)	3.18 sq ft
Rudder trim tab span	36.4 in
Rudder trim tab mean chord	6.3 in
Rudder trim tab travel	
Right (from rudder trailing edge)	12°
Left (from rudder trailing edge)	12°

Fuselage

Maximum width	4 ft 8.5 in
Maximum height	7 ft 4 in
Length (tip of nose to tip of tail)	53 ft 5.75 in

Engine

Number	2
Type	Wright Cyclone
Designation	R-2600-13 or -29
Number of cylinders	14 - double row
Gear ratio	16:9
Supercharger gear ratio	
Low	7.06:1
High	10.06:1

Power settings:

Condition	rpm	Manifold pressure (In of H_g)
Take-off	2600	46
NRP	2400	40
Cruise	2100	29
Approach	2000	20
For tests	1800	24

Propellers

Manufacturer	Hamilton Standard
Type	Controllable pitch

Number of blades	3
Diameter	12 ft 7 in
Blade type	6359 A-18
Control type	Hydromatic full feathering
Hub type	23E50-473
Pitch setting	
Low (fine)	22°
High (coarse)	90°

Landing gear (estimated data)

Main gear assembly	
Weight of retractable portion	500 lb (each)
Radius of gyration of retractable portion about retraction pivot	48 in
Nose gear assembly	
Weight of retractable portion	200 lb
Radius of gyration of retractable portion about retraction pivot	46 in

Weight	25,637 lb

Moments of inertia (estimated)

I_{XX}	63,000 slug ft^2
I_{ZZ}	120,000 slug ft^2
I_{XZ}	-1930 slug ft^2

FIG A-1 TEST AIRPLANE B-25J NO 328

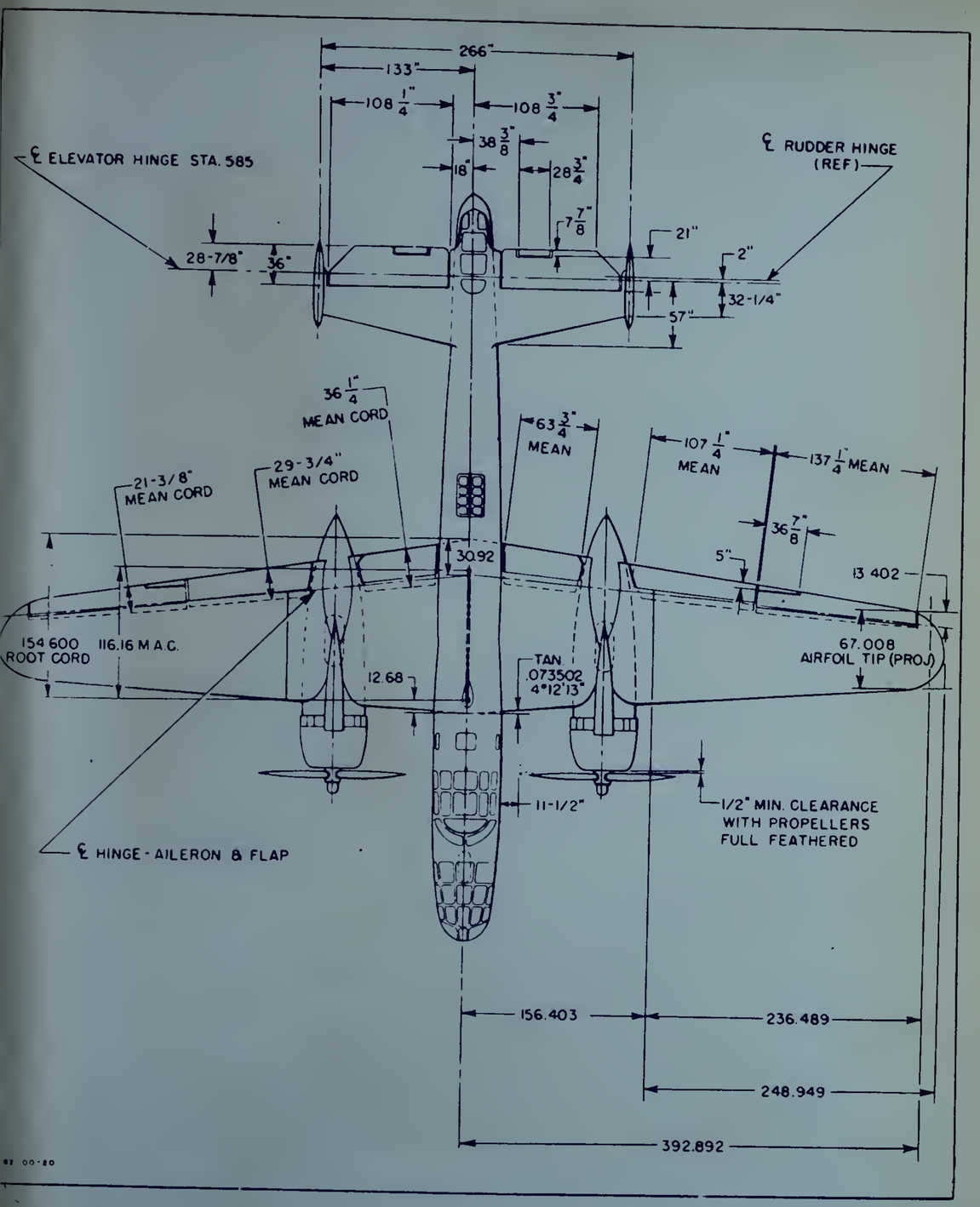

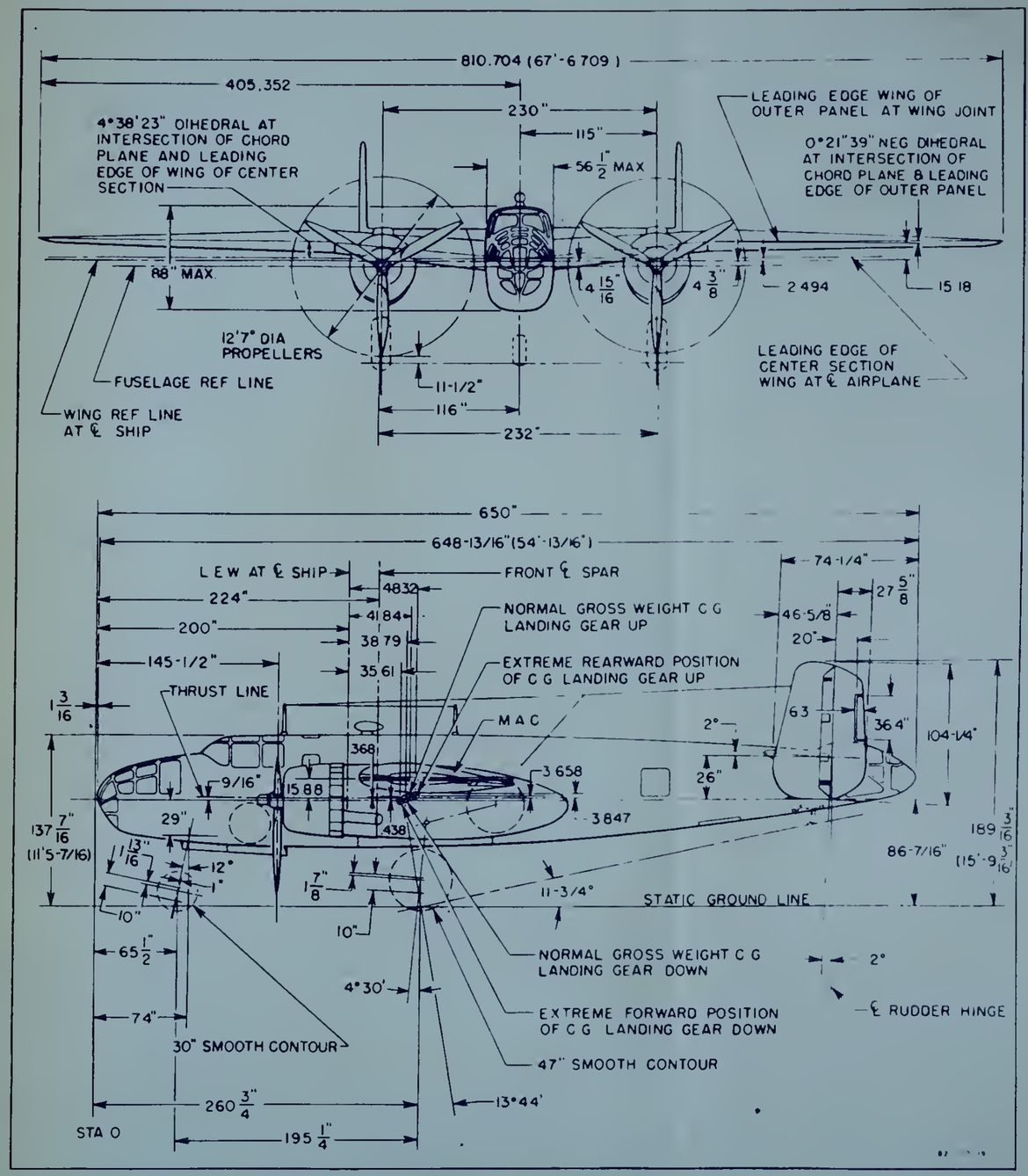

FIG. A-2. TEST VEHICLE DIMENSIONS

APPENDIX B

INSTRUMENTATION AND CALIBRATION

A. INSTRUMENTATION

As noted in the Introduction, finding the performance function by means of a pulse input has the advantages of keeping the response within the linearity limits of deviation from the equilibrium flight conditions, and of requiring a minimum of instrumentation. The devices required for applying the input pulses were designed to accomplish the following functions:

1. Allow rotation of the control surfaces between any desired limits, with positive stops at the ends of the arc of travel.

2. Allow variations in the size of the pulse.

3. Allow the pulse to be applied in both directions, that is, allow changes in the position of the mechanism relative to the pilot's controls without altering the pulse size. This function also allows the pilot to hold two controls rigidly against stops while the aircraft is responding to a pulse imparted by the third control.

4. Allow quick disconnect so as to make it possible to remove all impediments from full use of the pilot's controls in case of emergency.

The mechanisms employed were chosen from many possible designs as the simplest that could perform the above functions and still be fabricated with a minimum of machining. The aileron pulsing mechanism, shown in Figures B-1, B-2, and B-3, consists of a plate mounted on the right control wheel which is slotted to receive two pivoted bars which are set to give the desired size of pulse. A slotted length of duralumin angle, hinged at one edge, was mounted on a shelf fastened to the top of the control column. The slot allowed a single stop to be positioned so that the chosen pulse could be initiated at any trim condition by moving the single stop against either one of the stops on the wheel plate. The hinged edge allows the stop to be thrown out of position in order to clear the aileron control in case of emergency in flight. Approximately 45 degrees of wheel rotation were used in applying the desired aileron pulse.

The mechanism used for applying rudder pulses is shown in Figures B-4 and B-5. Choice of the design selected was dictated by the limited installation space and by the requirement that the pulse setting and quick disconnect units must be easily accessible to the co-pilot in flight. The mechanism in its final configuration consists of a long rod, one end of which is attached to the right rudder pedal. The other end of the rod slides in a block which is pivoted at the center, and mounted on a plate fixed to the aircraft structure. The block receiving the sliding rod is cut away at the top so that a stop pin welded to the sliding rod may move in the slot thus provided. The cover of the block is made up of a frame hinged at the inboard edge and containing two stop bars connected by a positioning screw to provide adjustment of pulse size. In addition, both bars, holding the set pulse size, may be moved by means of a second screw to permit engaging the pin on the sliding rod with either of the stop bars when in the trim condition. The hinge on the inboard side allows the block cover to be moved clear of the rod stop, thus quickly and positively freeing the rudder controls. Figures B-4 and B-5 show the cover block clear of the rod stop in the stowed condition. Approximately 0.3 in. of linear throw of the rudder pedals provided the desired rudder pulse size.

The microsyn pickoff units installed for measurement of control surface rotation were of the variable transformer type designed by Dr. R.K. Mueller of the M.I.T. Instrumentation Laboratory. The installation of these units in the right and left wing are shown in Figures B-6 and B-7 respectively. The mounting positions and linkage lengths are identical in each wing. The final determination of linkage sensitivity, that is, pickoff rotation per control surface rotation, was governed by accessibility in the wing or rudder cavity, linearity limits of the pickoff (approximately 150 milli-radians), and the maximum control surface motion anticipated in obtaining the desired magnitude

of response. Shielded pickoff leads were used throughout, and, as shown in Figs. B-6 and B-7, safety brackets were attached to the microsyn mountings to prevent any possible damage or jamming of controls in case the linkage worked free at the pickoff rotor.

The rudder pickoff installation is shown in Fig. B-8. The linkage is similar to those used in the wings, the bell crank at the rudder control serving as the initial point of motion measurement.

The rate gyros employed were elevation and deflection gyros developed by the Instrumentation Laboratory, M.I.T. The characteristics of these gyros were modified to suit the measurement requirements of the project by changing the damping, and were installed as roll and yaw rate gyros respectively.

Laboratory calibration of the gyros prior to installation in the aircraft was necessary to determine the excitation currents desired for the elastic restraints and the signal generators (pick-offs), the temperature required for the damping fluid, and the friction torque level.

The friction torque level was first determined to judge whether the gyros would provide a satisfactorily sensitive response to allow measurements of the desired accuracy and precision. The final results are shown in Figures 9 and 10 for the roll and yaw rate gyros, respectively. The maximum friction torque level for the roll gyro was 50 dy cm, and for the yaw gyro was 140 dy cms, and the unbalance was reduced to a torque level below that of the friction level. The maximum friction torque level for the roll rate gyro represents an angular velocity input of 0.25 milli-radians/sec and for the yaw rate gyro, the maximum friction torque represents an angular input velocity of 0.7 milli-radians/sec. This friction level is considered satisfactory since the oscillograph record ordinates can be measured only to a maximum accuracy of .01 inch, the latter figure representing approximately 1/2 milli-radians/sec in

most of the records.

The rate gyro equations of motion were investigated to make certain that the desired characteristic could be obtained. The general equation representing both gyros is:

$$W_{(\ )}\ {}^{HS}{}_{(link)(M_g M_c)} = I_{(c)(eff)}\ \ddot{A}_c + c_c\ \dot{A}_c + S_{(er)(A_c M_c)}\ A_c$$

where the subscript c refers the indicated quantity to the computer shaft, and the subscript g refers the indicated quantity to the gimbal shaft.

This equation may be reduced to the general form of the second-order differential equation yielding

$$\frac{A_c}{W_{(\ )}} = S_{(g)(WA)}\ \frac{1}{[1 - (FR)^2] + j\ 2(DR)(FR)}$$

where

$$(DR) = \frac{c_c}{2I_{c(eff)}\ W_n}$$

$$(FR) = \frac{W_f}{W_n}\ ;\quad W_n{}^2 = \frac{S_{(er)(AM)}}{I_{c(eff)}}$$

To determine the gyro undamped natural frequency, the effective moment of inertia at the computer shaft was measured using low elastic restraint currents and no damping. The period was recorded on a brush type oscillograph, and the moment of inertia was then determined from the following equation:

$$I_{c(eff)} = \frac{S_{(er)(AM)}}{4\pi^2}\ T^2 = 264\ \text{dyne-cm-sec}^2$$

Rechecks at different values of elastic restraint verified the above figure. To establish the amount of elastic restraint desired on the gyros, maximum rates of roll and yaw for the magnitude of control surface deflection inputs anticipated were determined from B-25 roll rate data $(\frac{pb}{2U})$ and from Cornell Laboratory Reports covering rate responses to step inputs of control

deflection (Refs. 4 and 5). The maximum rates determined were 0.4 rad/sec in roll and 0.5 rad/sec in yaw. The elastic restraint units were then calibrated for both gyros, as shown in Figs. B-11 and B-12, using various values of elastic restraint current. The maximum rate tabulated for each sensitivity indicates the rate input for the particular sensitivity which will rotate the gyro computer shaft 150 milliradians. At deflections exceeding this value, the signal generators become nonlinear. The overall sensitivities of the elastic restraints, considering both excitation current and angular displacement as inputs are:

$$S_{(roll)(er)(A,\ i^2;\ M)} = 1820\ \frac{\text{dyne cm}}{(\text{ma})^2\ \text{rad}}$$

$$S_{(yaw)(er)(A,\ i^2;\ M)} = 512\ \frac{\text{dyne cm}}{(\text{ma})^2\ \text{rad}}$$

Selection of the desired undamped natural frequency depends on the desired frequency response of the gyro. The rate gyros must accurately reproduce aircraft response below about 10 rads/sec, offering negligible or minimum attenuation and phase shift, while at the resonant structural vibration frequencies of the airplane, the attenuation must be a maximum. Previous instrumentation work on the B-25 has indicated that the most pronounced resonant frequencies were found at 16 and 30 cps. To fulfill the response requirements outlined above, the following acceptable limits for the gyro characteristics were determined:

Undamped Natural Frequency, n_n = 5 - 8 cps

Damping Ratio, (DR) = 0.6 - 1.0

With the above ranges, elastic restraint currents were selected to satisfy both undamped natural frequency and maximum rate input requirements.

A damping fluid was then selected to fit the above requirements of DR.

Figure B-13 shows the viscosity vs temperature characteristics of damping fluid DCC 350, which was the fluid used in both gyros. DCC 350 offered the smallest gradient of viscosity to temperature of any of the fluids available having the viscosity range desired.

The following chracteristics, coefficients, and sensitivities describe the gyros as used in the final test flights:

	Roll rate gyro	Yaw rate gyro
$I_{(c)(eff)}$	264 dy cm sec^2	264 dy cm sec^2
$c_{(c)}$	17200 $\frac{dy\ cm}{rad/sec}$	24000 $\frac{dy\ cm}{rad/sec}$
Damper temperature	160° F	177° F
$S_{(er)(AM)}$	3.8×10^5 $\frac{dy\ cm}{rad}$	4.65×10^5 $\frac{dy\ cm}{rad}$
W_n	38 rad/sec	42 rad/sec
n_n	6.05 cps	6.7 cps
(DR)	.857	1.08

The gyros were mounted in a dustproof container and secured in the airplane on an adjustable mount which allowed aligning the gyros with the horizontal. Since the B-25 trims at 175 mph in a nose high attitude with its horizontal reference line 3.6° above the horizontal, the gyro container must be tilted accordingly. The adjustable mount is shown in Fig. B-14, and the gyro container in position on the mount is shown in Fig. B-15. The gyro container utilized three thermostatically controlled heaters to maintain a fixed ambient temperature for the gyros.

Figure B-16 shows the amplifier panel. Four channels of amplification were used to amplify the pick-off voltages representing total aileron deflection, rudder deflection, angular velocity in yaw, and angular velocity in roll. Each amplifier channel performed three functions (1) amplified the AC pick-off signal, (2) demodulated the AC signal, and (3) amplified the resulting DC signal. The output of each amplifier channel is controlled by 12 attenuation

settings in order to adjust oscillograph current to give the desired oscillograph displacement.

The oscillograph used is shown in Fig. B-17. It is a 12-channel Consolidated Recording Oscillograph. The dynamics of the oscillograph galvanometer units have a negligible distortion effect in reproducing the inputs introduced by the amplifier outputs. The natural frequency of the units used is 120 cps and the DR is 0.7 approx.

The stiffness current regulator shown mounted in position in Fig. B-16 is a closed-loop feedback regulator functioning to hold the stiffness current at a set current within 1 percent variation. Figures B-15 and B-17 show the exposed regulator chassis, the chassis having been removed from its case.

To integrate the added instrumentation with the instrumentation previously existing in the aircraft, an additional junction box was installed. It's location is noted in Fig. B-17.

The three-phase, 400-cycle thyratron controlled inverter initially installed was found to give unsatisfactory regulation for the needs of this project. Consequently, it was replaced by a USAF PU-16 single-phase inverter, which was found to give satisfactory regulation. This change necessitated use of a phase splitter and stepdown transformer to obtain the 3 phase, 28v gyro wheel supply. A block diagram of the overall instrumentation system is shown in Figure B-26.

As shown in Fig. B-26 the output of each pickoff was loaded with a 1000-ohm resistance to reduce the noise level and the null voltage. A variable resistance and a variable inductance were placed in series with the pickoff excitation coils (P.O. coils in series). The resistance was used to set the desired excitation current, and the inductance was used to bring the pickoff outputs into proper phase.

B. CALIBRATION

The objective of the measuring system calibration for this project was to establish overall sensitivities, expressing inputs to the measuring instruments in terms of output linear displacements at the oscillographs. The sensitivities are expressed in such a manner that multiplication of any displacement on the oscillograph record by the appropriate sensitivity yields the measured quantity in the desired units. These sensitivities are:

$S_{(ail)(X_{osc}\ \delta_a)}$ deg/in

$S_{(rud)(X_{osc}\ \delta_r)}$ deg/in

$S_{(roll\ gyro)(X_{osc}\ W_X)}$ $\frac{deg/sec}{in}$

$S_{(yaw\ gyro)(X_{osc}\ W_Z)}$ $\frac{deg/sec}{in}$

For purposes of simplicity and system flexibility, the overall sensitivities listed above were broken into two component sensitivities, one representing the instrument sensitivity and one representing the indicating system sensitivity. The instrument sensitivity is a fixed quantity determined in the case of the control surface rotations by the linkage sensitivities and the signal generator excitation current, and in the case of the rate gyros by the elastic restraint current and the signal generator excitation current.

The indicating system sensitivity may be varied at will by changing the attenuation setting at the amplifier. The amplifier sensitivity allows the desired size of recorded input pulses and output angular velocities to be selected. Selection of the proper size of recorded displacements is governed on one hand by the linearity limits of the oscillograph trace and on the other hand by the size record required for ease of analysis.

In order to obviate the necessity for calibration of each amplifier at

each attenuation setting, a ''master'' pickoff and a calibration voltage source, the latter providing 12 voltage stops, were employed. The master pickoff was calibrated (Figure B-18) to determine the limits of linearity. The sensitivity determined was $S_{(mpo)(A_{mpo}\ e_{mpo})} = 4\ \frac{m\ volts}{division}$, with 300 master -p.o. divisions as the limit of the linearity range. The master pickoff was then used to ''buck-out'' or neutralize the voltage produced by the instrument pickoffs. Thus, instrument sensitivities were obtained both in terms of voltage output for input rotation or angular velocity and in terms of master pickoff output angle for input rotation or angular velocity.

The master pickoff is shown in Fig. B-19. The master pickoff could be plugged into any of the pickoff outputs by means of bayonet jack receptacles on the amplifier panel. As shown in Fig. B-26, the particular pickoff output could then be switched from the amplifiers to the master pickoff.

The procedure for obtaining the instrument sensitivities was straightforward. For the ailerons, a propeller bubble protractor, measuring to 0.1 degree accuracy was used to measure the angle of both ailerons with respect to the horizontal, and the total aileron differential angle thus obtained. For each measured δ_a, the corresponding voltage was recorded. This voltage was then nulled by the MPO and the corresponding angle of the MPO recorded. The voltage representing total aileron angle was achieved by adding the voltages of the two aileron pickoff outputs in series.

For calibration of the rudder deflection to MPO angle, the same system was used as outlined for the ailerons with the exception of the means of measuring rudder deflection. Figure B-20 shows the method employed. The center of rotation of the rudder was determined by means of a plumb bob. A piece of mirror was then attached to the rudder at the center of rotation, and the plumb bob lined up with the center of a sector of a circle, the latter being graduated in mils. Measurements were then read by means of a

telescope equipped with a hair line.

Figure B-21 shows the set-up used to calibrate the gyros. On a small turntable, having a selection of 4 speeds, an inclined plate was mounted to receive the gyro container. The can was so aligned that the spin axis of the roll rate gyro was rotated a measured angle about the gimbal axis. With the two gyros properly aligned within the can, this also rotated the input axis of the yaw gyro about its spin axis by the same measured angle. As a consequence, the input to each gyro was calculated in the following manner:

Roll gyro $\quad W_X = W_{TT} \sin \theta$

Yaw gyro $\quad W_Z = W_{TT} \cos \theta$

where W_{TT} is the angular velocity of the turntable, and θ is the measured angle of tilt.

The calibration curves for all four measuring instruments showing the measured quantity vs MPO divisions (each div. = approx. 2 mils) and, for the gyros, the measured quantity vs pickoff output voltage are shown in Figs. B-22 through B-25.

The instrument sensitivities thus determined are

[aileron] $S_{(ail)(e_o\ \delta_a)}\ S_{(MPO)(A_{MPO}\ e_o)} = S_{(ail)(M)(A_{MPO}\ \delta_a)} = 0.0281 \frac{deg}{div}$

[rudder] $S_{(rud)(e_o\ \delta_r)}\ S_{(MPO)(A_{MPO}\ e_o)} = S_{(rud)(M)(A_{MPO}\ \delta_r)} = 0.00846 \frac{deg}{div}$

[roll gyro] $S_{(rg)(e_o\ W_X)}\ S_{(MPO)(A_{MPO}\ e_o)} = S_{(rg)(M)(A_{MPO}\ W_X)} = 0.994 \frac{mils/sec}{div\ MPO}$

[yaw gyro] $S_{(yg)(e_o\ W_Z)}\ S_{(MPO)(A_{MPO}\ e_o)} = S_{(yg)(M)(A_{MPO}\ W_Z)} = 1.228 \frac{mils/sec}{div\ MPO}$

The indicating system sensitivities were determined on each flight whenever data was recorded. The indicating system sensitivity is made up of the amplifier sensitivity, oscillograph sensitivity and master pickoff sensitivity, that is:

$$S_{(\text{ind sys})(X_{osc};\ A_{MPO})} = S_{(MPO)(e\ A_{MPO})}\ S_{(amp)(i,e)}\ S_{(osc)(X_{osc}\ i)}$$

Upon the completion of each series of flight runs the measuring instruments were switched away from the inputs to the amplifiers, and a 12-step voltage source switched onto the amplifier inputs (shown in Fig.B-19). As the voltage was varied through the 12 steps, a record was made on the oscillograph. These same 12 voltage steps were then applied to the master pickoff, the latter instrument being rotated until each calibration voltage was nulled and the corresponding output angle of the master pickoff was recorded. Thus increments of oscillograph displacement corresponding to increments of MPO angle were available for each test flight, and an overall indicating system sensitivity was available without knowledge of the oscillograph and amplifier component sensitivities. That is,

$$S_{(\text{ind sys})(X_{osc}\ A_{MPO})} = \frac{\Delta A_{MPO}}{\Delta X_{osc}}$$

The overall system sensitivity for each measuring channel was thus available by combining instrument and indicating system sensitivities. Therefore, the general expression of the sensitivity is

$$S_{(q\ \text{chan})(X_{osc}\ q)} = S_{(\ )(M)(A_{MPO};\ q)}\ S_{(\ )(\text{ind sys})(X_{osc}\ A_{MPO})}$$

To determine the system errors and uncertainties, static tests were made on the ground. A known value of each quantity to be measured was applied to the respective measuring instruments, and an oscillograph record made of the outputs. The calibration source voltages were then recorded at the same attenuation settings, and a record of master pickoff angles recorded for each calibration voltage. In this manner the overall sensitivity could be compared with the product of the instrument sensitivity and the indicating system sensitivity.

The comparison was found to be:

Measured quantity	$S_{(\ )(total)(\ )}$	$S_{(\ )(ind\ sys)(\ )}$	$S_{(\ )(M)(\ )}$	$S_{(\ )(total)(\ )}$ by components	Average Error (% of aver. sensitivity)
W_X	52.9 $\frac{mils/sec}{in}$	55.0 $\frac{MPO\ div}{in}$	0.993 $\frac{mil/sec}{MPO\ div}$	54.7 $\frac{mil/sec}{in}$	1.7
W_Z	61 $\frac{mils/sec}{in}$	50.0 $\frac{MPO\ div}{in}$	1.228 $\frac{mil/sec}{MPO\ div}$	61.5 $\frac{mil/sec}{in}$	0.4
δ_a	4.155 $\frac{deg}{in}$	148 $\frac{MPO\ div}{in}$	0.0281 $\frac{deg}{MPO\ div}$	4.16 $\frac{deg}{in}$	0.07
δ_r	0.895 $\frac{deg}{in}$	104 $\frac{MPO\ div}{in}$	0.00846 $\frac{deg}{MPO\ div}$	0.880 $\frac{deg}{in}$	0.9

The linearity limits and of the measuring system components are as follows:

Component	Linearity Range
Master P.O.	±300 divs (150 mils)
Aileron Defl.	30° total deflection
Rudder Defl.	±7° rudder deflection
Roll gyro	±0.3 rad/sec
Yaw gyro	±0.35 rad/sec
Oscillograph defl.	±2.7 in (approx.)

The largest source of error in the measuring system lies in the insensitivity of the voltmeter used as an indicator when nulling a voltage with the master p.o. Efforts to reproduce results have produced variations as high as 4 divisions of the MPO, with an average error of 1 to 1 1/2 divisions. This represents an error, or null voltage, of 4 to 6 mv in matching voltages.

A change in the instrumentation was effected just prior to the final test flight (See Flight Record - Appendix D). The gyro container was secured rigidly to the aircraft structure during flight in order to eliminate recording vibrations set up by the gyro container mount and the Lord shock mounts. This modification resulted in removing an undesirable 10 cps transient from the records which occurred whenever the aircraft was responding to input pulses. This change made it possible to make the shock mounts ineffective during flight, and yet to free them when desired in order to protect the gyros from landing shock.

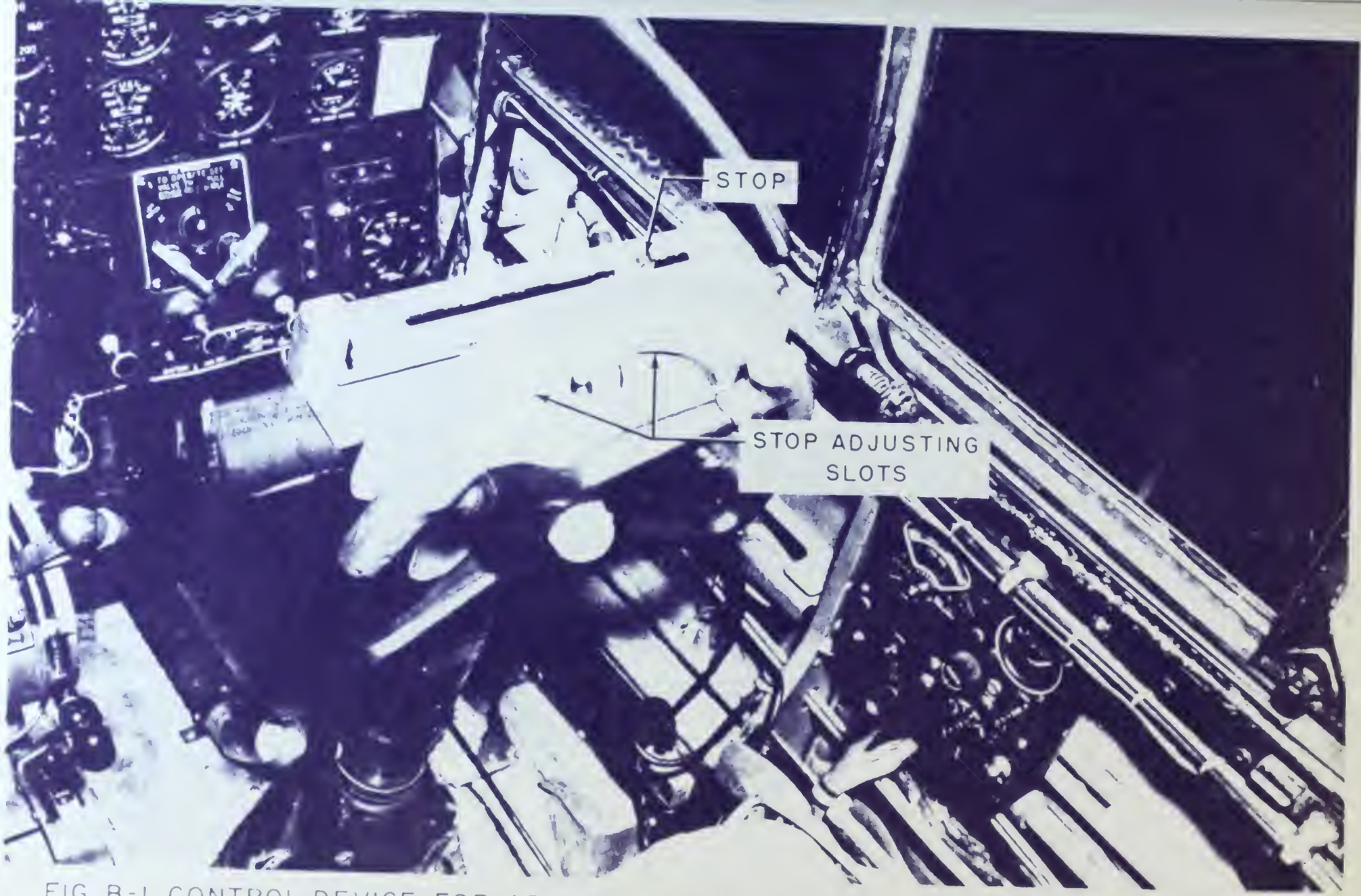

FIG B-1 CONTROL DEVICE FOR APPLYING AILERON PULSE - VIEW LOOKING FORWARD PILOT'S COMPARTMENT

FIG. 8 CONTROL DEVICE FOR APPLYING AILERON PULSE - VIEW LOOKING AFT INTO PILOTS COMPARTMENT

FIG B-3 CONTROL DEVICE FOR APPLYING AILERON PULSE - RIGHT SIDE VIEW

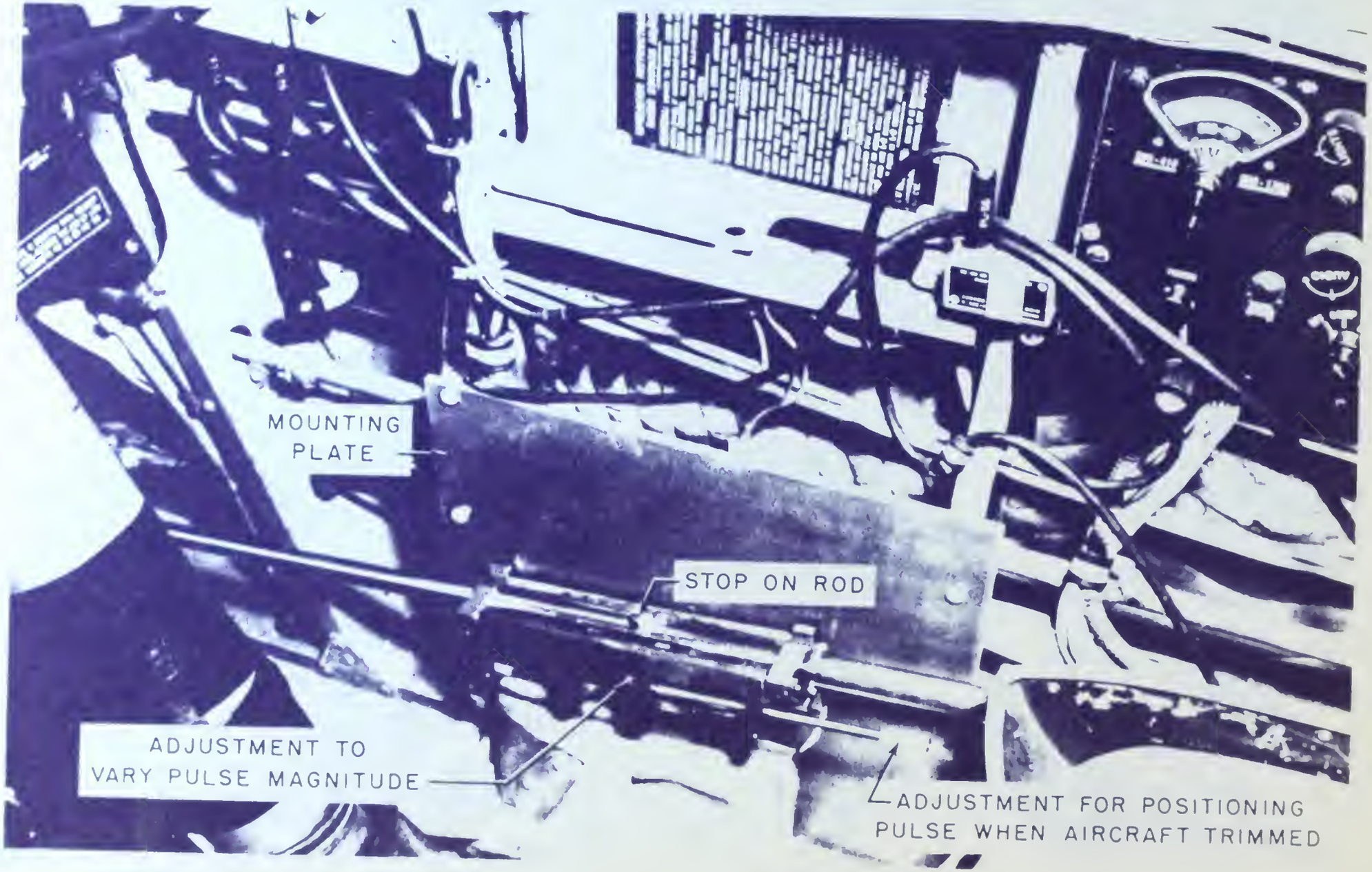

FIG B-4 CONTROL DEVICE FOR APPLYING RUDDER PULSE - SIDE VIEW

FIG B-5 CONTROL DEVICE FOR APPLYING RUDDER PULSE - TOP VIEW

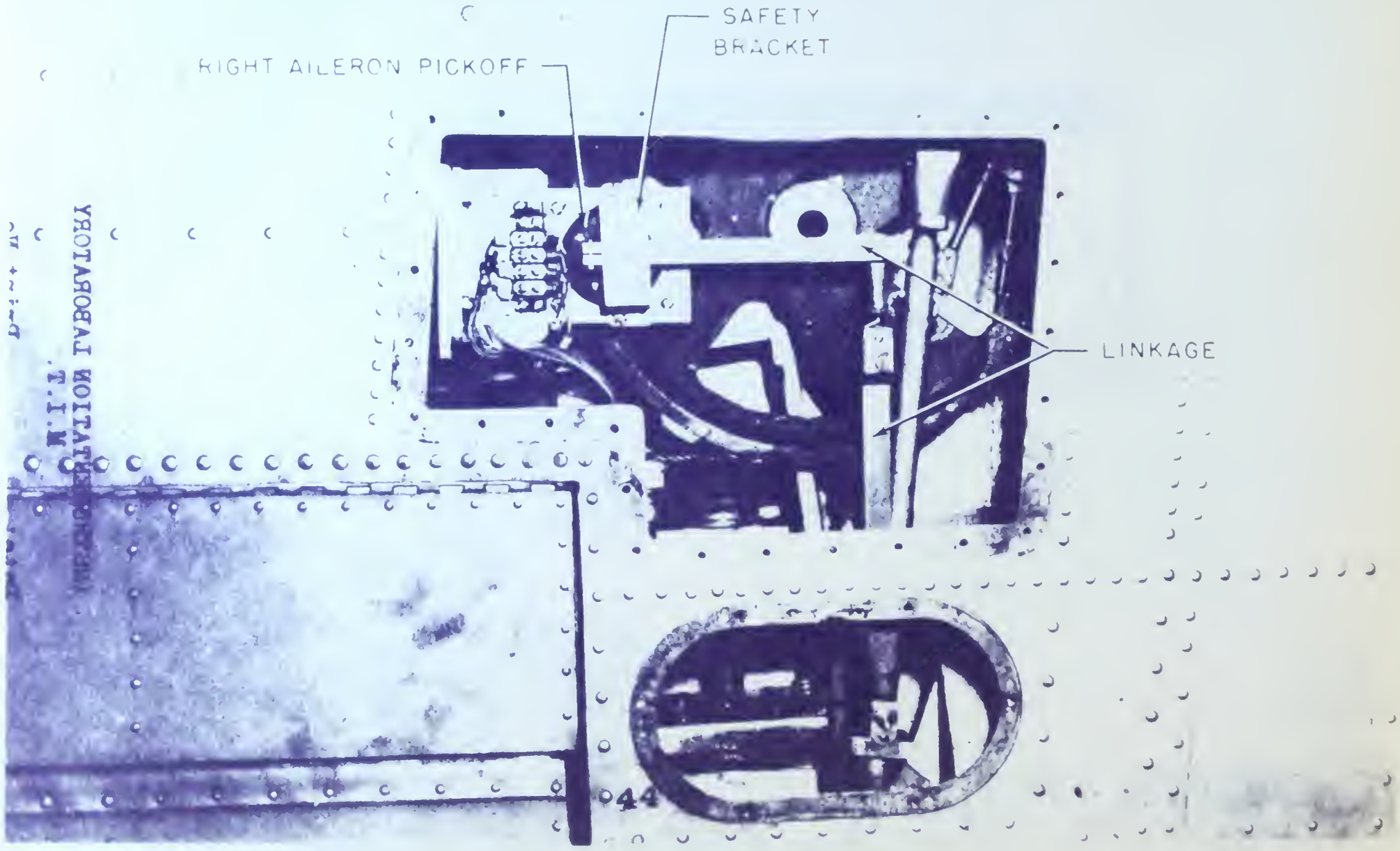

RIGHT WING VIEWED FROM BELOW

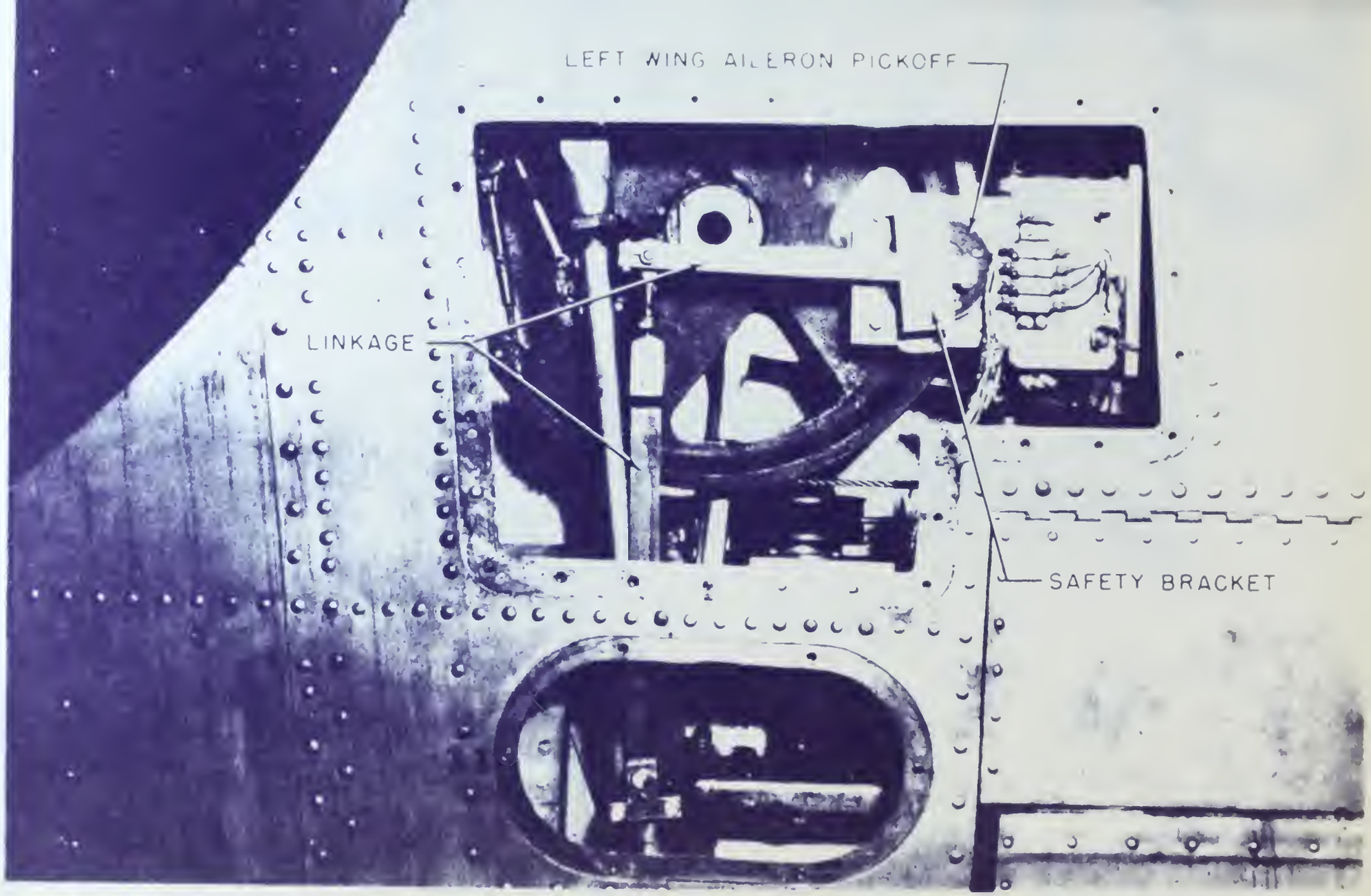

FIG B-7 AILERON PICKOFF INSTALLATION, LEFT WING - VIEWED FROM BELOW

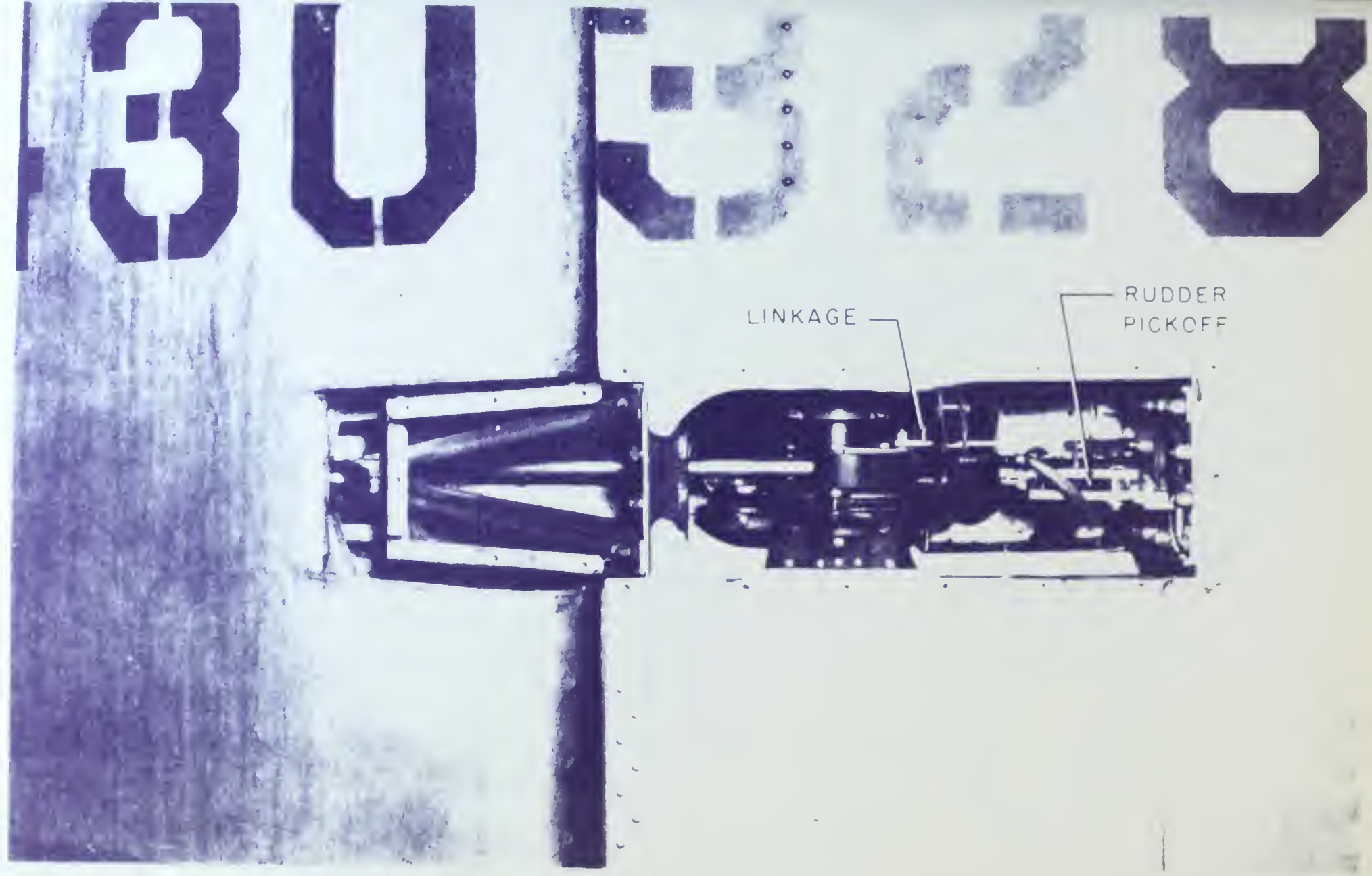

RUDDER PICKOFF INSTALLATION, RIGHT RUDDER VIEWED FROM

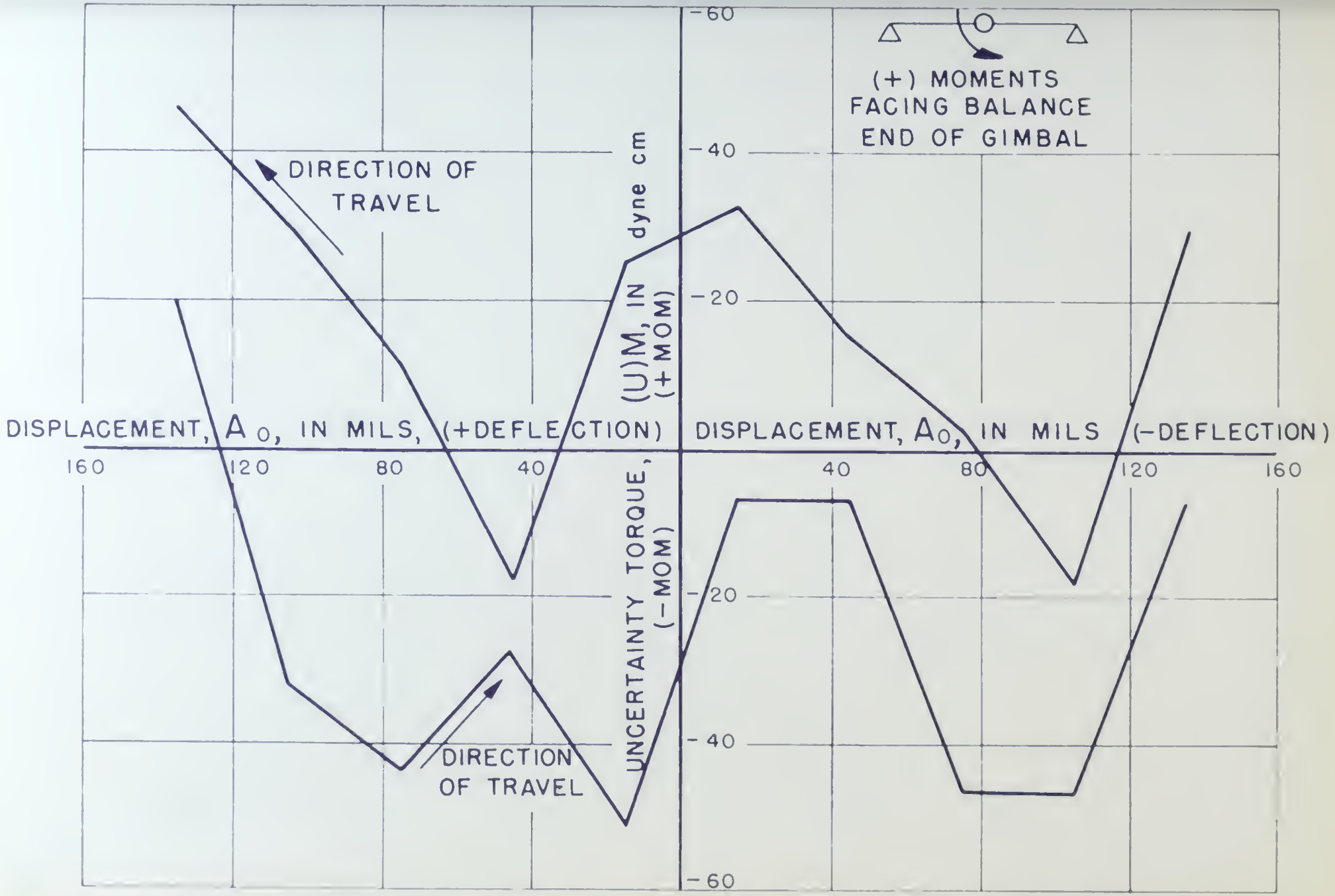

FIG.B-9 UNCERTAINTY MOMENT VS COMPUTER SHAFT ROTATION FOR ROLL RATE GYRO.

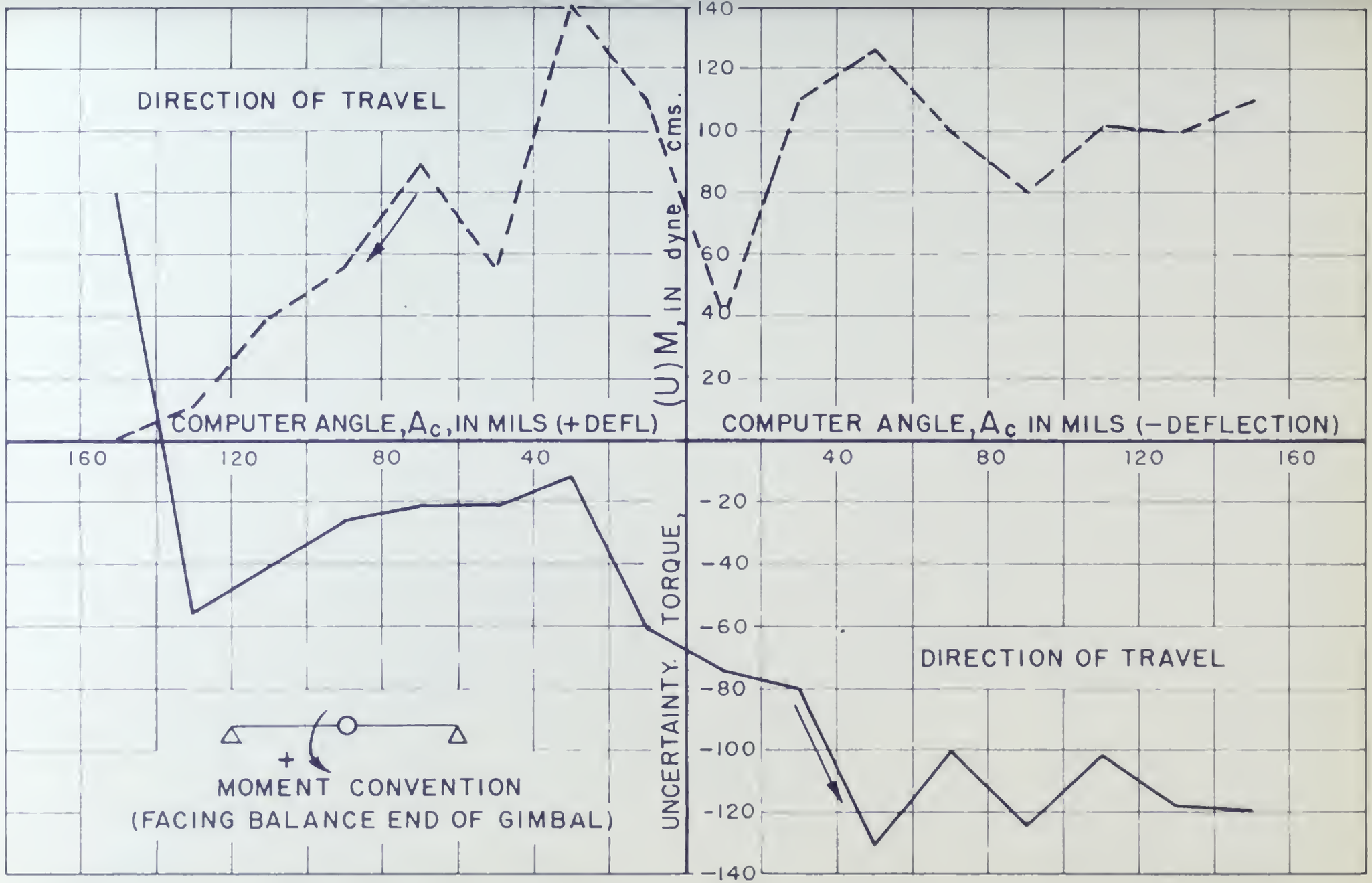

FIG. B-10. UNCERTAINTY MOMENT VERSUS COMPUTER SHAFT DEFLECTION FOR YAW GYRO

FIG. B-11
ROLL RATE GYRO
ELASTIC RESTRAINT CALIBRATION

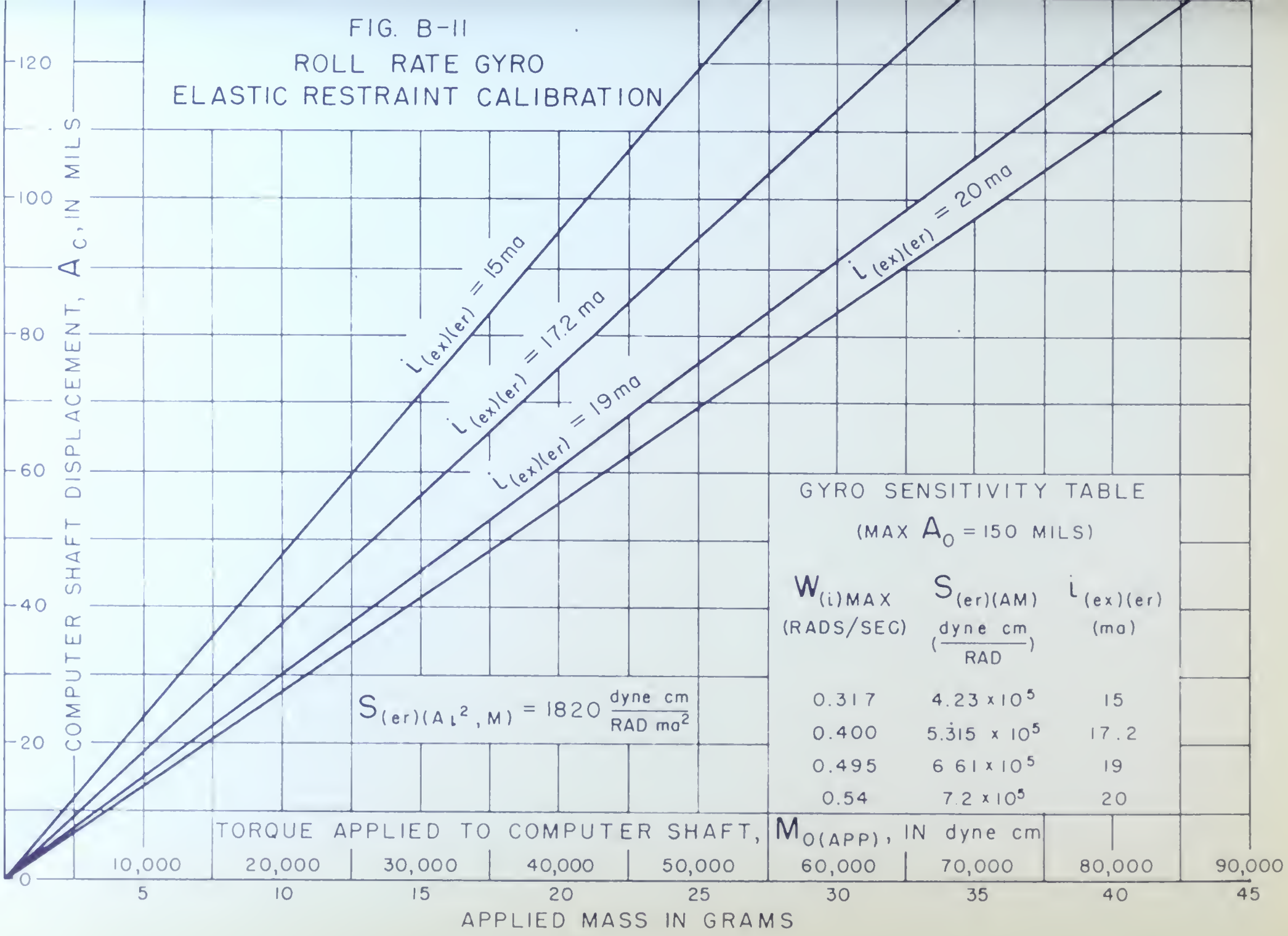

GYRO SENSITIVITY TABLE

(MAX A_O = 150 MILS)

$W_{(i)MAX}$ (RADS/SEC)	$S_{(er)(AM)}$ $(\frac{\text{dyne cm}}{\text{RAD}})$	$i_{(ex)(er)}$ (ma)
0.317	4.23×10^5	15
0.400	5.315×10^5	17.2
0.495	6.61×10^5	19
0.54	7.2×10^5	20

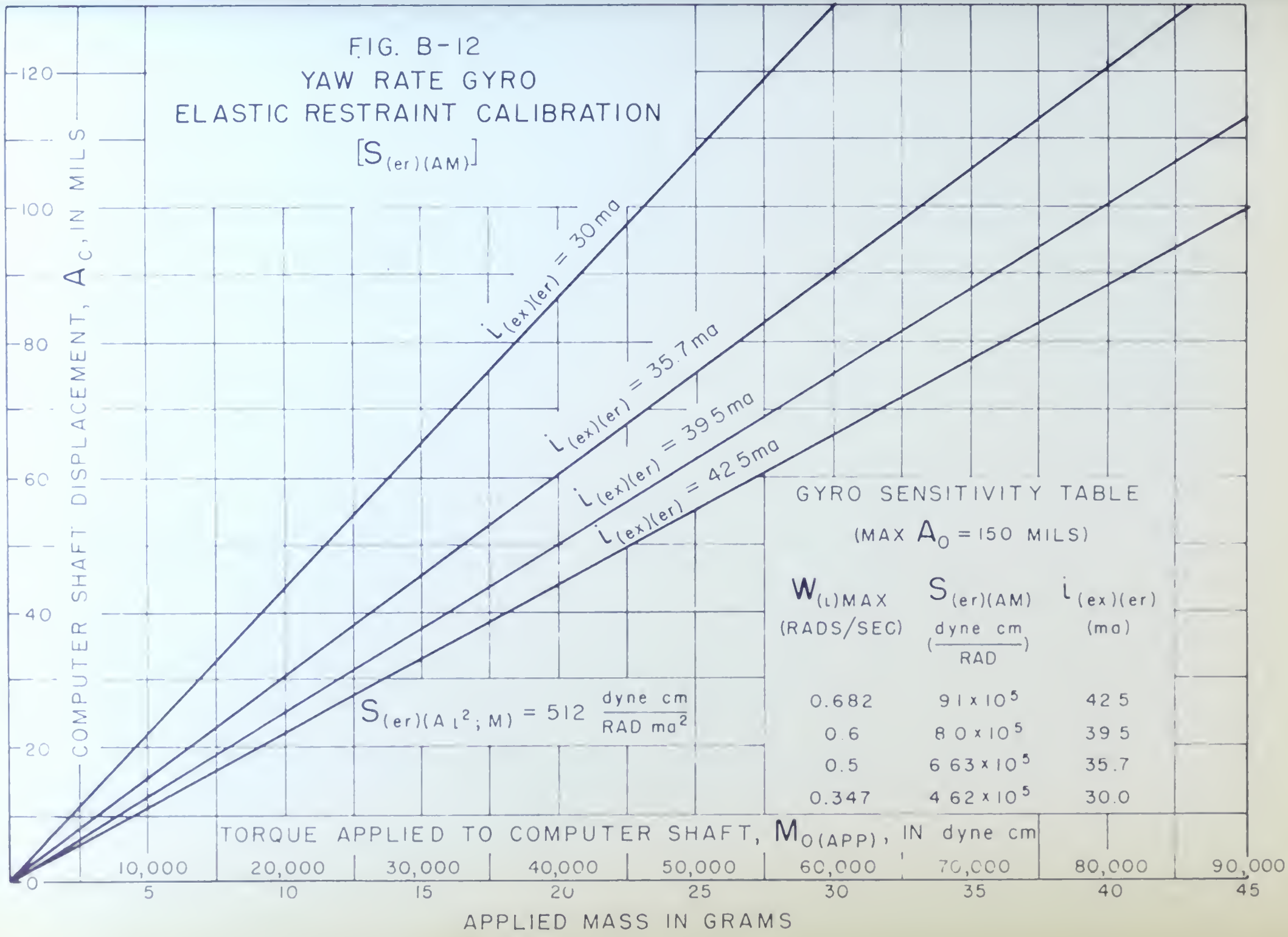
FIG. B-12
YAW RATE GYRO
ELASTIC RESTRAINT CALIBRATION
[S(er)(AM)]
COMPUTER SHAFT DISPLACEMENT, Ac, IN MILS
120
100
80
60
40
20
0
i(ex)(er) = 30ma
i(ex)(er) = 35.7ma
i(ex)(er) = 39.5ma
i(ex)(er) = 42.5ma
GYRO SENSITIVITY TABLE
(MAX A0 = 150 MILS)
W(L)MAX (RADS/SEC) | S(er)(AM) (dyne cm / RAD) | i(ex)(er) (ma)
0.682 | 9.1 x 10^5 | 42.5
0.6 | 8.0 x 10^5 | 39.5
0.5 | 6.63 x 10^5 | 35.7
0.347 | 4.62 x 10^5 | 30.0
S(er)(A L^2; M) = 512 dyne cm / RAD ma^2
TORQUE APPLIED TO COMPUTER SHAFT, M0(APP), IN dyne cm
10,000
20,000
30,000
40,000
50,000
60,000
70,000
80,000
90,000
0
5
10
15
20
25
30
35
40
45
APPLIED MASS IN GRAMS

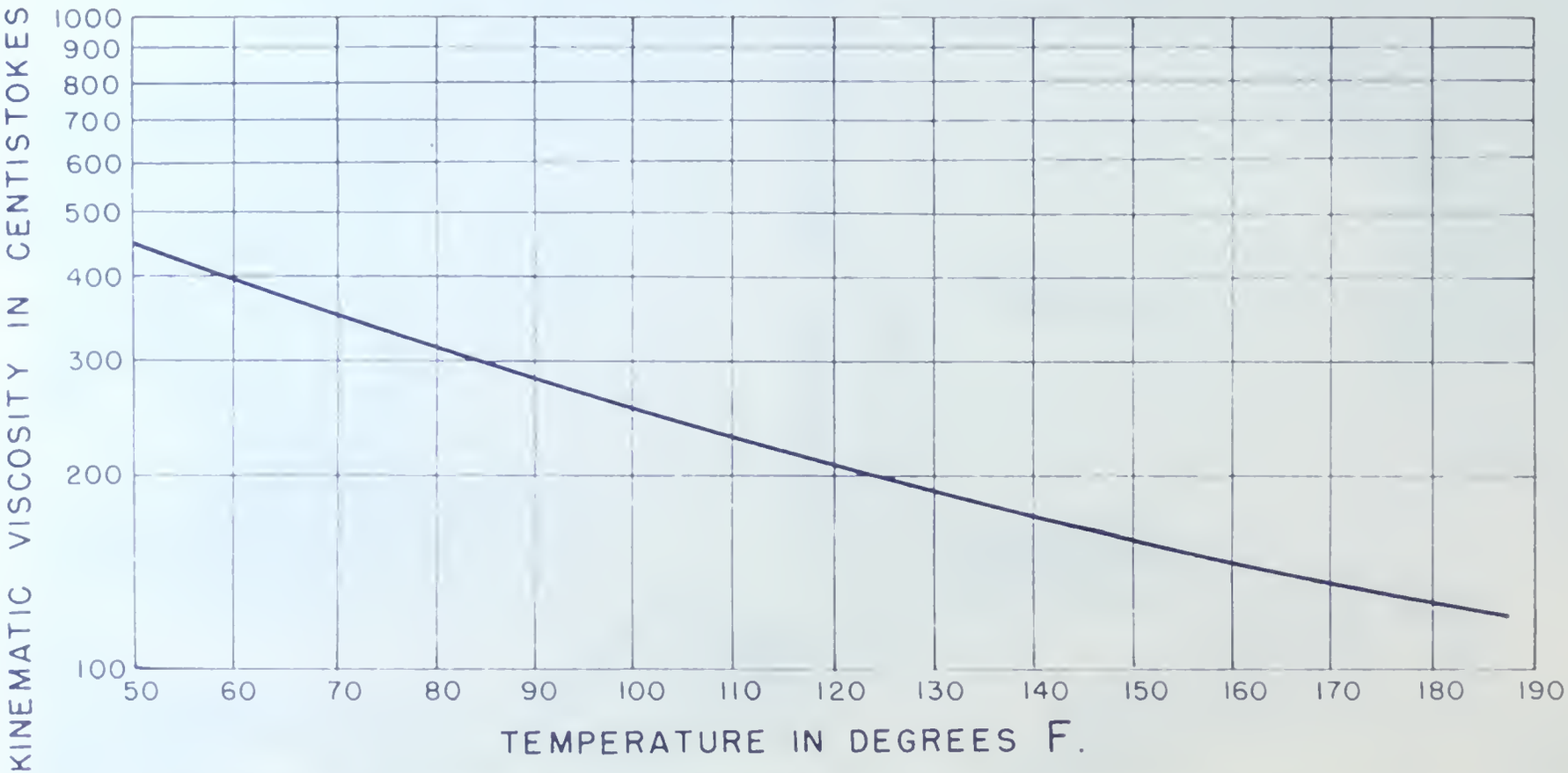

FIG. B-13 TEMP.- VISC. CURVE FOR DOW CORNING DAMPING FLUID NO. 350 DCC.

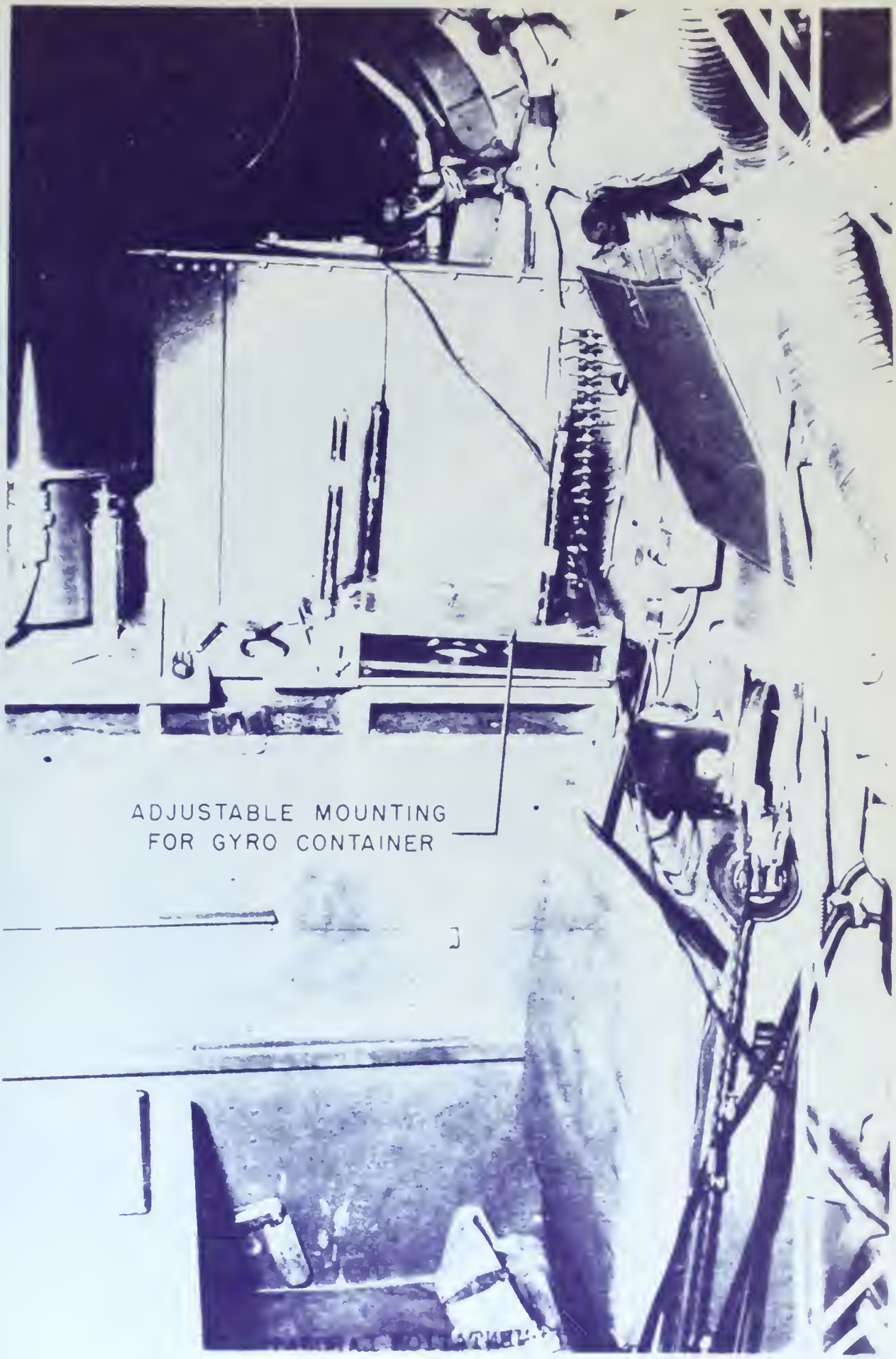

FIG B-14 ADJUSTABLE MOUNT FOR GYRO CONTAINER - VIEW LOOKING FORWARD

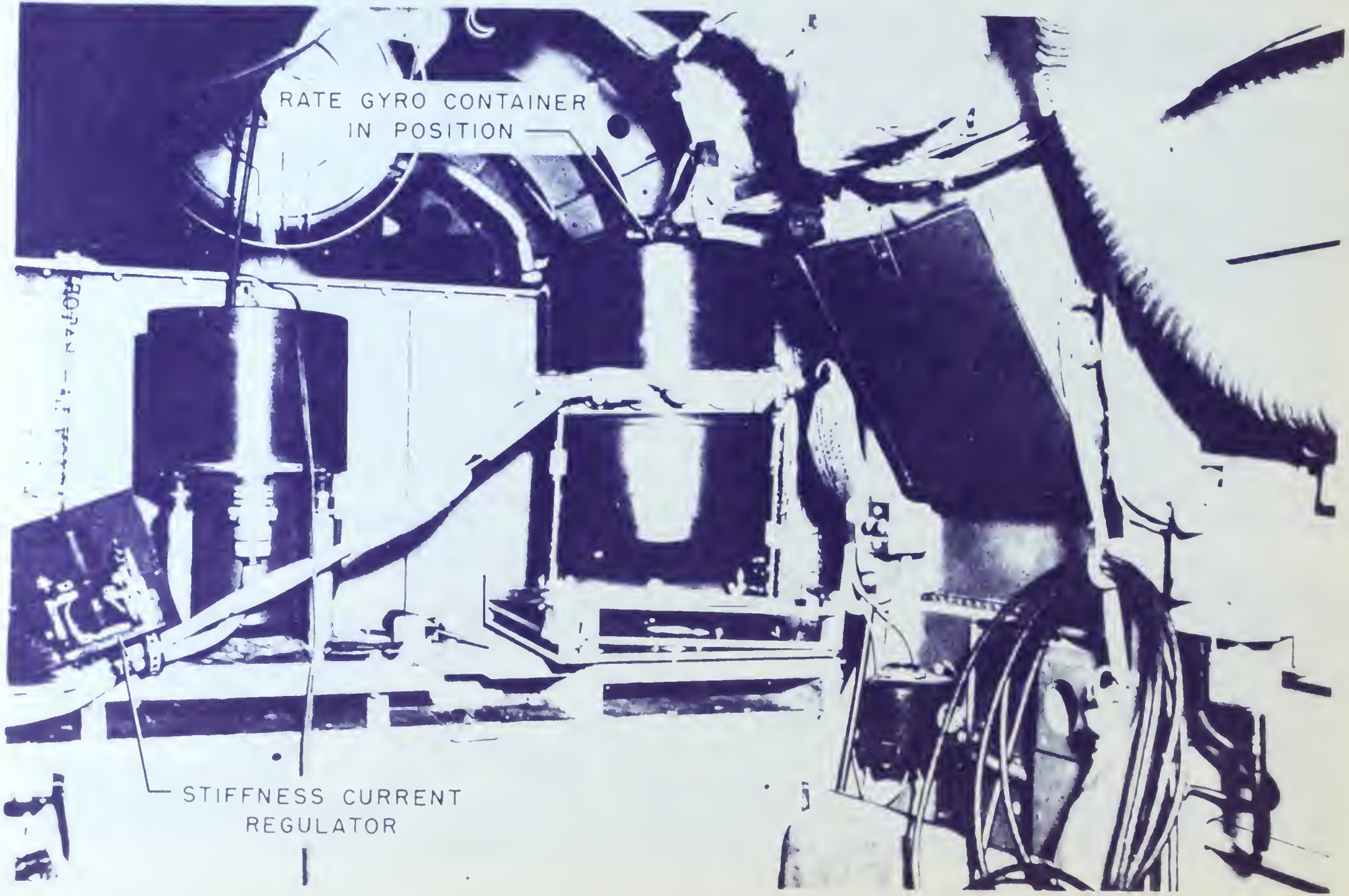

FIG B-15 LOCATION OF GYROS - LOOKING FORWARD IN AFTER COMPARTMENT

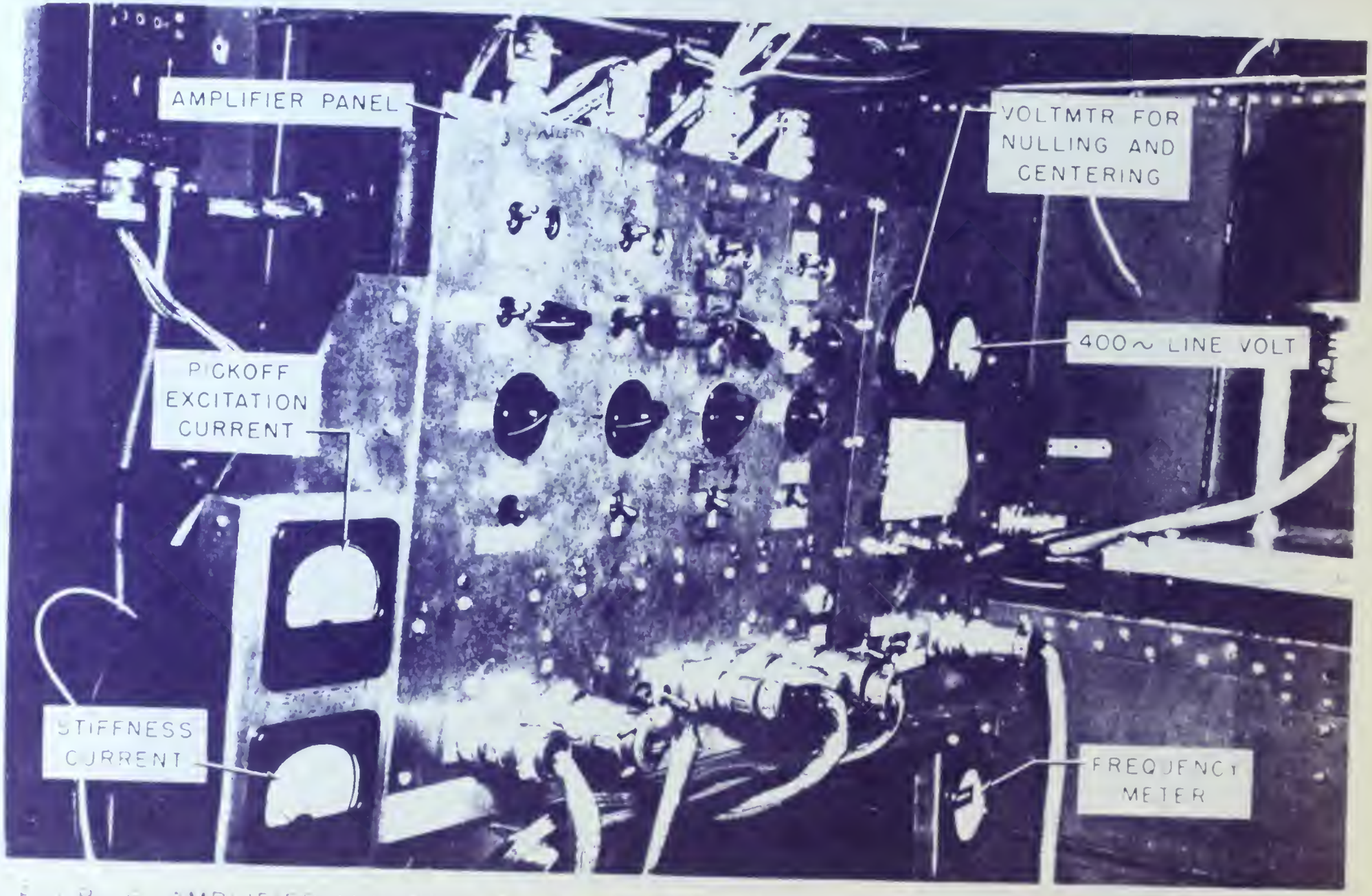

FIG 5 AMPLIFIER AND CONTROL PANEL - BRIDGE VIEW LOOKING FORWARD AND LEFT

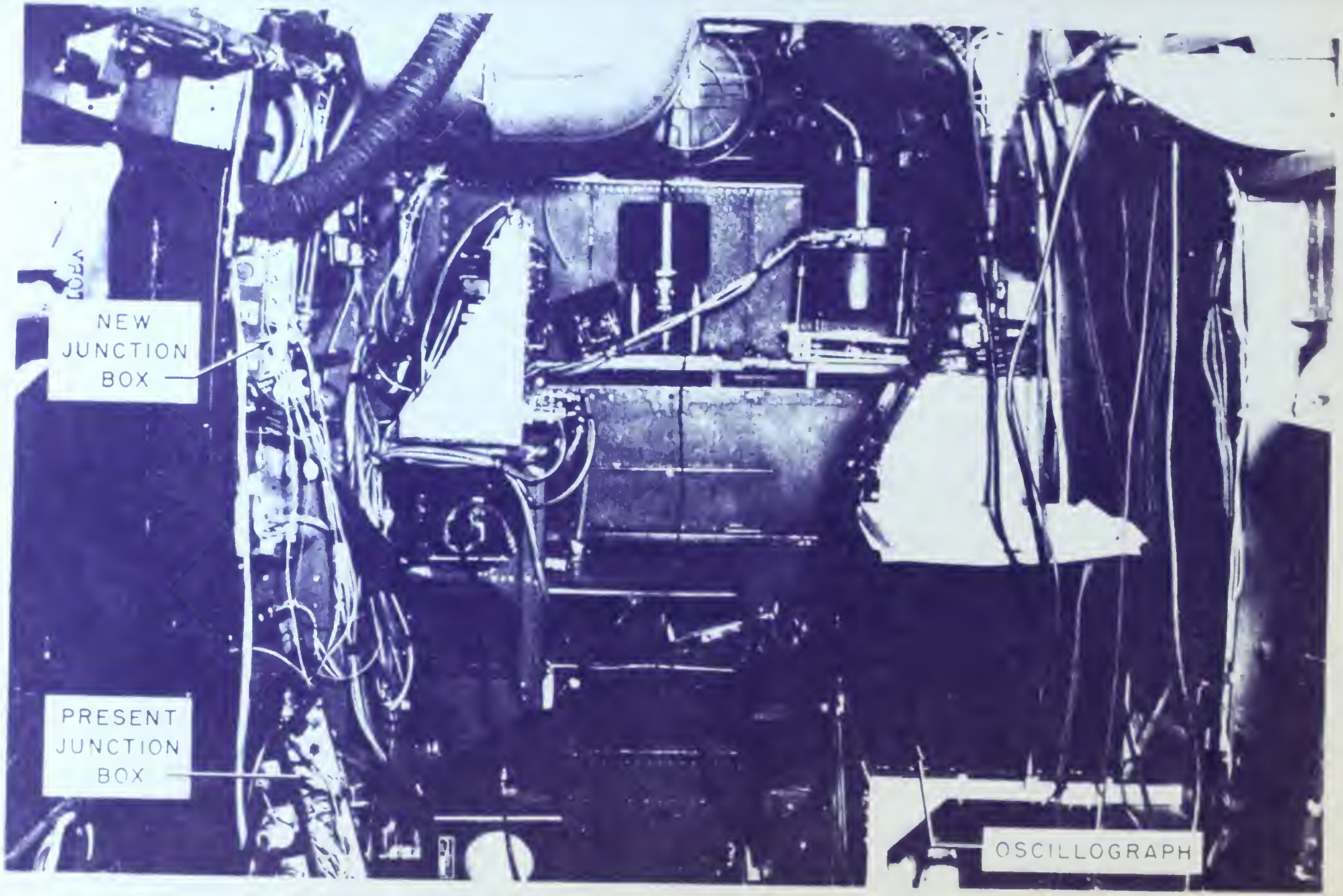

FIG. 5.12 INSTRUMENTATION IN AFTER COMPARTMENT - LOOKING FORWARD

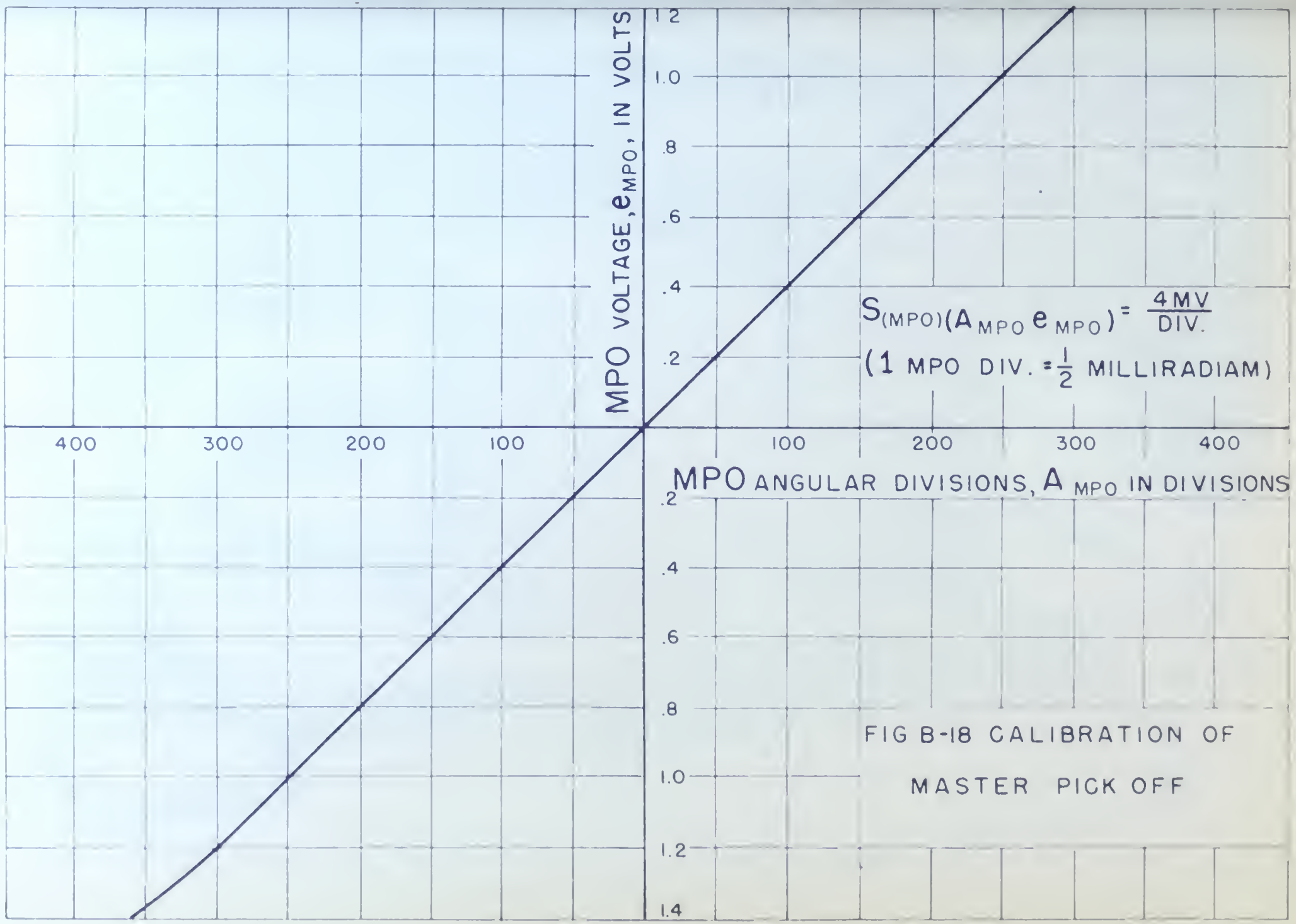

FIG B-18 CALIBRATION OF MASTER PICK OFF

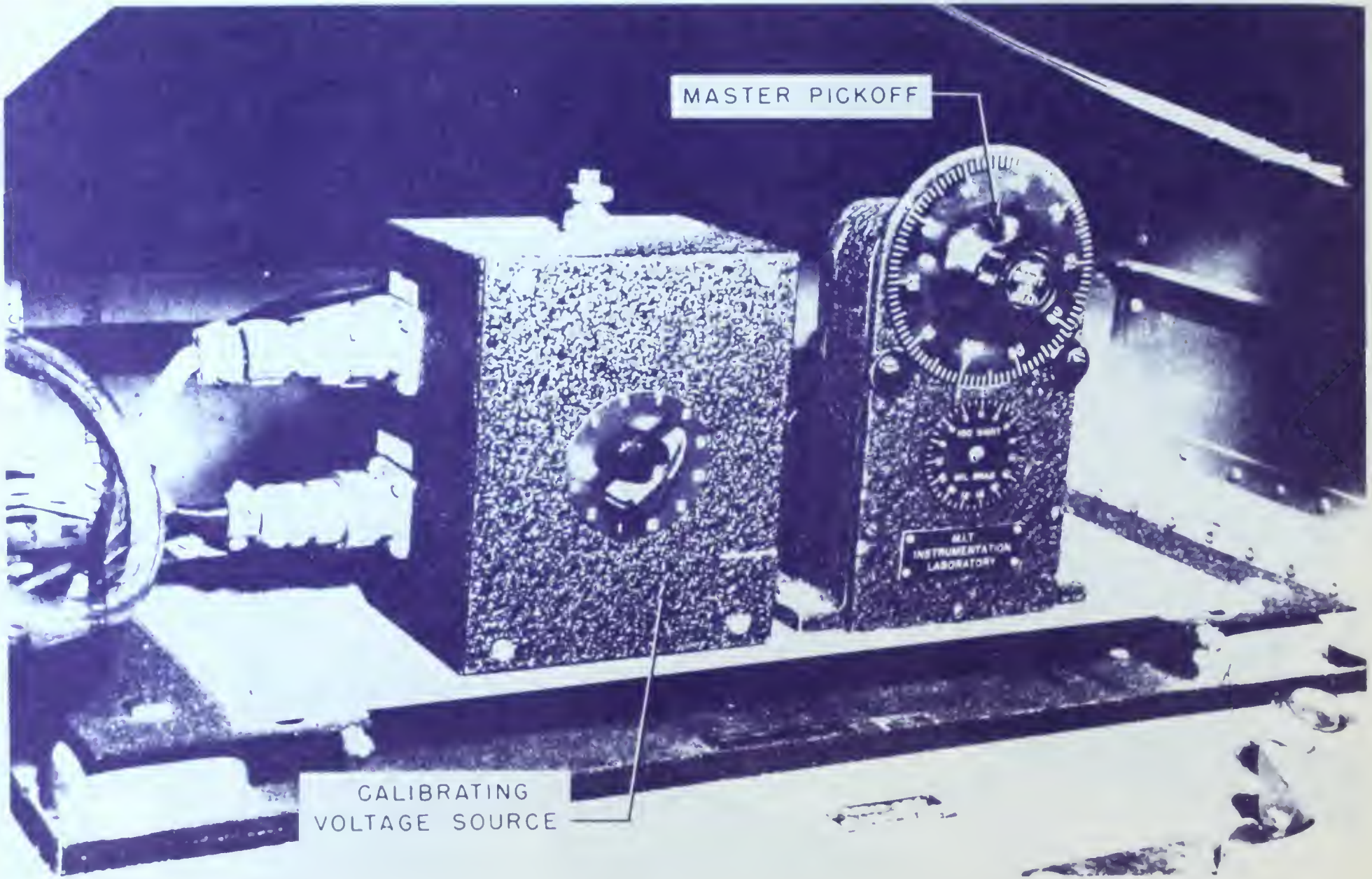

FIG B-19 MASTER PICKOFF AND CALIBRATING VOLTAGE SOURCE - LOCATED BELOW AMPLIFIER PANEL

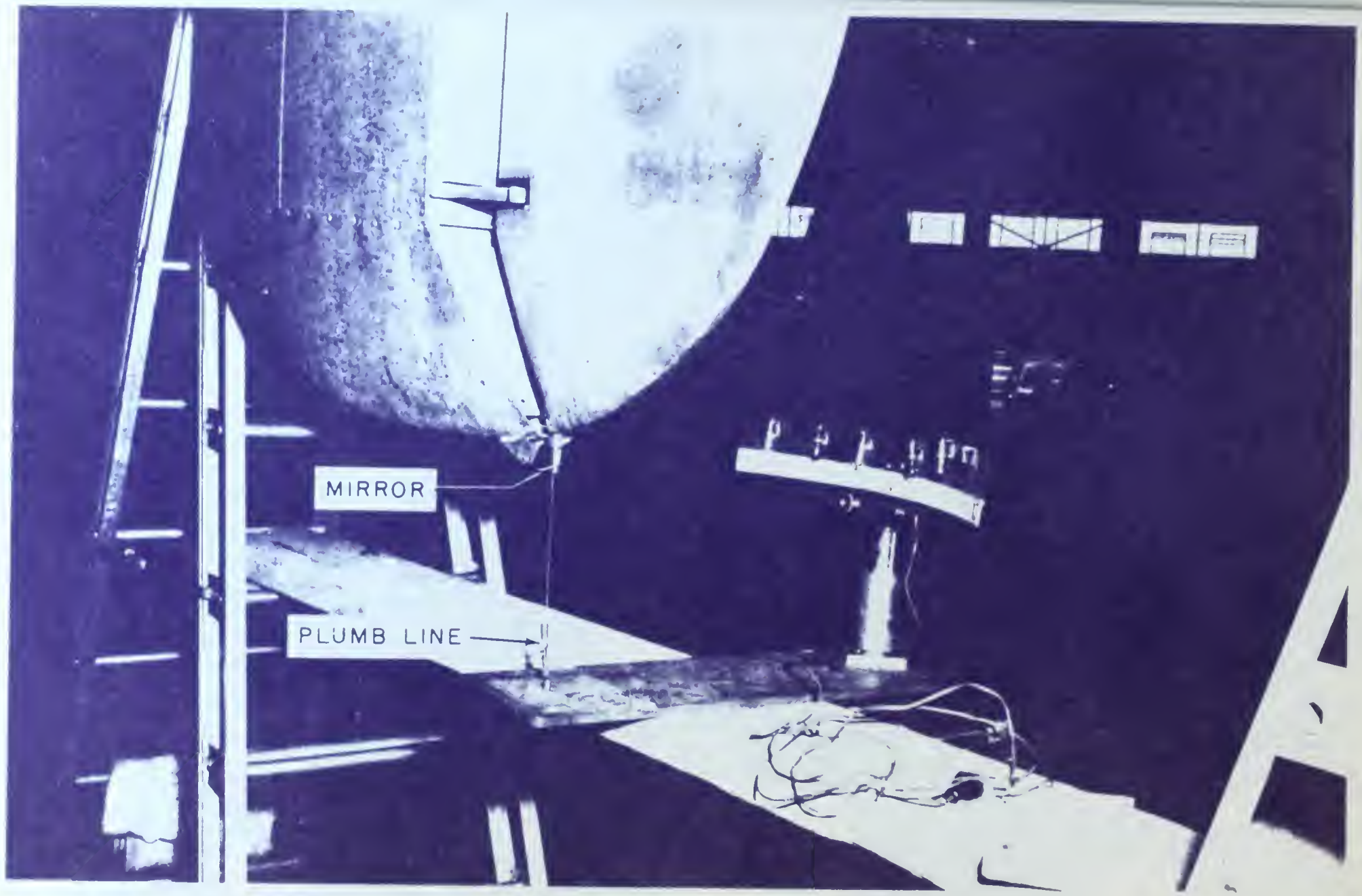

FIG B-20 RUDDER CALIBRATION SETUP

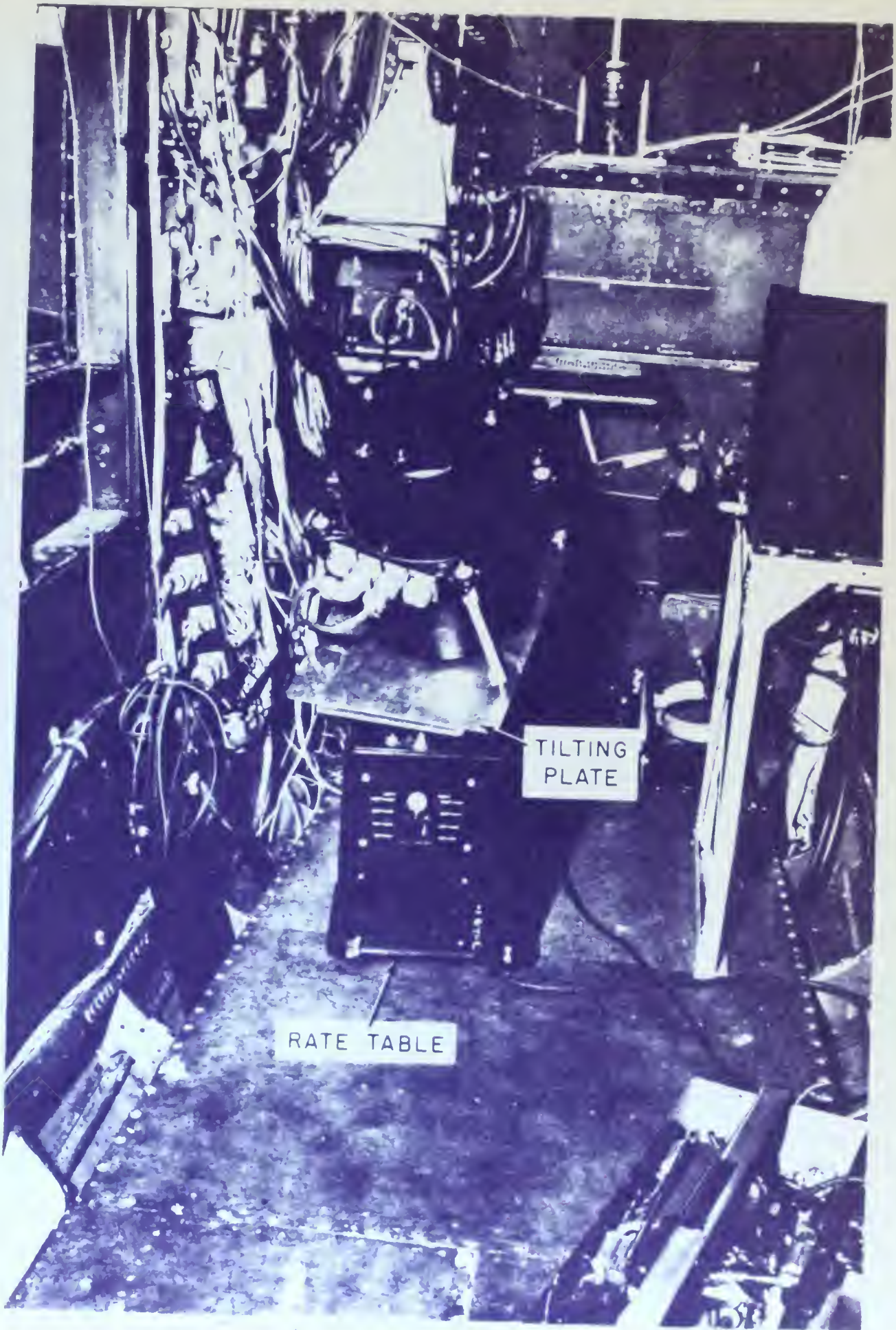

FIG B-21 SETUP USED FOR GYRO STATIC CALIBRATION

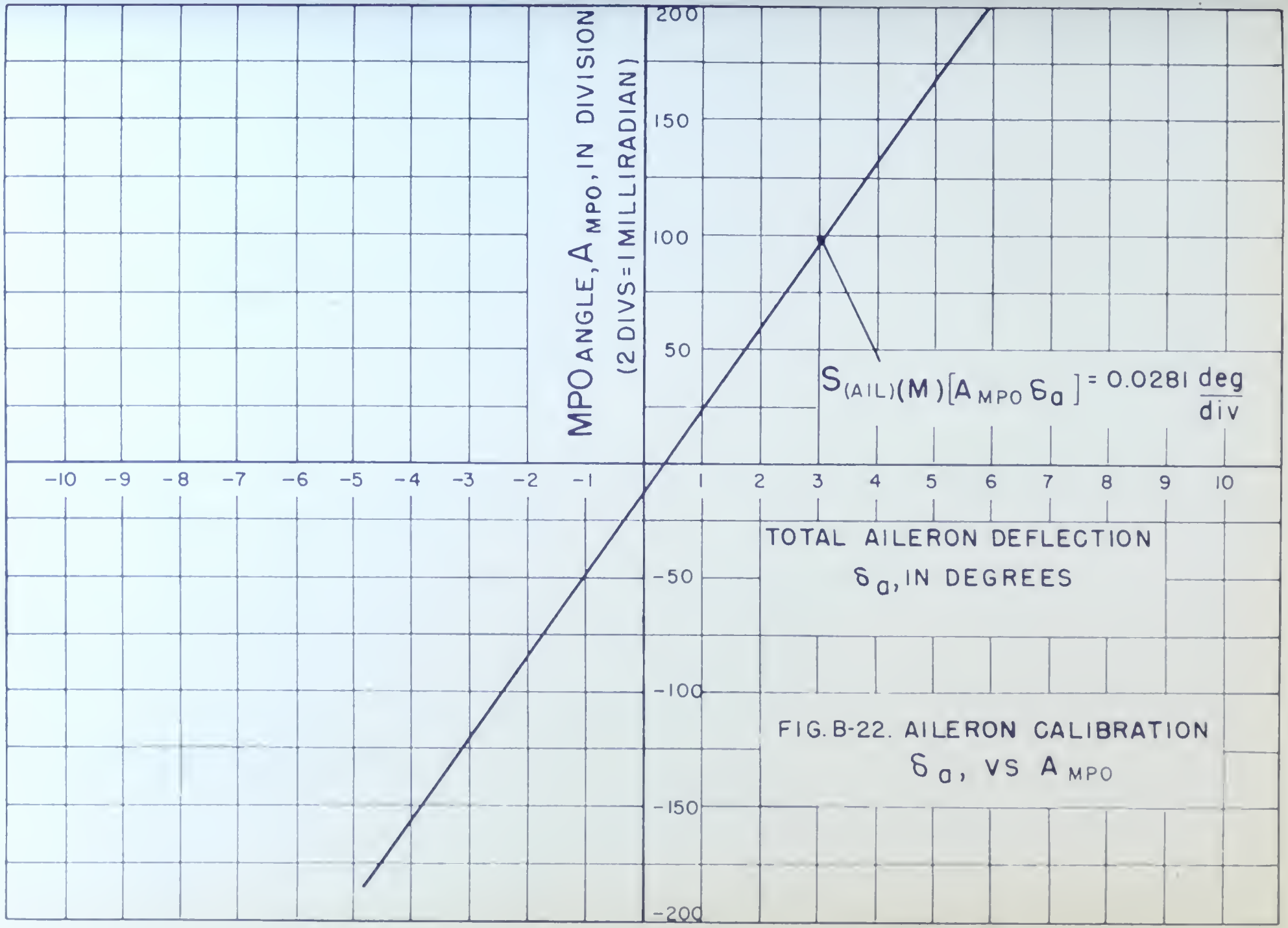

FIG. B-22. AILERON CALIBRATION
δ_a, VS A_{MPO}

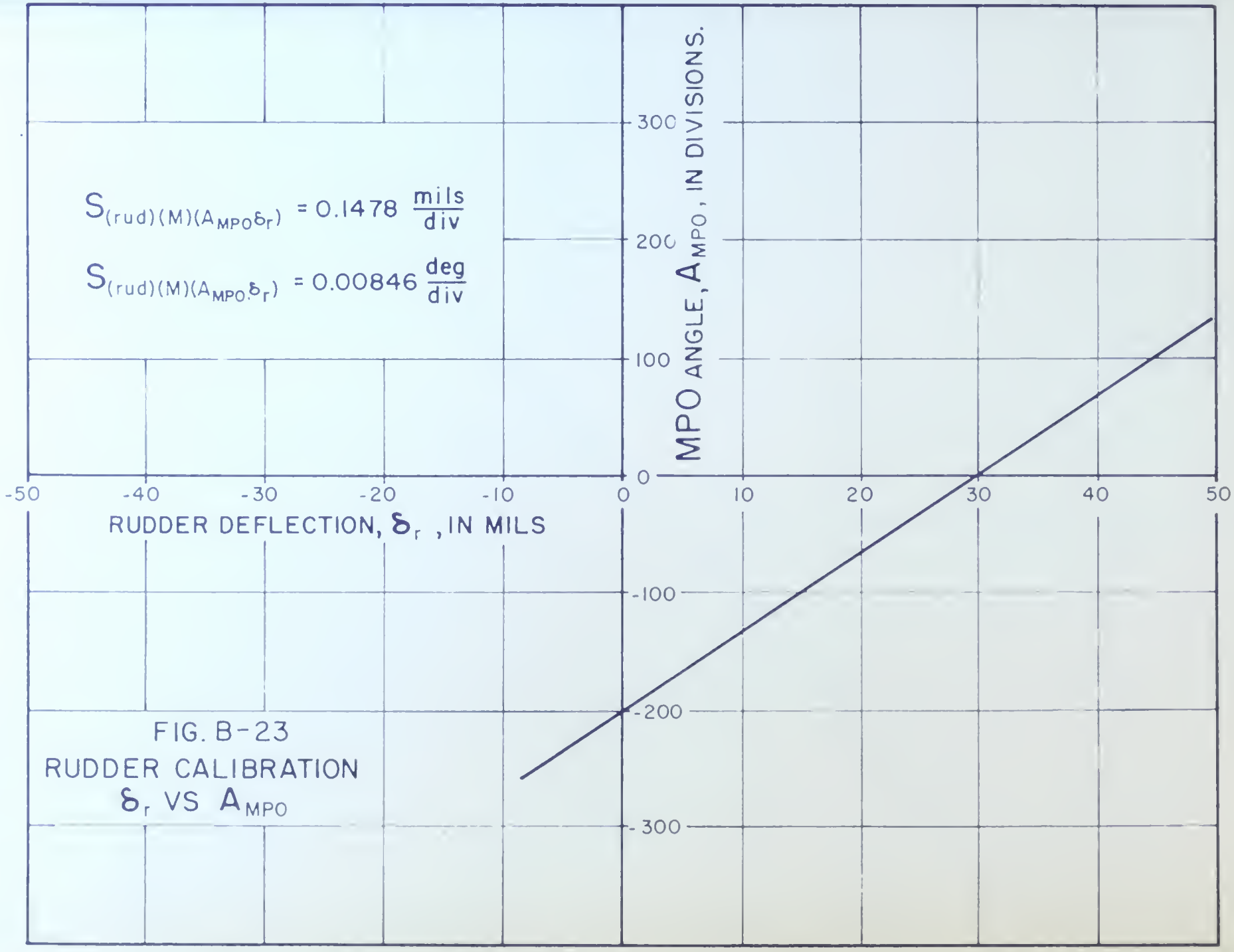

FIG. B-23
RUDDER CALIBRATION
δ_r VS A_{MPO}

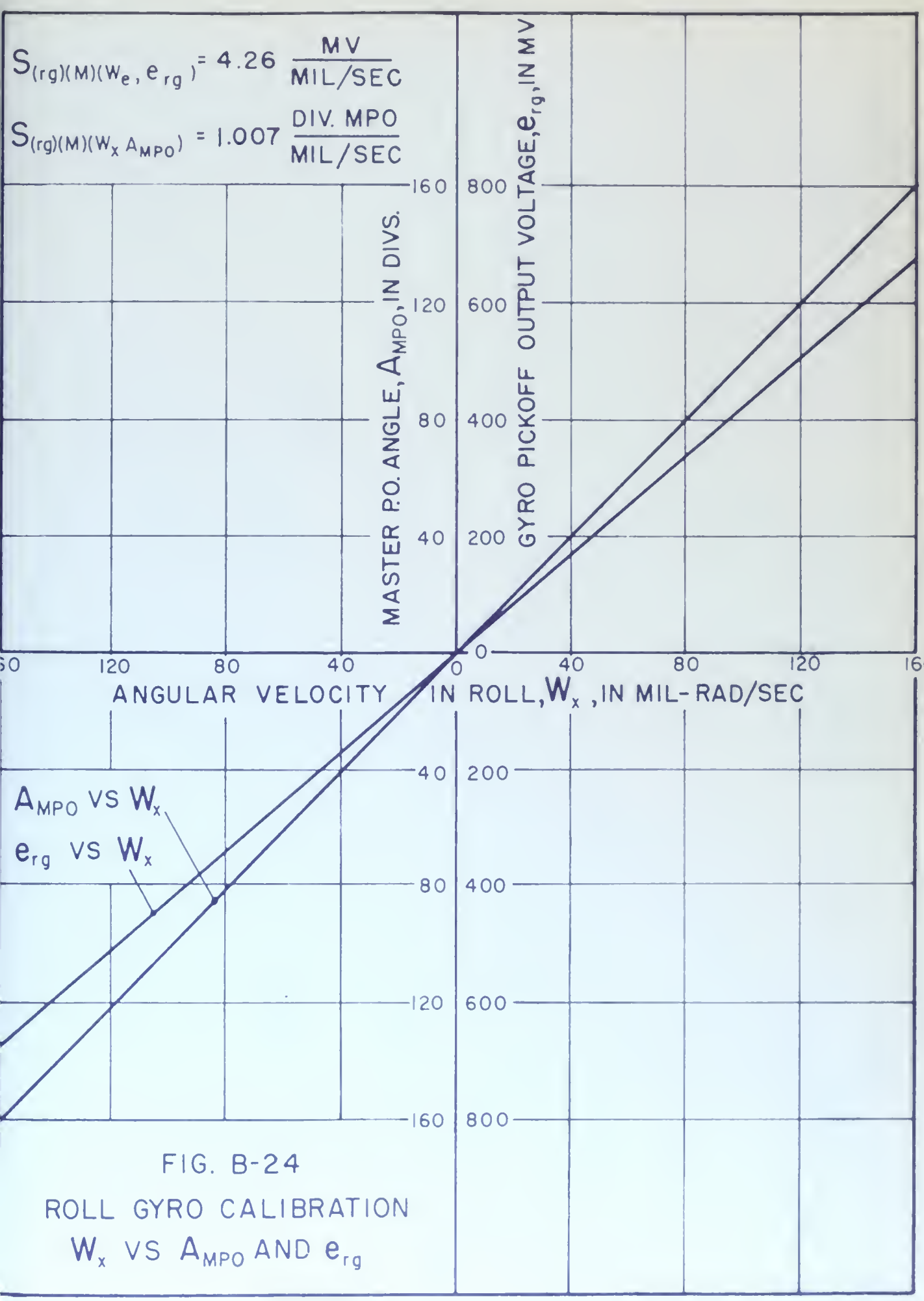

FIG. B-24

ROLL GYRO CALIBRATION

W_x VS A_{MPO} AND e_{rg}

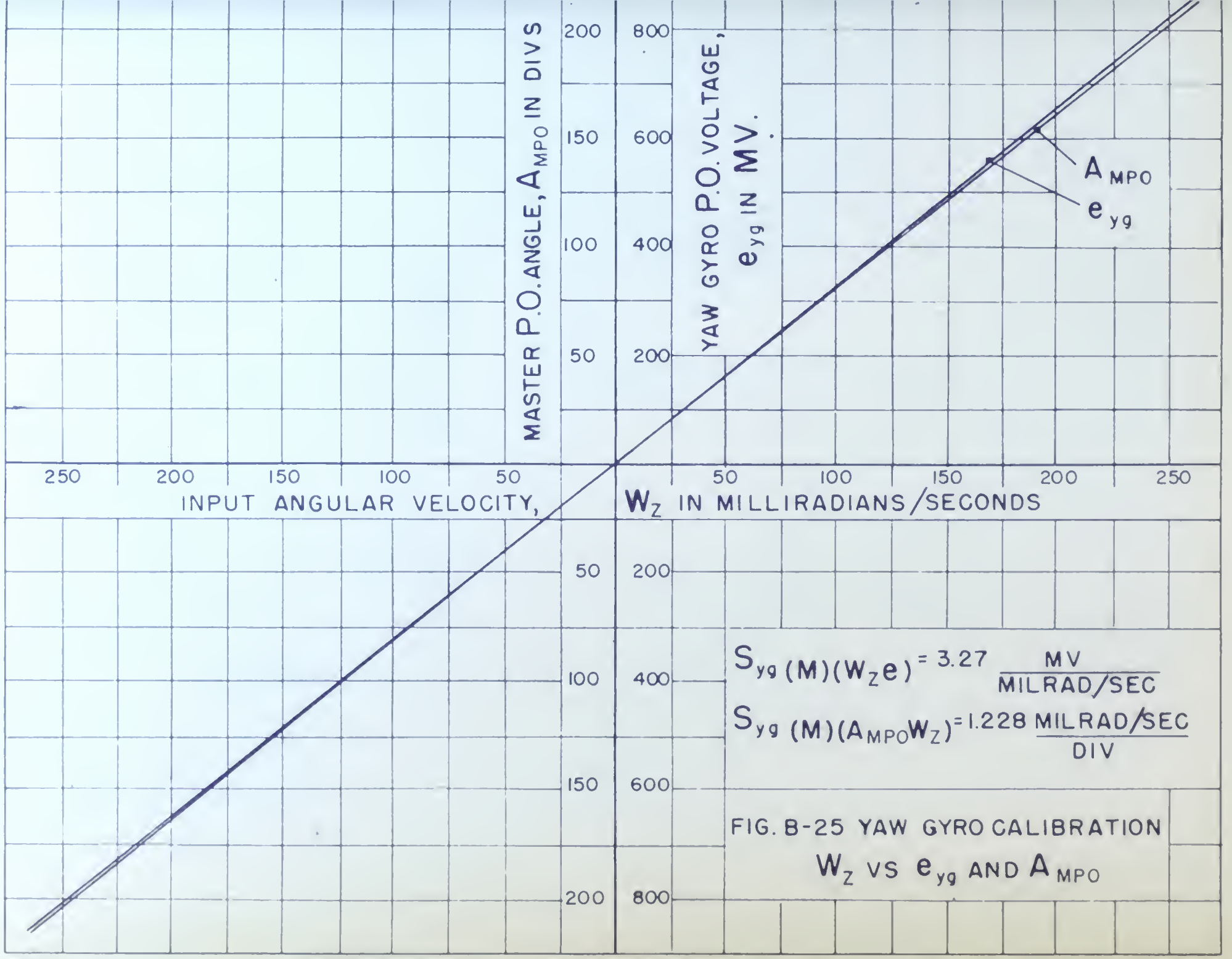

$S_{yg}(M)(W_Z e) = 3.27 \frac{MV}{MILRAD/SEC}$

$S_{yg}(M)(A_{MPO} W_Z) = 1.228 \frac{MILRAD/SEC}{DIV}$

FIG. B-25 YAW GYRO CALIBRATION

W_Z VS e_{yg} AND A_{MPO}

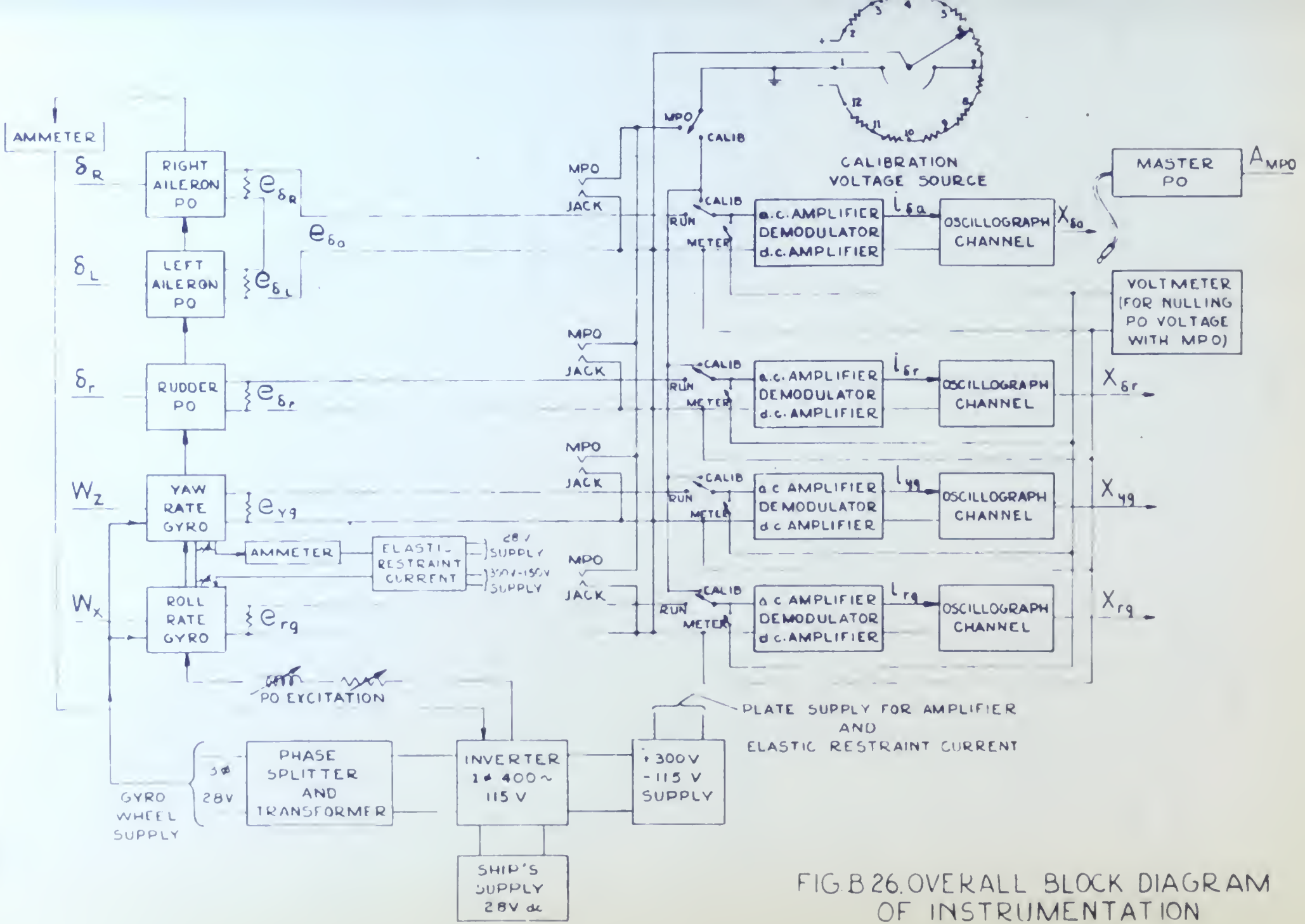

FIG. B 26. OVERALL BLOCK DIAGRAM OF INSTRUMENTATION

APPENDIX C

ANALYSIS OF A DIVERGENT TRANSIENT RESPONSE

References (2) and (3) point out that the approximation of the Fourier Transform is applicable only to stable systems. This can be easily seen from a consideration of the transient response of a system described by a characteristic equation having a positive root. For such a response, the sum

$$\sum_{n = 1,2,\ldots} q_{out}(t_n) e^{-jn\Delta\tau w}$$

will not converge. This condition is found in the lateral motion of many airplanes, where the positive root is associated with the motion called spiral divergence.

Since the B-25J used in the present investigation did not exhibit this type of response, a simple dynamic system illustrating divergent motion is analyzed in this appendix, using the finite pulse method.

Consider the system schematically pictured in Fig. C-1. The mass, m, in this figure is assumed to be supported in the gravity field by a rigid, massless, rod. The Laplace Transform of the characteristic equation for the small angles of motion considered in Fig. C-1, (Ref. 8), is

$$[m\ell s^2 + C\ell s - mg]\,\Theta = 0 \qquad (C\text{-}1)$$

Assume that a forcing function is applied consisting of a unit triangle of force, $UT(t - \Delta\tau)$ which is described by

$F = 0 \qquad 0 > t$

$F = \frac{1}{\Delta\tau} t \qquad 0 \leq t \leq \Delta\tau$

$F = 2 - \frac{1}{\Delta\tau} t \qquad \Delta\tau \leq t \leq 2\Delta\tau$

$F = 0 \qquad t > 2\Delta\tau$

$\Delta\tau = 0.1$ second

The transformed equation of motion becomes

$$[m\ell s^2 + C\ell s - mg]\Theta(s) = (LT)[UT(t - \Delta\tau)] \qquad (C\text{-}2)$$

where

$$(LT)[UT(t - \Delta\tau)] = \frac{(1 - e^{-\Delta\tau s})^2}{\Delta\tau\ s^2}$$

Solving for $\Theta(s)$,

$$\Theta(s) = \frac{(1 - e^{-\Delta\tau s})^2}{(\Delta\tau\ s^2)(m\ell)(s^2 + \frac{C}{m}s - \frac{g}{\ell})} \qquad (C\text{-}3)$$

In this investigation of the B-25J lateral motion, the response which was measured was the angular rate in roll or yaw. For this reason, the time rate of change of the angular position Θ will be considered as the output in this example. The rate of change of this output, $\dot{\Theta}$, is given by

$$\dot{\Theta}(s) = \frac{(1 - e^{-\Delta\tau s})^2}{\Delta\tau\ m\ell\ s(s^2 + \frac{C}{m}s - \frac{g}{\ell})} \qquad (C\text{-}4)$$

Factoring the characteristic equation,

$$s = -\frac{C}{2m} \pm \sqrt{\frac{C^2}{4m^2} + \frac{g}{\ell}}$$

Let

$$a = -\frac{C}{2m} + \sqrt{\frac{C^2}{4m^2} + \frac{g}{\ell}}$$

$$-b = -\frac{C}{2m} - \sqrt{\frac{C^2}{4m^2} + \frac{g}{\ell}}$$

Note that a is always positive and that a and b are positive, real numbers.

By appropriate substitution of a and b, the equation of motion, eq. (C-4) can be written,

$$\dot{\Theta}(s) = \frac{(1 - e^{-\Delta\tau s})^2}{\Delta\tau\ m\ell\ s\ (s - a)(s + b)} \qquad (C\text{-}5)$$

The performance function $(PF)_{[F, \dot{\Theta}]}$ is defined as

$$(PF)_{[F, \dot{\Theta}]} = \left. \frac{(LT)\ \dot{\Theta}(t)}{(LT)\ F(t)} \right|_{s = j\omega}$$

Then,

$$(PF)_{[F, \dot{\Theta}]} = \frac{1}{ml} \frac{j\omega}{(j\omega - a)(j\omega + b)} \qquad (C-6)$$

A value of 0.1 was assigned to a, and a value of 2.0 to b. The value of 0.1 for a is such that the amplitude of the divergence will double in 6.93 seconds. Some airplanes have this much divergence at high angles of attack. The value of 2.0 for b is somewhat small compared with that for the highly damped motion of most airplanes. The major consideration in the choice of these roots was to choose values that would reduce the calculations as much as practicable, and yet that would retain some semblance to those encountered in airplane lateral performance functions.

These choices were consistent with the choice of m and l as 1 and 2 respectively. The units are those of any consistent set of physical units.

Substituting these numbers and letting

$$s = j\omega$$

the performance function becomes

$$(PF)_{[F, \dot{\Theta}]} = \frac{1}{2} \frac{j\omega}{(j\omega - 0.1)(j\omega + 2)} \qquad (C-7)$$

This performance function is plotted in Fig. C-5.

Returning to eq. (C-5), by the inverse Laplace transformation the time response was obtained and plotted in Fig. C-2.

In Fig. C-3, the portion of the curve of Fig. C-2 beyond 5 seconds was plotted on semi-log paper, thus enabling determination of the divergent root. The straight line was extended to zero time and the intercept found. Having thus found an expression for the divergent component of the response, it was

subtracted from the total response leaving the remainder shown in Fig. C-4. The integral of this remainder is convergent and its approximate Fourier Transform is

$$(FT)\dot{\Theta}_{(rem)}(t) = (FT)[UT(t)] \sum_{n = 1,2\ldots} \dot{\Theta}(t_n)e^{-jn\Delta\tau\omega}$$

Since the system is linear, the performance function determined from the response curve can be expressed as the sum of components; i.e.,

$$(PT)_{[F,\ \dot{\Theta}\ ]} = \frac{(LT)[q_o(t)]_{(divergent)}}{(LT)[q_{in}(t)]} + \frac{(FT)[q_o(t)]_{(rem)}}{(FT)[q_{in}(t)]}$$

$$+ \frac{(FT)[(RT)[q_o(t_o)]_{(rem)}}{(FT)[q_{in}(t)]} \qquad (C-8)$$

The last two terms on the right side of eq. (C-8) were determined by approximating the Fourier Transform by triangles. The first term can be determined since the analytical expression for $q_o(t)_{divergent}$ is known, and since

$$(LT)[q_{in}(t)] = (FT)[q_{in}(t)]$$

This analytical expression for the divergent component of the response as determined from the time response is

$$(LT)[q_o(t)_{div}] = \frac{0.0231}{s - 0.1}\ ,$$

and

$$(PT)_{[F,\ \dot{\Theta}\ ](div)} = \frac{0.0231}{(j\omega - 0.1)(FT)[UT(t)]e^{-j\Delta\tau\omega}}$$

From this, the amplitude ratio and phase angle can be calculated for any given ω .

The desired performance function can be obtained by performing the addition of complex quantities indicated in eq. (C-8).

Figure C-5 shows the comparison of the original performance function with the performance function obtained by analysis of the time response. The

accuracy with which the original performance function was duplicated shows that this is a useable method of determining a performance function from a divergent time response.

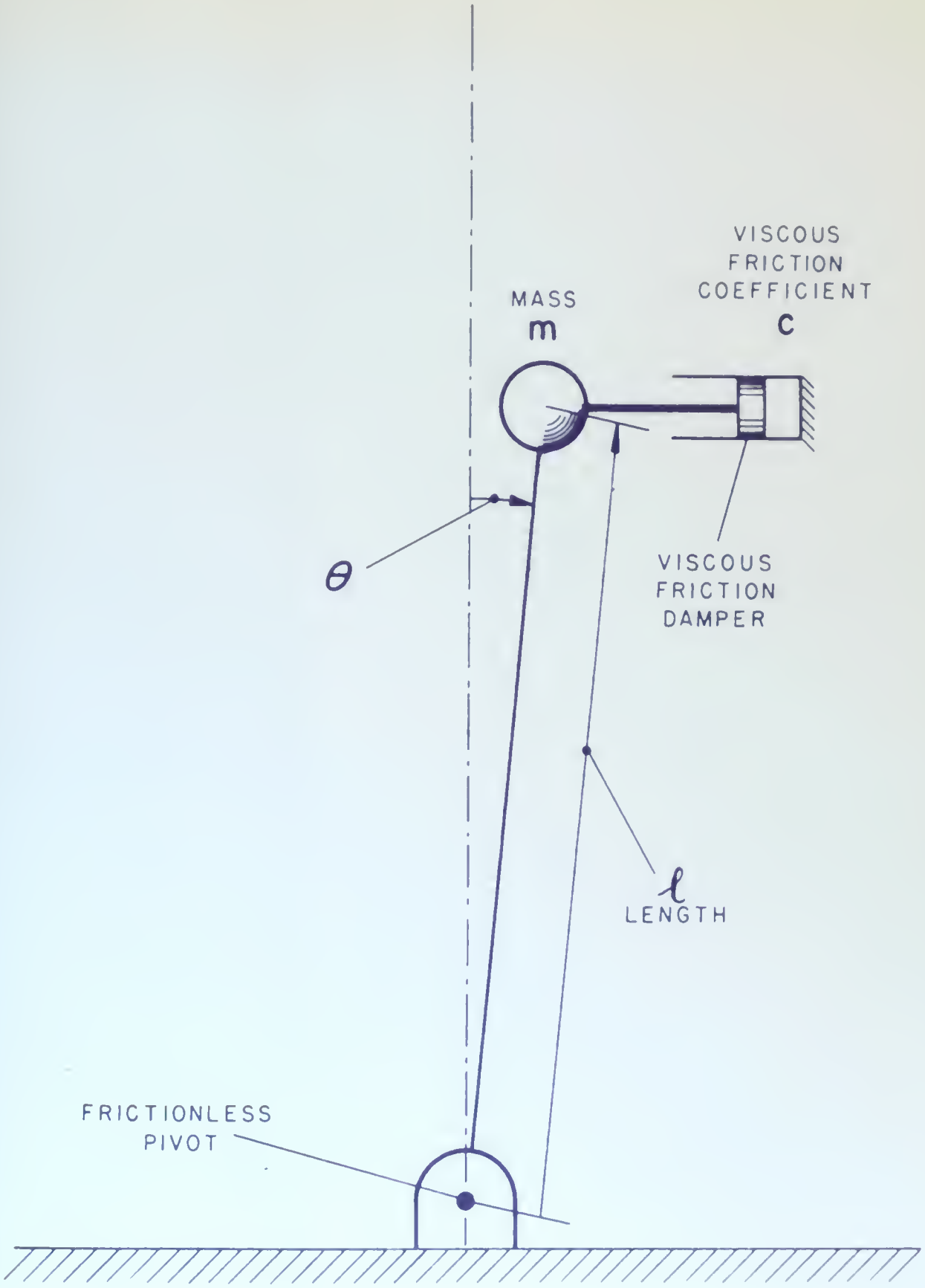

FIG. C-1 SCHEMATIC DIAGRAM OF SIMPLE DYNAMICAL SYSTEM

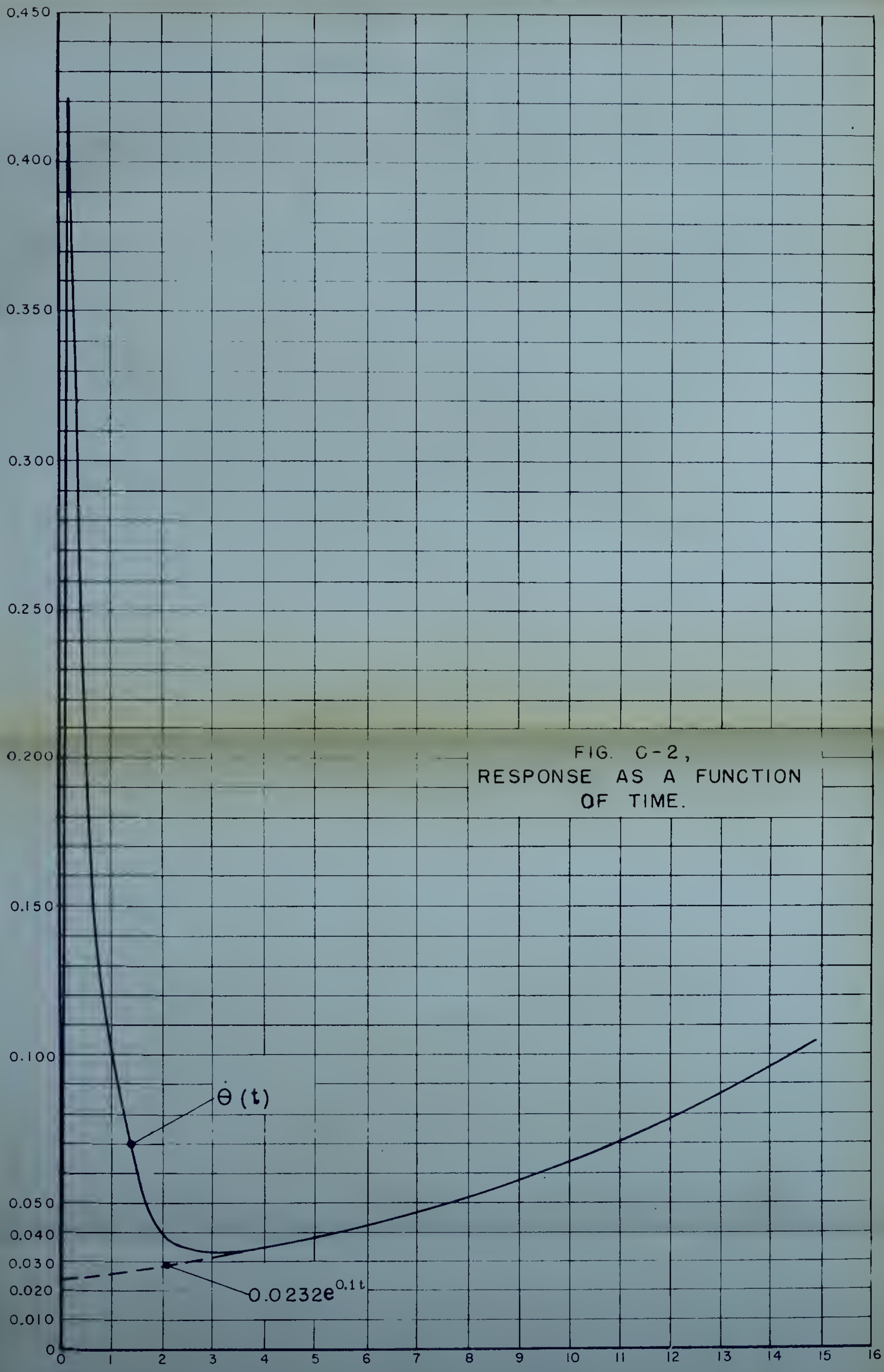

FIG. C-2,
RESPONSE AS A FUNCTION
OF TIME.

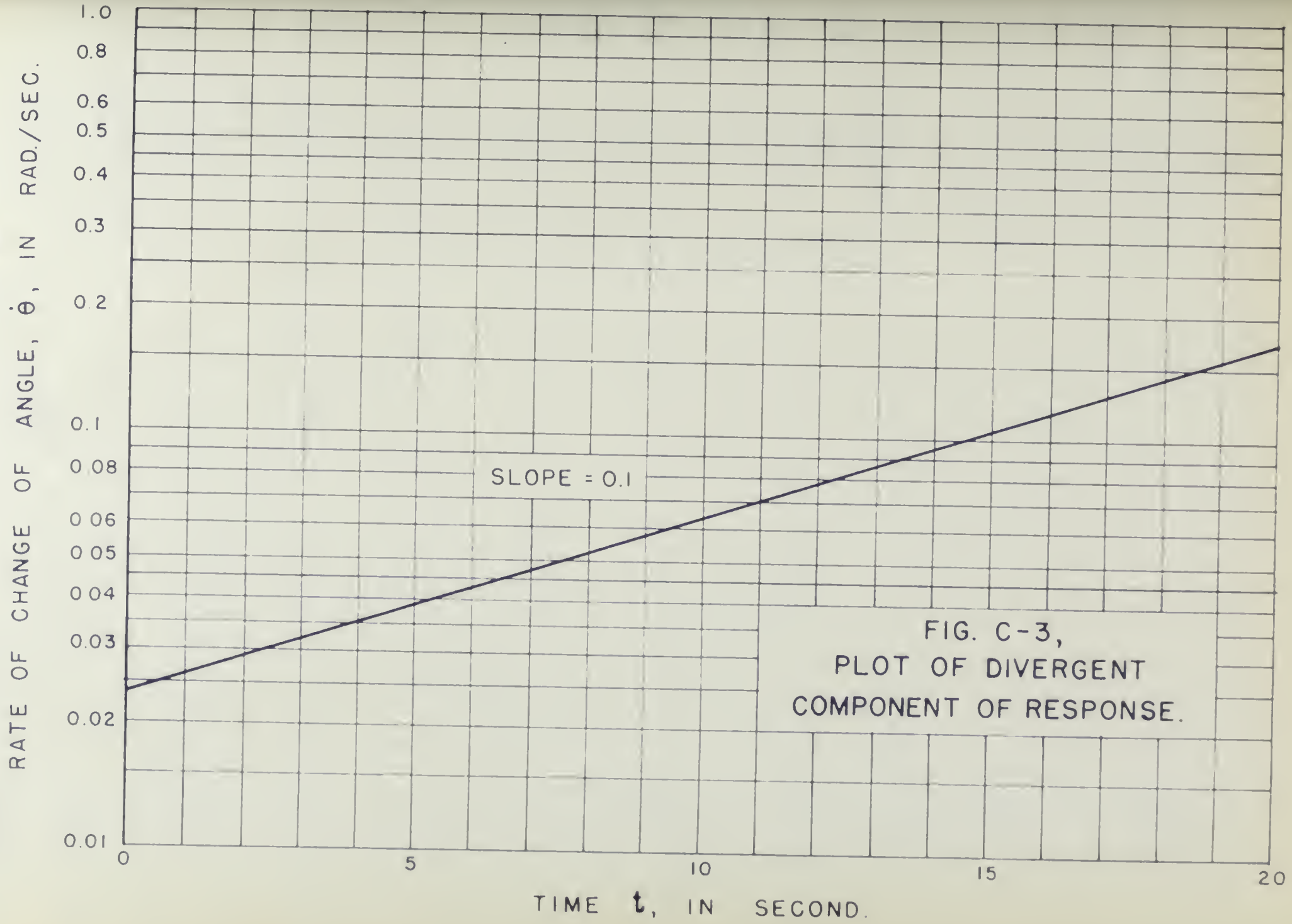

FIG. C-3,
PLOT OF DIVERGENT
COMPONENT OF RESPONSE.

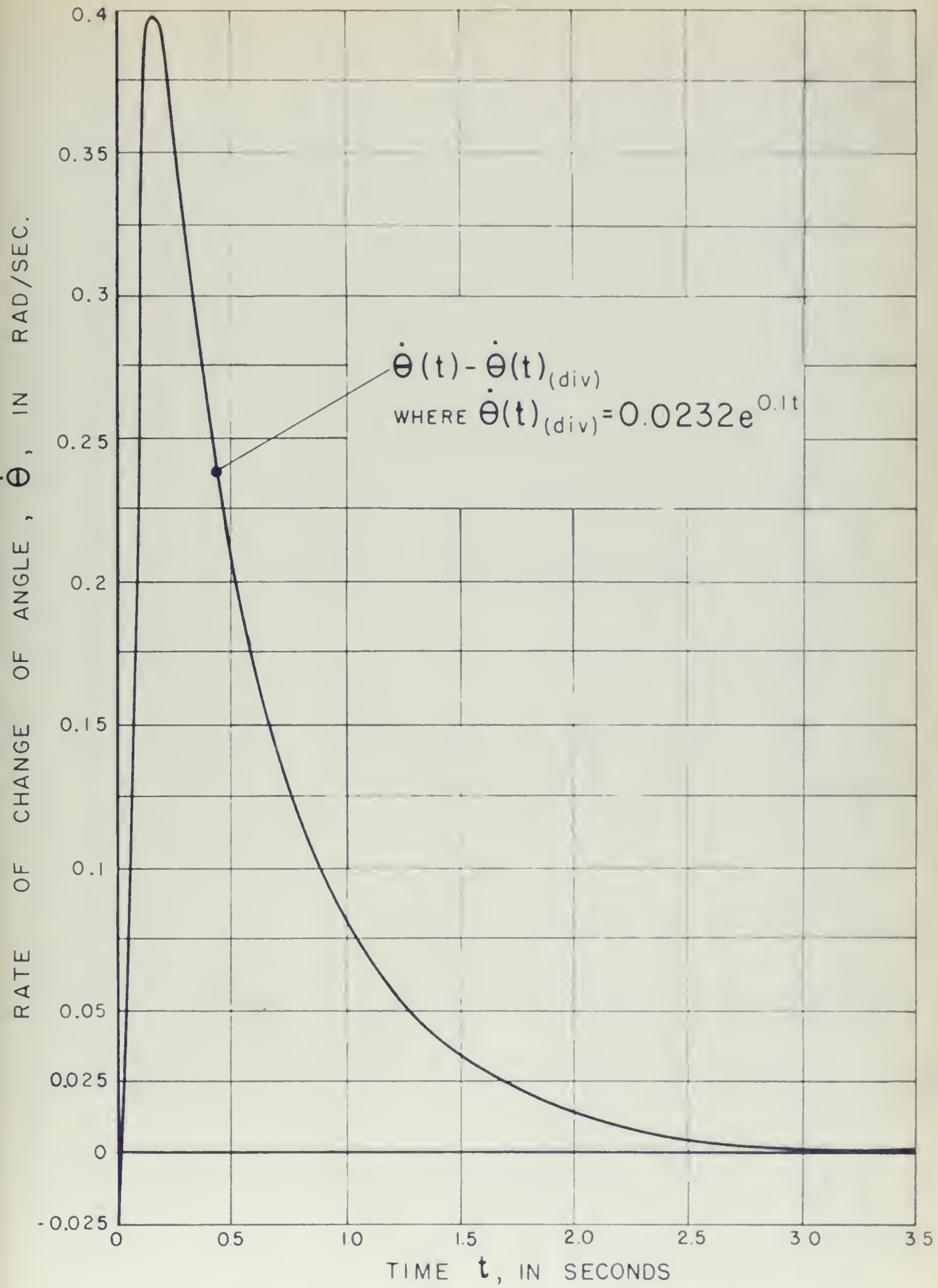

FIG. C-4, TIME RESPONSE WITH DIVERGENCE REMOVED.

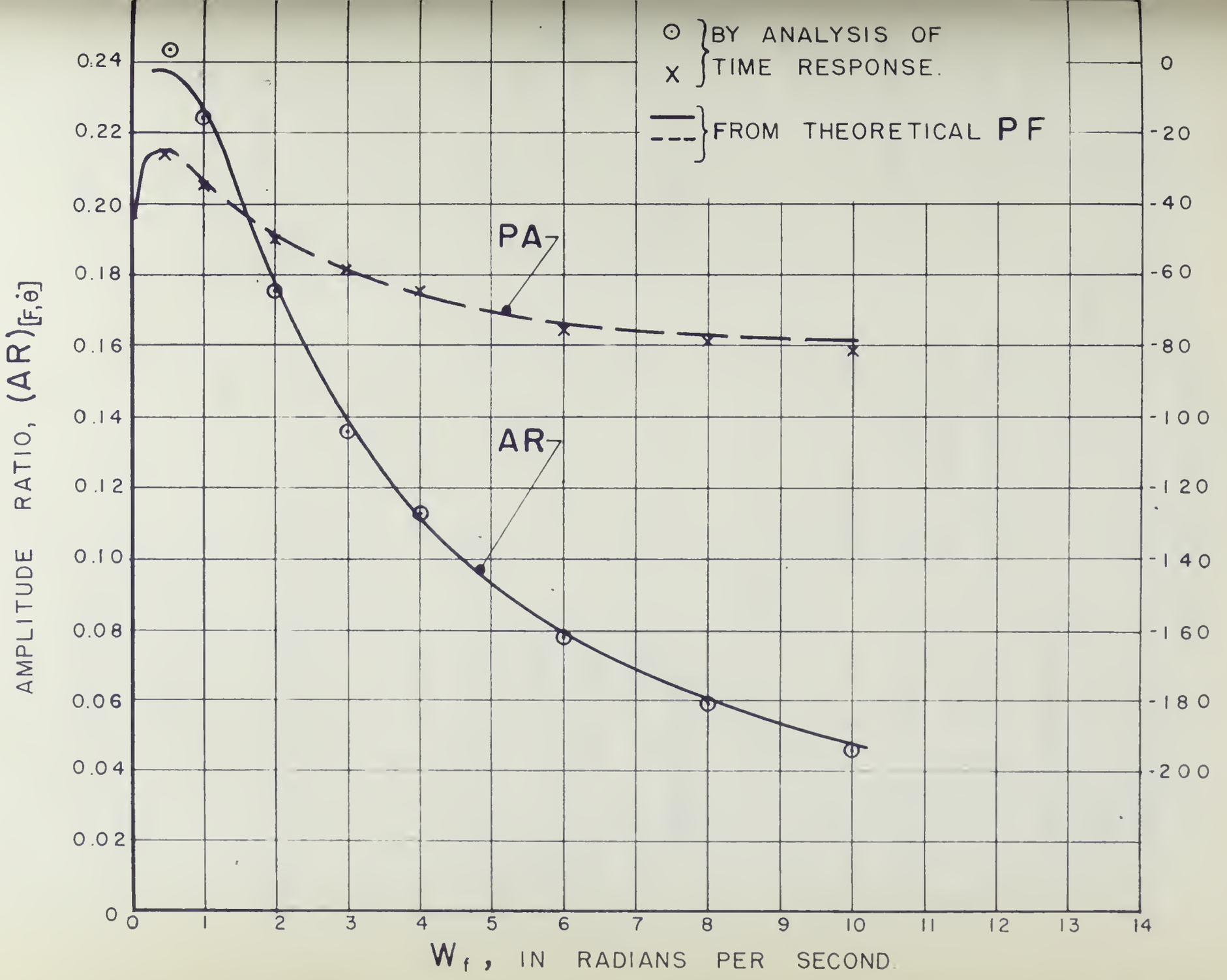

FIG. C-5. COMPARISON OF THEORETICAL AND MEASURED $PF_{[F,\dot{\theta}]}$.

APPENDIX D

DATA REDUCTION AND EVALUATION

The method used to obtain a desired performance function, knowing the time response of a system to a known input pulse, is outlined in Chapter I. In that chapter the method of approximating the mathematical expressions graphically (within the desired degree of accuracy) is covered. Reference 3 shows the method applied to a critically damped second order system, and outlines a method of attack to be used when more lightly damped oscillations are present in the time response. The process as above outlined has been applied to the oscillograph test records obtained in this investigation.

The oscillograph records provided the following information:

Input Pulses	Output Response
Aileron deflection, δ_a (+ defl)	Angular vel. in yaw and roll
Aileron deflection, δ_a (- defl)	Angular vel. in yaw and roll
Rudder deflection, δ_r (+ defl)	Angular vel. in yaw and roll
Rudder deflection, δ_r (- defl)	Angular vel. in yaw and roll

Sign conventions used in designating pulses correspond to NACA usage, i.e.,

(+) Aileron defl. - right aileron depressed

(+) Rudder defl. - rudder trailing edge moved to the left.

Reduction of the above listed recorded data would yield the following aircraft performance functions:

(1) $[PF]_{(A)(\delta_a, W_X)}$

(2) $[PF]_{(A)(\delta_a, W_Z)}$

(3) $[PF]_{(A)(\delta_r, W_X)}$

(4) $[PF]_{(A)(\delta_r, W_Z)}$

The time available for reduction of data was not sufficient to allow all these performance functions to be determined. Therefore, since this project is primarily concerned with the application of the pulse technique as a means of determining the performance function of any dynamical system, and since knowledge of the actual dynamics of the test vehicle is of secondary importance, the records were analyzed to achieve the following objectives:

(1) To determine the degree of accuracy or uncertainty in repeating results.

(2) To compare the results of determining the performance function by slightly variant graphical means.

(3) To compare the performance function as obtained by the pulse technique with the calculated performance function as determined from the aerodynamic derivatives obtained from wind tunnel tests.

(4) To reveal any inherent uncertainties or limitations in using the pulse technique to determine performance functions.

To obtain the data necessary to investigate the above objectives, the following analyses were actually made:

TABLE 1

Run No.	$[PF]_{[\ ]}$	Method	Direction of Pulse Input
4665	$[PF]_{[\delta_a\ W_X]}$	Graphical	(+) defl.
4661	$[PF]_{[\delta_a\ W_X]}$	Graphical	(-) defl.
4662	$[PF]_{[\delta_a\ W_X]}$	Graphical	(-) defl.
4665	$[PF]_{[\delta_a\ W_Z]}$	Graphical	(+) defl.
4662	$[PF]_{[\delta_a\ W_Z]}$	Graphical	(+) defl.
4665	$[PF]_{[\delta_a\ W_Z]}$	Numerical	(+) defl.

In determining the performance function graphically, three different methods were utilized to determine the amplitude ratio and phase angle at each selected forcing frequency. The first method utilized the general method as outlined in Ref. 3, that is, the graphical summation of input and output vectors as indicated in the following expression:

$$[PF] = \left. \frac{\Sigma\, q_{(out)}(\tau_n) e^{-jnw_f \Delta\tau_o} [FT][UT(t)]_o}{\Sigma\, q_{(in)}(\tau_n) e^{-jnw_f \Delta\tau_i} [FT][UT(t)]_i} \right|_{n = 1,2,3,4,5,....} \qquad (D\text{-}1)$$

Figure D-1 shows a sample plot of this method for $w_f = 1.25$ rad/sec using run number 4665, for determining the performance function $[PF]_{(A)(\delta_a\, W_X)}$. In this plot, the effect of the lightly damped sinusoid on the phase angle and amplitude ratio is apparent. Each cusp represents one half cycle of oscillation. In order for the amplitude to be attenuated to 0.05 of the original amplitude, the plot must be continued until a total of approximately 6.5 cusps have been plotted. The majority of the oscillograph records are not long enough to allow more than three or four cusps to be plotted, not is it practicable to obtain transient responses of this length with a usable uncertainty level. Thus the AR or PA, or both AR and PA are subject to error due to deleting the vector summation representing several additional half cycles of the oscillatory mode. Furthermore, the desired matching of the curve required that the response be divided into 0.1 sec increments, requiring that as high as 84 vectors be plotted (8.4 sec) at each forcing frequency — a tedious job resulting in a rather high degree of uncertainty.

In order to simplify the graphical method by requiring fewer vectors to be plotted to determine the AR and PA at each frequency, and to obviate the error incurred by omitting two or three half cycles of the oscillatory mode, a second graphical plotting system was used. In this system vectors were plotted in identically the same manner as previously discussed until

the time response was reduced to a remainder which was solely (for practical purposes) a pure damped sinusoid. At this point a single vector was added to the response vector summation to represent the contribution of the long ''tail'' of the sinusoid.

Figure D-2 is a sample plot of this method at the same forcing frequency and run (No. 4665) as used in Fig. D-1. The accuracy of this method depends on the accuracy with which the characteristics of the damped sinusoid may be determined. The characteristics were determined by the method demonstrated in Fig. 8 of Ref. 3. Knowing that the oscillatory motions in both yawing and rolling angular velocity have the same frequency and damping ratio (see eqs. (D-10) and (D-11) several records of both motions were used to measure the period and peak amplitude ratios, and average values for the parameters, DR and W_n, were thus obtained. The logarithmic decrement curves shown in Fig. 7 of Ref. 3 were used in determining DR. The records agreed quite closely in the period of the oscillation, but determination of DR required the average of several records, giving the following characteristics:

$$DR = 0.15$$

$$W_n = 1.45 \text{ rads/sec}$$

In the case of the rolling angular velocity response, it was found that the response was nearly a pure sinusoid after the third peak overshoot. (See Fig. D-5). As a consequence, the general performance function equation was rewritten, designating the time at the second peak overshoot as t_p, and the ordinate at t_p as q_p.

$$[PF]_{(\ )}(q_{in}, q_{out}) = \frac{\left[(\Sigma\, q_{(out)}(\tau_n)e^{-jnw_f\Delta\tau_o}\,[FT][UT(t)]_o\right]\Big|_{n=1,2,\ldots p}}{\left[(\Sigma\, q_{(in)}(\tau_n)e^{-jnw_f\Delta\tau_i})\,[FT][UT(t)]_i\right]\Big|_{n=1,2,\ldots}} \cdot \frac{\left[(\Sigma\, q_o(\tau_n)e^{-jnw_f\Delta\tau_o})\,[FT][UT(t)]_o\right]\Big|_{n=p,p+1\ldots}}{\left[(\Sigma\, q_i(\tau_n)e^{-jnw_f\Delta\tau_i})\,[FT][UT(t)]_i\right]\Big|_{n=1,2,\ldots}} \quad \text{(D-2)}$$

(zero time lag, τ_o, is assumed in the preceding equation)

The second term in the numerator may now be replaced by a single vector representing the contribution of the damped sinusoid from t_p to infinity, yielding,

$$[PF]_{(q_{in}\ q_{out})} = \frac{\Sigma\ q_{(out)}(\tau_n)e^{-jnw_f\Delta\tau_o}\ [FT][UT(t)]_o \Big|_{n=1,2,\ldots p}}{\Sigma\ q_{(in)}(\tau_n)e^{-jnw_f\Delta\tau_i}\ [FT][UT(t)]_i \Big|_{n=1,2,\ldots}}$$

$$\frac{[[FT][q_{(out)(osc)}(\tau)]\ e^{-jpw_f\Delta\tau_o}}{\Sigma\ q_{(in)}(\tau_n)\ e^{-jnw_f\Delta\tau_i}\ [FT][UT(t)]_i \Big|_{n=1,2,3,\ldots}} \qquad (D\text{-}3)$$

where $\Delta\tau_o$ and $\Delta\tau_i$ are the time intervals used in the output and input respectively.

Any time later than the time at which the response becomes a pure sinusoid may be selected as the point at which the remaining oscillatory motion may be represented by the Fourier Transform of a damped sine or cosine wave. However, it is advantageous to use a ''peak point'' or a point where the sinusoid crosses the axis in order that the phase angle in the sinusoid expression may be eliminated. In these two cases the term is reduced to the following Fourier Transform expressions:

(t_p at peak)

$$[FT]q_{o(osc)} = \left[\ [FT]q_p\ e^{-DRw_n t}\ \cos w_o t\ \right]\ e^{-jpw_f\Delta\tau_o}$$

$$= \left\{ \frac{q_o(DR)}{w_n} \frac{\sqrt{1 + (\frac{FR}{DR})^2}\ \left| \tan^{-1}(\frac{FR}{DR}) - \tan^{-1}\frac{2(DR)(FR)}{1 - FR^2} \right|}{\sqrt{[1 - (FR)^2]^2 + [2(DR)(FR)]^2}} \right\} e^{-jpw_f\Delta\tau_o} \qquad (D\text{-}4)$$

(t_p at axis)

$$[FT]q_{o(osc)} = \left[\ [FT]q_p\ e^{-(DR)(w_n)t}\ \sin w_o t\ \right]\ e^{-jpw_f\Delta\tau_o}$$

$$= \left\{ \frac{q_o\ w_o}{w_n^2} \left[\frac{-\tan^{-1}\frac{2(DR)(FR)}{1 - (FR)^2}}{\sqrt{[1 - (FR)^2]^2 + (2(DR)(FR)^2}} \right] \right\} e^{-jpw_f\Delta\tau_i} \qquad (D\text{-}5)$$

The time, t_p should be chosen to fall on one of the ordinates determined by the choice of $\Delta\tau_o$ to avoid disturbing the area approximation originally established by the isosceles triangles. If a peak maximum or minimum is selected as t_p, the area approximation by triangles is interrupted even through t_p may lie on one of the ordinates of the fitted triangle. In this case, a right triangle term must be added to the Fourier Transform of the output if the resulting output vector is to be exactly correct. However, the initial amplitude of the cosine wave starting at t_p was small enough in the runs analyzed in this project to render the right triangle term ineffectual in changing the AR or PA of the performance function. The method is demonstrated in Fig. D-4.

Figures D-1, D-2 and D-3 compare the two graphical methods used in determining the performance function, $[PF]_{(A)(\delta_a,\ W_X)}$. Figure D-1 shows the AR and PA determined by plotting the maximum number of vectors available from the oscillograph record. Figure D-2 shows the same AR and PA at the same forcing frequency as determined by representing the output divided in two parts in the method just described. Figure D-3 shows a comparison of the AR and PA results determined by each method. It was found that the maximum error in the first method, Fig. D-1, appeared at the resonant frequency.

The third method used for determination of the performance function from pulse response data is the method described in Ref. 3, Section IV. The oscillatory mode was determined as previously described, and subtracted from the output response from $t = 0$ to ∞. As shown in Fig. 9 of Ref. 3, the remainder of the output response is no longer zero at $t = \tau_o$, and a term must be added to account for the right triangular area at the time origin, which is not included in the area approximated by

the isosceles triangles approximating the remainder of the response. The resulting expression is that given by eq. 40 of Ref. 3.

$$[PF]_{(\ )(q_{in}\ q_{out})} = \frac{[FT][q_{o(osc)}(t)] + [q_{o(rem)}(\tau_o)][FT][(URT)(t)]}{\sum_{n=1,2,\ldots} q_{(in)}(\tau_n)e^{-jnw_f\Delta\tau_i}\ [FT][(UT)(t)]_i} +$$

$$\frac{\Sigma[q_{o(rem)}(\tau_n)]e^{-jnw_f\Delta\tau_o}\ [FT][(UT)(t)]_o \quad n=1,2,\ldots}{\Sigma\,[q_i\ (\tau_n)]e^{-jnw_f\Delta\tau_i}\ [FT][(UT)(t)]_i \quad n=1,2,\ldots} \qquad (D\text{-}6)$$

Figures 3-1 and 3-2 show the amplitude ratio and phase angle respectively of the performance function for aileron deflection input and roll response output. The phase angles shown have been corrected for gyro phase lag as obtained from the Fig. D-13. Undamped natural frequencies and damping ratio for both gyros are found in Appendix B. In figures 3-1 and 3-2 three experimental performance functions are shown which are the result of analyzing graphically three different oscillograph records (runs 4665, 4661 and 4662). The uncertainty in reproducing results may be observed from these plots. The curve shown represents the average value of the three experimental points at each frequency. The greatest deviation from the average occurs at $w_f = 1.25$ where the maximum variation in AR is 5.9 percent. The average variation is 1.6 percent. As noted in the sample oscillograph records, Figs. D-5 and D-6, no two input pulses were identical. Consequently, each response is different which necessitated independent analysis of each record. The reliability of the pulse input technique in reproducing results appears to be excellent, judging from the results of this limited investigation.

From the experience gained in use of the analyzing systems previously outlined, the following advantages and disadvantages were noted in applying these systems to time records having a long ''tail'' due to a lightly damped sinusoid.

TABLE 2

METHODS OF ANALYZING THE RESPONSE

Method of Analysis		Advantages	Disadvantages
No.	Description		
(1)	Vector addition of isoscles triangles over entire oscill. record. (No breakdown of components)	Simple and straight-forward. Accuracy dependent only on degree of approx. of time response and on satisfactory length of OSC record to include entire response.	1. Analysis slow and tedious due to large number of vectors required. 2. Difficult to separate noise from intelligence at large values of time.
(2)	Similar to (1) to $t = t_p$ plus a single vector representing pure damped sinusoid $t \geq t_p$	Fast and as accurate as any method investigated.	1. Depends on ability to determine accurately q_p, DF w_n of the oscillatory mode. 2. Depends on accuracy of locating t_p at a peak or null.
(3)	Addition of remainder, osc. mode, and right triangle. Over entire range, $0 \leq t \geq \infty$		1. (Same as 1) under Method (2). 2. Involves additional source of error in subtracting ordinates to remove osc. mode. 3. Requires fit of right triangle.

The only remaining curve shown in Figs. 3-1 and 3-2 which has not been discussed is the calculated performance function using wind tunnel stability derivatives for the B-25. Due to differences between the model used in the wind tunnel tests and the actual airplane, these derivatives have been modified to more closely represent the true derivatives of the aircraft. The derivatives that were not available from wind tunnel tests were estimated on the basis of previous engineering experience with comparable aircraft configurations. For use as a means of comparison in this project, the derivatives were corrected to include the values of moment of inertia about the X and Z axes as found for the B-25 used in the testing configuration (See Appendix A).

The derivatives as used to determine a calculated performance function are as follows:

$$L_p = \frac{\partial C_\ell}{\partial(\frac{pb}{2U})} \frac{\rho S b^2 U}{4 I_{XX}} = -2.71 \text{ 1/sec}$$

$$L_r = \frac{\partial C_\ell}{\partial(\frac{pr}{2U})} \frac{\rho S b^2 U}{4 I_{XX}} = +.673 \text{ 1/sec}$$

$$L_v = \frac{\partial C_\ell}{\partial \beta} \frac{\rho S b^2 U}{2 I_{XX}} = -.00964 \text{ 1/ft-sec}$$

$$L_{\delta a} = \frac{\partial C_\ell}{\partial \delta_a} \frac{\rho S b U^2}{2 I_{XX}} = -3.175 \text{ 1/sec}^2$$

$$N_{\delta a} = \frac{\partial C_n}{\partial \delta_a} \frac{\rho S b U^2}{2 I_{ZZ}} = +.133 \text{ 1/sec}^2$$

$$N_p = \frac{\partial C_n}{\partial(\frac{pb}{2U})} \frac{\rho S b U}{4 I_{ZZ}} = -.10 \text{ 1/sec}$$

$$N_v = \frac{\partial C_n}{\partial \beta} \frac{\rho S b U}{2 I_{ZZ}} = +.00648 \text{ 1/ft-sec}$$

$$N_r = \frac{\partial C_n}{\partial\left(\frac{br}{2U}\right)} \frac{\rho USb^2}{4I_{ZZ}} = -.428 \text{ 1/sec}$$

$$Y_v = \frac{\partial C_Y}{\partial \beta} \frac{\rho SU}{2m} = -.13 \text{ 1/sec}$$

$$N_{\delta r} = \frac{\partial C_n}{\partial \delta_r} \frac{\rho SbU^2}{2I_{ZZ}} = -1.66 \text{ 1/sec}^2$$

Alt. = 10,000 ft

Air spd = 175 mph

I_{XZ} = -1930 slug ft^2

I_{XX} = 63,000 slug ft^2

I_{ZZ} = 120,000 slug ft^2

Weight = 26,000 lb

The sign convention for the derivatives and equations of motion and the symbols representing displacements, moments, velocities, etc., are in accordance with NACA designation system. Positive directions along the axes, viewed from the origin, are forward, right wing, and down for the X, Y, and Z axes respectively.

The following assumptions were made in writing the equation of motion:

1. Damping moments due to control surface motion are negligible.
2. The wind axes and the aircraft reference axes are considered to be superimposed.
3. No gyroscopic effects were considered.

The equations of motion are:

a. Summation of forces along Y axis

$$m\dot{v} + mUr = \frac{\partial Y}{\partial v} v + \frac{\partial Y}{\partial \phi} \phi \qquad \text{(D-7)}$$

b. Summation of rolling moments

$$I_{XX} \dot{p} = \frac{\partial L}{\partial v} v + \frac{\partial L}{\partial p} p + \frac{\partial L}{\partial r} r + I_{XZ} \dot{r} + \frac{\partial L}{\partial \delta_a} \delta_a \qquad \text{(D-8)}$$

c. Summation of yawing moments

$$I_{ZZ} \dot{r} = \frac{\partial N}{\partial v} v + \frac{\partial N}{\partial p} p + \frac{\partial N}{\partial r} r + I_{XZ} \dot{p} + \frac{\partial N}{\partial \delta_a} \delta_a \qquad \text{(D-9)}$$

Dividing each equation by the appropriate moment of inertia or the mass, taking the Laplace transform and solving for p and r, the following performance functions were obtained:

$$[PF]_{(\delta_a W_X)} = \frac{-3.175\ S\ (S^2 + .586S + 1.6)}{(S^2 + .377\ S + 1.78)(S + 2.9)(S - .0013)} \qquad (D\text{-}10)$$

where $p = W_X$.

$$[PF]_{(\delta_a W_Z)} = \frac{.184\ (S + 3.51)(S + 1.097)(S - .837)}{(S^2 + .377\ S + 1.78)(S + 2.9)(S - .0013)} \qquad (D\text{-}11)$$

where $r = W_Z$.

The calculated performance function $[PF]_{(\delta_a W_X)}$ shown in Figs. 3-1 and 3-2 have the same general shape as the experimental performance function. The misalignment of the resonant frequencies of the two plots is indicated in the difference in characteristics of the oscillatory modes of the calculated and experimental performance functions. The characteristics for the calculated and experimental oscillatory modes are:

	DR	W_n
Experimental	.15	1.45
Calculated	.141	1.36

Since the oscillatory mode is the predominant mode in establishing the peak values of the performance function, the difference in the magnitude of the two peaks should represent approximately the same percentage difference as indicated by the difference in their damping ratios. From Fig. 3-1 the peak of the experimental performance function is 93.8 percent of the peak value of the calculated performance function, while the corresponding ratios of the two DR is 93 percent.

The calculated performance function shows a very small divergent root. However, it is difficult to state whether the B-25J actually is spirally divergent or not. The oscillograph time records do not indicate a divergence.

However, in order to determine whether such divergence exists, it would be necessary to take a record of at least 15 seconds to determine the presence of this unstable mode. During this period small perturbations in roll or yaw due to disturbances of the air mass would probably nullify the accuracy of any such record. In any case, for practical considerations, a root as small as the calculated performance function indicates, whether positive or negative, would have negligible effect on the performance function.

The sensitivities were compared using the following assumptions:

1. The unstable root encountered in the characteristic equation of the calculated performance function was considered negligible (0.0013 = 0),

2. The experimental performance function contains no divergent roots. (An assumption implicit in positioning the base line.)

Using the first assumption, the sensitivity for the calculated response was determined by rewriting the performance function as a sensitivity multiplied by a frequency function. The same assumption applied to the experimental curve gives the ratio of the area under the response curve in the time domain to the area under the input curve in the time domain as the sensitivity of the experimental performance function.

To determine the area contributed by the oscillatory mode of the response extending beyond the limits of the oscillograph record, the area was measured out to $t = t_p$, (t_p again representing the point at which the response becomes a pure damped sinusoid) and the curve beyond time t_p was integrated analytically and added to the area from $t = 0$ to t_p. The expression thus becomes

$$S_{(A)(\delta_a W_X)_{experimental}} = \frac{\left[\sum_{n=1,2,\ldots p} q_o(\tau_n)\,\Delta\tau_e\right] + \int_{t=p_0}^{t=\infty} q_p(\tau)\, e^{-D R W_n t} \cos w_o t}{\left[\sum_{n=1,2,\ldots} q_i(\tau_n)\,\Delta\tau_i\right]}$$

The sensitivities thus determined are:

$$S_{(A)(\delta_a W_X)_{(calc)}} = -.992 \text{ 1/sec}$$

$$S_{(A)(\delta_a W_X)_{(exper)}} = -.945 \text{ 1/sec} \quad (\text{Run No. 4666 Input} = +\delta_a)$$

$$= -1.080 \text{ 1/sec} \quad (\text{Run No. 4665 Input} = +\delta_a)$$

$$= -.985 \text{ 1/sec} \quad (\text{Run No. 4661 Input} = -\delta_a)$$

$$= -.990 \text{ 1/sec} \quad (\text{Run No. 4662 Input} = -\delta_a)$$

$$S_{(A)(\delta_a W_X)_{(exper)(av)}} = -1.0 \text{ 1/sec}$$

An additional sensitivity for comparison with the above may be obtained from flight test data for the B-25, utilizing curves of $\frac{Pb}{2U}$ vs δ_a (Ref. 4). From these curves, the sensitivity is,

$$S_{(A)(\delta_a W_X)_{(F)(\text{test data})}} = -.90 \text{ 1/sec}$$

The comparison of experimental and calculated sensitivities are in close agreement, as is the check with flight test roll rate data (Ref. 4).

The performance function for yawing velocity response to aileron input is shown in Figs. 3-3 and 3-4. The yawing velocity response as shown in Fig. D-5 appears to be an excellent example to illustrate the limitations of the pulse input technique. As noted in Fig. D-5, the response is essentially oscillatory, the first lobe (positive) indicating the adverse yaw effect in which side slip has taken place to give the high righting moment responsible for the second lobe (negative) being of greater amplitude than the first lobe. The pattern of this response is noted in detail since its effect in the graphical analysis is important.

The type of output response pattern found in yawing velocity for aileron input shows the same summation pattern at each of the low frequencies. Comparing Fig. D-7 with Fig. D-2, it is seen that the end point of each

summation is well away from the origin, and that small errors made in plotting will offer very little error to either the AR or the PA of the total output vector. Also, the comparison at these low frequencies with the AR and PA of the calculated performance function is satisfactory both in yaw and in roll. (See Fig. 3-1 and 3-2 for roll, and Fig. 3-3 and 3-4 for yaw.) However, as the frequency increases, and $W_f \Delta\tau$ increases correspondingly, the vector summation of the yaw vectors begin to ''wind up,'' the end points never getting very far from the origin. Note the difference in the summation as shown for W_f = 1.5 rad/sec in Fig. D-7 and the summation as shown for W_f = 5.0 rad/sec in Fig. D-8. This clearly indicates that any uncertainty entering the summation, regardless of its nature, will impart a much higher uncertainty effect to the PA of the output vector (end-point to origin) than in the case where the end-point is well removed from the origin. The uncertainty of the results thus are increased by two factors as the frequency increases,

1. The large relative size of the last vector in the summation in comparison with the resultant output vector, and

2. The accumulated errors from measuring ordinates from the record.

Consequently, each system of analysis as covered in Table 2 must be analyzed and tested to determine the relative uncertainty in approximating the Fourier Transform under conditions where the response is composed in the main of an oscillatory motion. The general effort is to establish the system of analysis that will produce the fewest inaccuracies in approximation and the fewest uncertainties in plotting.

Investigation of the method listed in Table 2 as (2), the one used most extensively in determining the response vectors for the performance function in roll for an aileron input, certain inherent uncertainties are noted. Again, it is emphasized that these uncertainties become increasingly

important as the response becomes more predominately oscillatory. These uncertainties affecting the magnitude and phase angle of the output vector are listed in order of the importance of the error they present.

1. Uncertainty in determining the time at which a mode has reached its peak value on the time response, or the time at which the output time response crosses the base line. That is, correct determination of the location of t_p. Figures D-5 and D-6, actual oscillograph records, show the cause for this uncertainty. The records are of too short duration to show more than a maximum of one full cycle of the pure damped sine wave. Therefore, although the DR and W_n of the oscillating mode may be well established by comparison of many records, the low flat-topped lobes and the low slope of the curve, plus the fact that the noise to signal level is becoming quite high at low amplitudes, all tend to make the selection of the exact point at which the curve peaks or crosses the base line somewhat uncertain within about ± 0.1 second. The effect of such an error can be observed best at high frequency. If W_f = 6 rads/sec and $\Delta\tau = 0.1$, and the final output vector is approximately the length of the vector representing the oscillatory mode, an error as high as 30 degrees in PA may exist. As the end point moves further from the origin, this possible maximum error reduces accordingly.

2. Uncertainty in determining DR and W_n of the oscillatory mode.

3. Uncertainty in determining the amplitude of the oscillatory mode.

On the basis of the above uncertainty at high frequency in adding a vector representing the Fourier Transform of the oscillatory mode, it may be concluded that the greater the time, t_p, the less the uncertainty. This may be observed in eq. (D-3). To simplify that expression consider $\Delta\tau_o = \Delta\tau_i$, then

$$[PF]_{(\ )(q_i q_o)} = \frac{\Sigma\, q_o(\tau_n) e^{-jnw_f \Delta\tau_o}}{\Sigma q_i(\tau_n) e^{-jnw_f \Delta\tau_i}} \Bigg|_{n = 1,2,3,\ldots}^{n = 1,2,\ldots p}$$

$$+ \frac{\left[[FT]q_{o(osc)}(t)\right] e^{-jp\Delta\tau_o w_f}}{[FT][UT(t)]_i \quad \Sigma\, q_i(\tau_n) e^{-jnw_f \Delta\tau_i}} \Bigg|_{n = 1,2,\ldots}$$

The larger t_p becomes, the greater the percentage of the graphical analysis that is accomplished with the same degree of approximation in both numerator and denominator. If the oscillograph record were long enough, the best results at high frequency would be obtained by continuing summation of the output vectors until such time as the end point is clearly indicated. This allows the same degree of approximation in obtaining both the output vector and the input vector throughout the entire summation. However, in addition to the tedium of plotting a large number of vectors, uncertainties are introduced by the oscillograph record in picking off ordinates well out in the time respcnse. The noise to signal ratio becomes high, and drift of the baseline appears to be one of the evils of the long record.

The most uncertain of the graphical methods for use with the highly oscillating type response is the method which subtracts the pure oscillatory mode from the entire response. In this case, the subtracted oscillatory mode represents a high percentage of the total response. This large portion of the response is represented by a single vector which is an exact Fourier Transform. Consequently, the output, in the extreme case where the response is almost entirely oscillatory, is represented exactly, and the input is approximated. The result is that at high frequency, the output reaches a certain fixed phase angle, due to the predominance of the oscillatory

mode, and the input continues to shift phase angle rapidly. Therefore, it appears that at very high frequency the oscillatory part of the output will eventually lead the input. The lagging phase of the remainder should theoretically compensate in such a manner that the vector representing the total performance function will have the proper phase angle. But, the vector representing the remainder is very small, and therefore, although its phase lag may be increasing in a like manner to the denominator (input), its contribution to the phase angle of the vector summation is very small. Furthermore, the additional manipulation of the time response data in obtaining a breakdown into components offers added uncertainty in the vector summation.

Sample records are provided to show the vector summation using method (3) in which the oscillatory mode is removed from $t = 0$ to $t = \infty$ and represented by an exact Fourier Transform, and method (2) in which the Fourier Transform of a sine wave starting at t_p is added to the output summation for $t = 0$ to $t = t_p$. Figures D-9 and D-10 respectively show these two cases. Note that in Fig. D-9 the vector representing the oscillatory mode is the largest of the three vectors comprising the total response vector. Furthermore, it has attained its maximum lagging phase angle to within about 5 degrees. The phase angle from the performance function at $W_f = 6$ by this method is -49 degrees (corrected for gyro phase angle from Fig. D-14). Figure D-10 shows the results of using the same approximation in both input and output over the greater part of the response, method (2). The addition of the vector representing the sine wave summation is nearly negligible in its effect on the total response vector. The phase angle at this same frequency by this method, (2), is -87.5 degrees.

As previously discussed, adding the sine term involves uncertainty in properly locating t_p. This error may be reduced to a negligible size or

eliminated by the following means. Select t_p where the output crosses the base line and observe the magnitude of the vector resulting in comparison with the magnitude of the last vector in the summation from t = 0 to t = t_p. If the vectors are approximately the same size, no appreciable error will result from an error in locating t_p. If the vector representing the added sine term is large compared to the last vector of the summation, t_p should be moved to the next null point of the time response, which will decrease the magnitude of the sine wave amplitude by the factor $e^{-W_n(DR)(T/2)}$.

It is the opinion of the authors that the added sine wave method of component summation is subject to the least inaccuracies, of the methods investigated, in determining the performance function of a response which is essentially oscillatory. The method affords the same degree of approximation in both the input and response, until such time as the response is subjected to inaccuracies of noise and instrumentation. At this point (t_p) the small remainder is represented by an exact transform.

Referring again to Figs. 3-3 and 3-4, the effects of various analysis methods in obtaining the performance function are shown. The method numbers are those listed in Table 2. As previously noted, the variation in PA from the calculated performance function at high frequencies is very high, and it is difficult to explain the variation in terms of the dynamics of the airplane. The assumptions listed in setting up the theoretical equations of motion for the test vehicle, limit the phase shift to 90 degrees of lag at high frequencies. However, refinements which were excluded by these assumptions may add about 10 to 15 percent additional phase lag at high frequency, as shown in the theoretical performance function found in Ref. 7. The performance function applies to the B-26, an aircraft similar in dimensions and mass configuration to the B-25J. The experimental PA, at high frequencies are in disagreement with the calculated performance functions determined both for the B-25 and the B-26. However, the very low AR at the frequencies of

uncertain phase angles makes PA uncertainty relatively unimportant in determining the performance functions.

The scattering of points in the doubtful phase angle range shows the effect of various methods of determining the transform of the response. It was found by halving the $\Delta\tau_o$, the phase angle was negligibly affected. Compare Fig. D-8 with Fig. D-11. This indicates that $W_f\Delta\tau$ has not reached a critical value. (Ref.3).

The sensitivities for this performance function were determined in the same manner as used in the performance function for rolling velocity response to input aileron responses.

As previously noted, the calculated performance function, (eq. D-11), has a very small root in the denominator. Such a small root either positive or negative would not be apparent in the time response and would be implicitly considered to be zero by the action of drawing in the base line. To be consistent for comparative purposes, the same assumption must be made with the calculated performance function.

Thus, to get a valid comparison let $jw - 0.0013 = jw$ in the calculated performance function. Then by writing the performance function as a sensitivity multiplied by a frequency function, a sensitivity that can be compared with the ratio of the areas under the experimental output and input curves is obtained. The comparison is:

$$S_{(A)[\delta_a W_Z]_{calc}} = 0.209 \text{ 1/sec}$$

$$S_{(A)[\delta_a W_Z]_{exper}} = .167 \text{ 1/sec} \qquad \text{(from run no. 4665 + } \delta_a \text{ input)}$$

$$S_{(A)[\delta_a W_Z]_{exper}} = .172 \text{ 1/sec} \qquad \text{(from run no. 4662 } -\delta_a \text{ input)}$$

In general, the results obtained bring out several points concerning the application of the pulse technique as a means of determining the

performance functions of dynamical systems. Results obtained in rolling velocity response for aileron inputs showed very close agreement with the theoretical performance function throughout the entire range of frequencies investigated. The comparison of time response patterns or conformations indicate the response pattern involving the least inaccuracies in analysis is one which responds quickly, reaching its maximum amplitude in the early part of the time response. Under these conditions, the end point will usually be well removed from the origin, and uncertainties in added vectors representing the Fourier Transforms of oscillatory modes, right triangles, etc. will have a minimum effect on the AR and PA of the performance function, until very high frequencies and small AR prevail.

A potential source of error lies in establishing the true baseline for each response and input time record. An error in the location of this line produces a double error in the results in that as much false area is added to one side of the line as is subtracted from the other side of the line. In the case of records having the long tail characteristic of a lightly damped oscillatory mode, the envelope should be drawn in determining the base line, particularly if there is any drift in the center of the response record. This is demonstrated in Fig. 8, Ref. 3. In any case, measurements from the reference trace to the center-line should be made at short intervals and connected, rather than passing a line between two measured points at the extremities of the record. This corrects for warping of the record incurred in the drying process. If nominal care is exercised in laying out the baseline, and in picking off ordinates from the record, the uncertainties in reproducing results will be satisfactorily low.

FLIGHT TEST RECORDS

FLIGHT NO. 1

Date: 28 July 1949 Duration: 2.5 hrs

Airplane: B-25J No. 44-30328

Crew:

Pilot: C. O. Bostrom

Co-pilot: F. H. Michaelis

Observers: J. C. Wootton
A. A. Hollander

Purpose of Flight:

Instrument shakedown

Airplane configuration:

Gross Weight - 26,100

C. G. Percent MAC - 27.4

Instrumentation installed for recording elevator position, rudder position, rate of roll and rate of yaw.

Flight Procedure:

(1) Trimmed aircraft at 10,000 ft PA and 175 mph IAS.

(2) Observed action of oscillograph of input and response traces using test pulses of positive and negative aileron and rudder displacements.

(3) Obtained records of positive and negative ailerons and rudder pulses.

Results and Comments:

Frequency regulation of the inverter was very poor. Frequency varied from 380 cps to 405 cps. Noise level on the oscillograph records was so high that the records were not satisfactory for reduction.

FLIGHT NO. 2

Date: 2 August 1949 Duration: 1.5 hrs

Airplane: B-25J No. 44-30328

Crew:

Pilot: C. Collins

Co-pilot: J. B. Bain

Observers: F. H. Michaelis
J. C. Wootton

Purpose of Flight:

To obtain oscillograph records of airplane response to aileron and rudder inputs.

Airplane configuration:

Gross weight - 26,100

C. G. Percent MAC - 27.4

Flight Procedure:

(1) Trimmed at 10,000 ft PA and 175 mph IAS.

(2) Observed action of oscillograph traces for test pulses of positive and negative aileron pulses.

(3) Obtain records of positive and negative aileron and rudder pulses.

Results and Comments:

No records obtained due to malfunctioning of recording equipment.

FLIGHT NO. 3

Date: 2 August 1949 Duration: 1.5 hrs

Airplane: B-25J No. 44-30328

Crew:

Pilot: C. Collins

Co-pilot: J. B. Bain

Observers: F. H. Michaelis
J. C. Wootton

Purpose of Flight:

To obtain oscillograph records of aircraft response to aileron and rudder inputs.

Airplane configuration:

Gross weight - 26,100

C. G. Percent MAC - 27.4

Procedure this Flight:

(1) Trimmed at 10,000 ft PA and 175 mph IAS.

(2) Observed action of oscillograph traces for test pulses of positive and negative aileron pulses.

(3) Obtain records of positive and negative aileron and rudder pulses.

Results and Comments:

The records obtained had an unacceptable noise level, but were somewhat improved over preceding flights. Input pulses, while acceptable, were too long for ease of data reduction.

FLIGHT NO. 4

Date: 5 August 1949 Duration: 1.50 hr

Airplane: B-25J No. 44-30328

Crew:

Pilot: Capt. Warwick

Co-pilot: J. B. Bain

Observers: J. C. Wootton
F. H. Michaelis

Purpose of Flight:

To obtain oscillograph records of airplane response to aileron and rudder displacements.

Airplane configuration:

Gross weight - 26,100

C.G. Percent MAC - 27.4

Replaced faulty inverter, and installed new Lord shock mounts on gyro can.

Flight Procedure:

(1) Trimmed at 10,000 ft PA and 175 mph IAS.

(2) Observed action of oscillograph traces for test pulses of positive and negative aileron pulses.

(3) Obtain records of positive and negative aileron and rudder pulses.

Results and Comments:

Flight discontinued due to wiring difficulties.

FLIGHT NO. 5

Date: 5 August 1949 Duration: 1.5 hrs

Airplane: B-25J No. 44-30328

Crew:

Pilot: Capt. Warwick

Co-pilot: J. B. Bain

Observers: J. C. Wootton
F. H. Michaelis

Airplane configuration:

Gross weight - 26,100

C. G. Percent MAC - 27.4

Changes since last flight:

Loose connection in 300 volt system found and repaired.

Flight Procedure:

(1) Trimmed at 10,000 ft PA and 175 mph IAS.

(2) Observed action of oscillograph traces for test pulses of positive and negative aileron pulses.

(3) Obtain records of positive and negative aileron and rudder pulses.

Results and Comments:

The records obtained were considered to be useable. The noise was of insignificant amplitude, and the input pulses were of the correct size, however, the roll gyro picked up a vibration, apparently from its mount, signal of about 10 cps which would make data reduction somewhat difficult.

FLIGHT NO. 6

Date: 9 August 1949 Duration: 1.5 hrs

Airplane: B-25J No. 44-30328

Crew:

Pilot: C. Collins

Co-pilot: J. B. Bain

Observers: F. H. Michaelis
F. Smith

Airplane Configuration:

Gross weight - 26,100

C. G. Percent MAC - 27.4

Changes since last flight:

Intalled stop to remove shock mounts while airborne and wedged gyro container rigidly to airplane to eliminate vibration of the mount from being recorded.

Procedure this flight:

(1) Trimmed at 10,000 ft PA and 175 mph IAS.

(2) Observed action of oscillograph traces for test pulses of positive and negative aileron pulses.

(3) Obtain records of positive and negative aileron and rudder pulses.

Results and Comments:

The records obtained on this flight were very good. The attenuator settings used were:

Function	Attenuator
W_Z	3
W_X	4
δ_a	5
δ_r	8

These attenuations allowed the traces to remain on the paper and gave large enough traces to be readable. Eight records were taken and static

calibrations with the master pickoff were made in flight.

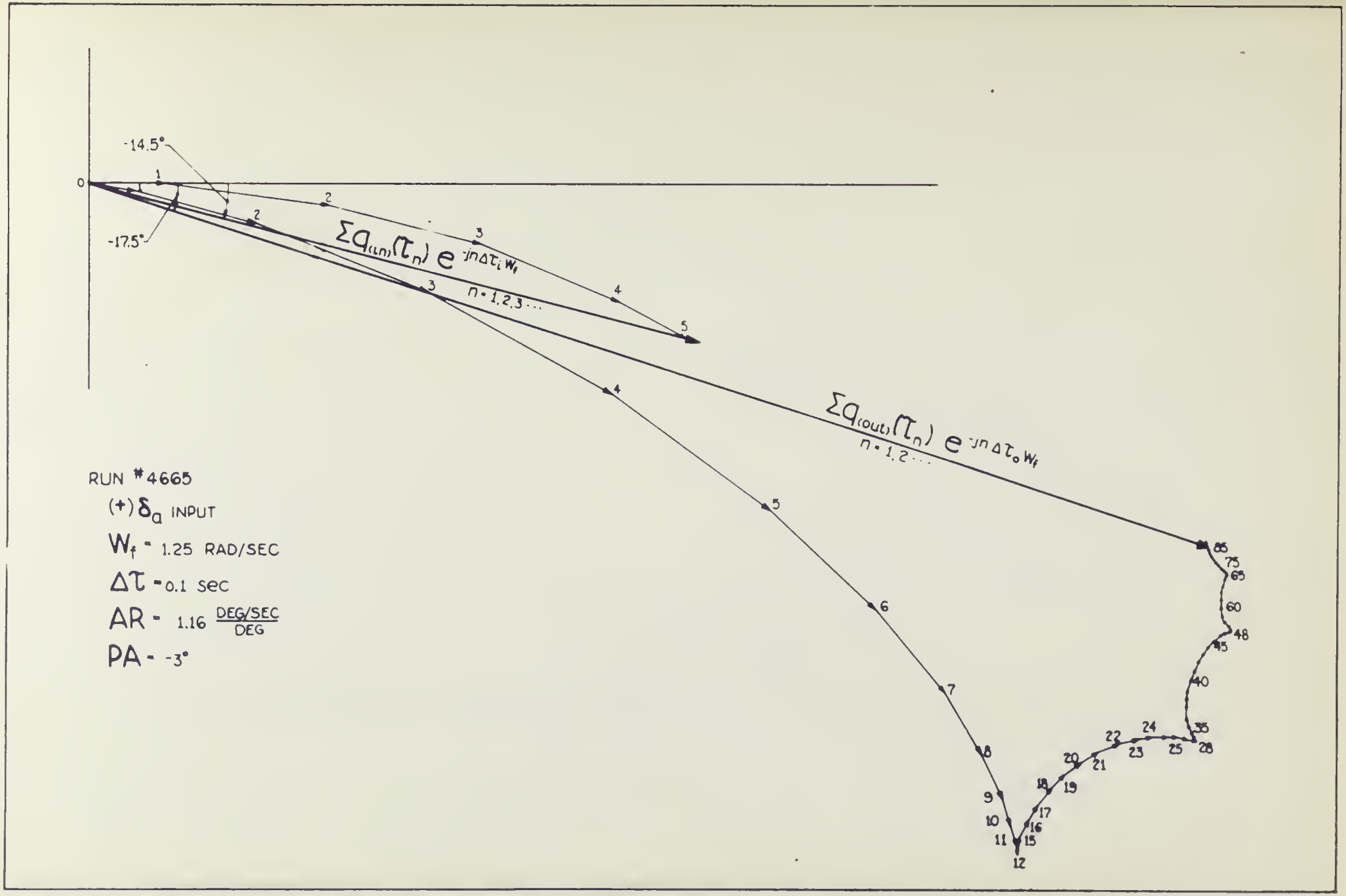

FIGURE D-1 DETERMINATION OF PERFORMANCE FUNCTION, $[PF]_{(A)(\delta_a W_f)}$, AT W_f = 1.25 RAD/SEC BY METHOD OF ANALYSIS (1) OF TABLE 2

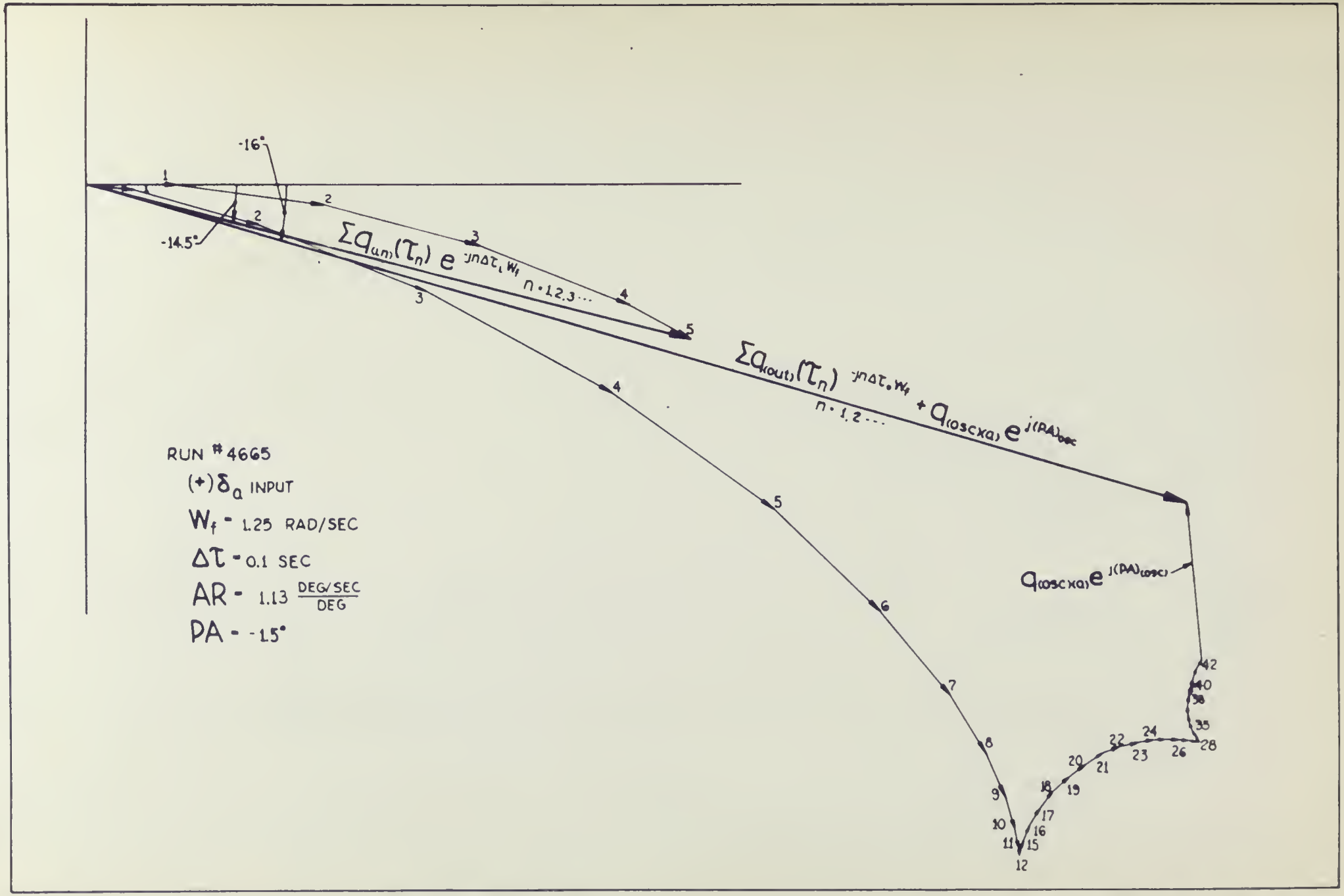

FIGURE D-2 DETERMINATION OF PERFORMANCE FUNCTION, $[PF]_{(A)(\delta_a W_f)}$, AT W_f = 1.25 RAD/SEC BY METHOD OF ANALYSIS (2) OF TABLE 2.

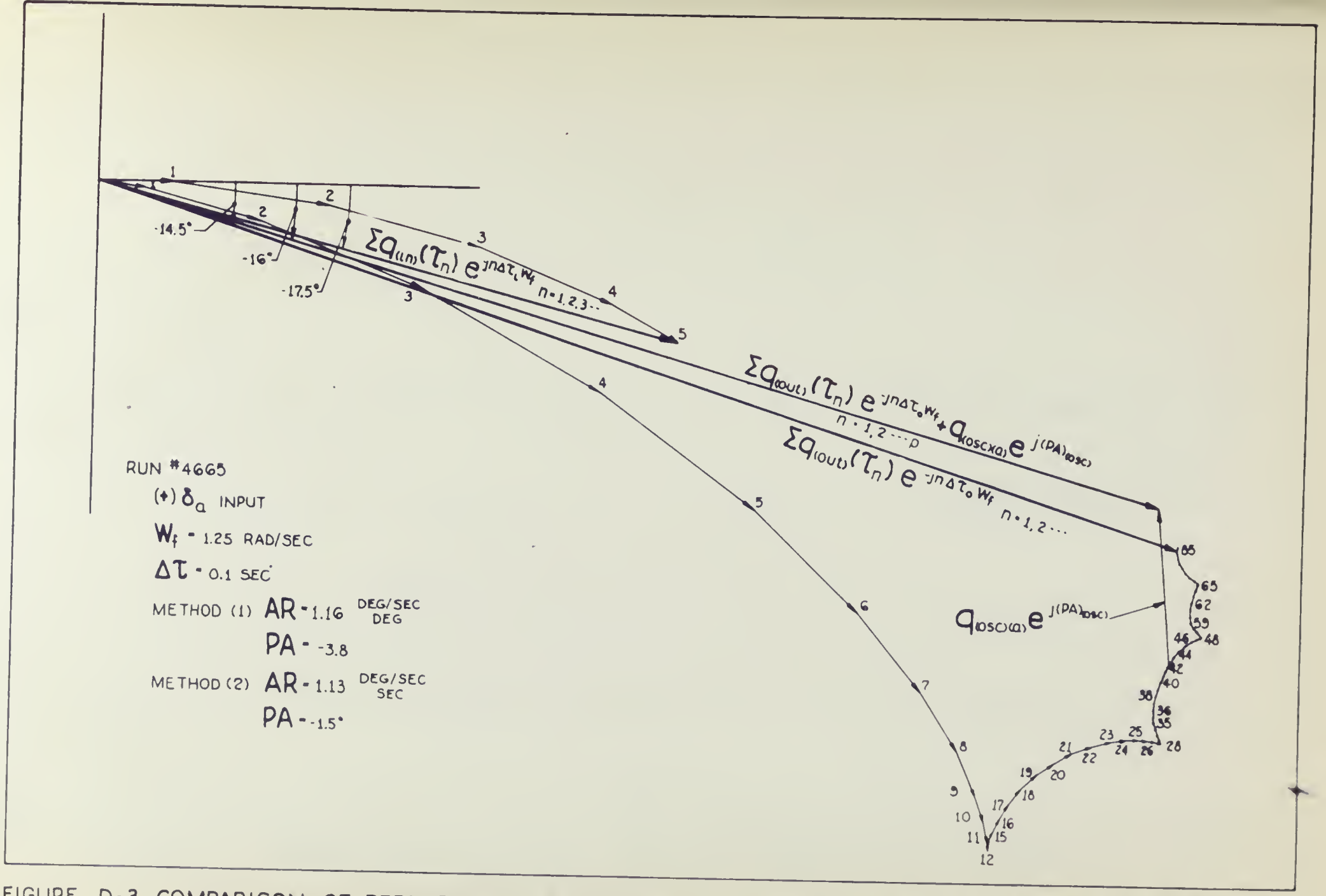

FIGURE D-3 COMPARISON OF PERFORMANCE FUNCTIONS AS DETERMINED AT W = 1.25 RAD/SEC BY METHODS OF ANALYSIS (1) AND (2) OF TABLE 2.

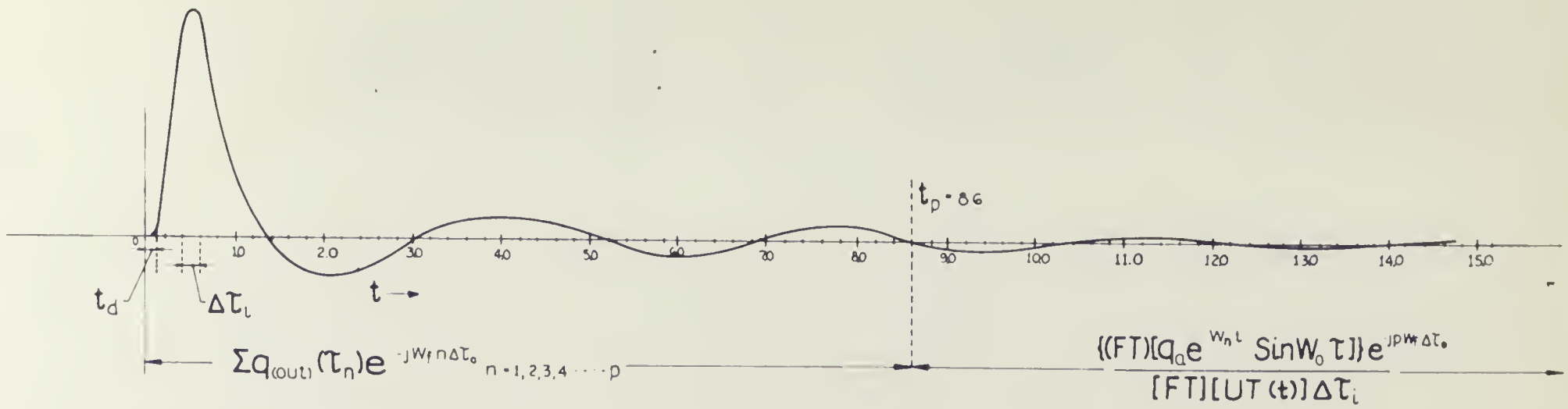

FIGURE D-4 DEMONSTRATION OF USE OF METHOD OF ANALYSIS (2) OF TABLE 2.

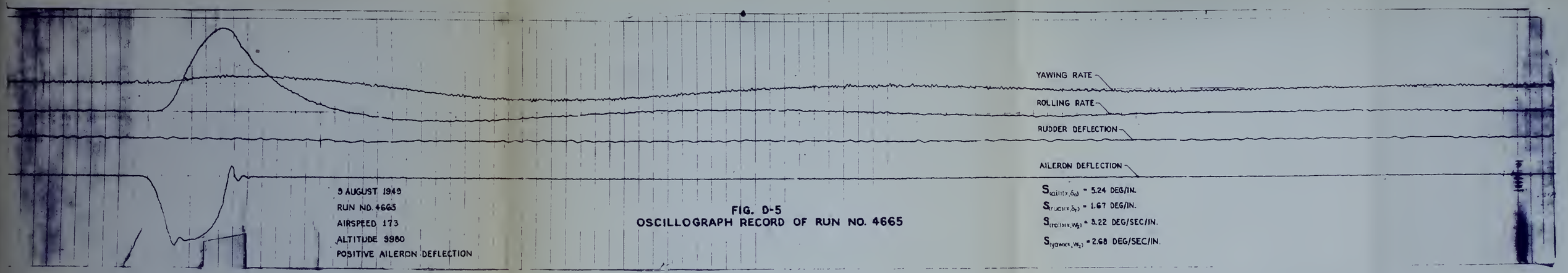

FIG. D-5
OSCILLOGRAPH RECORD OF RUN NO. 4665

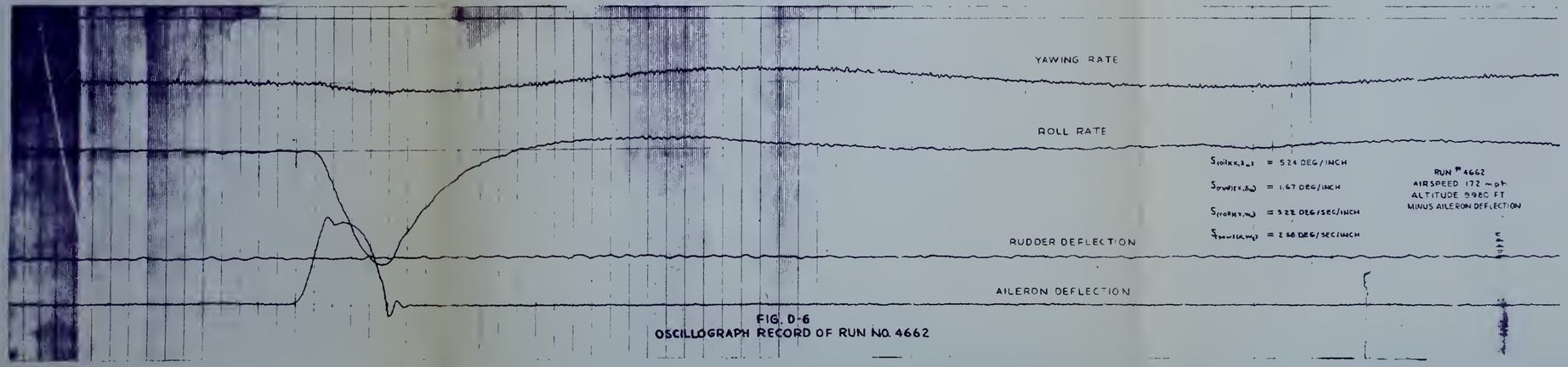

FIG. D-6
OSCILLOGRAPH RECORD OF RUN NO. 4662

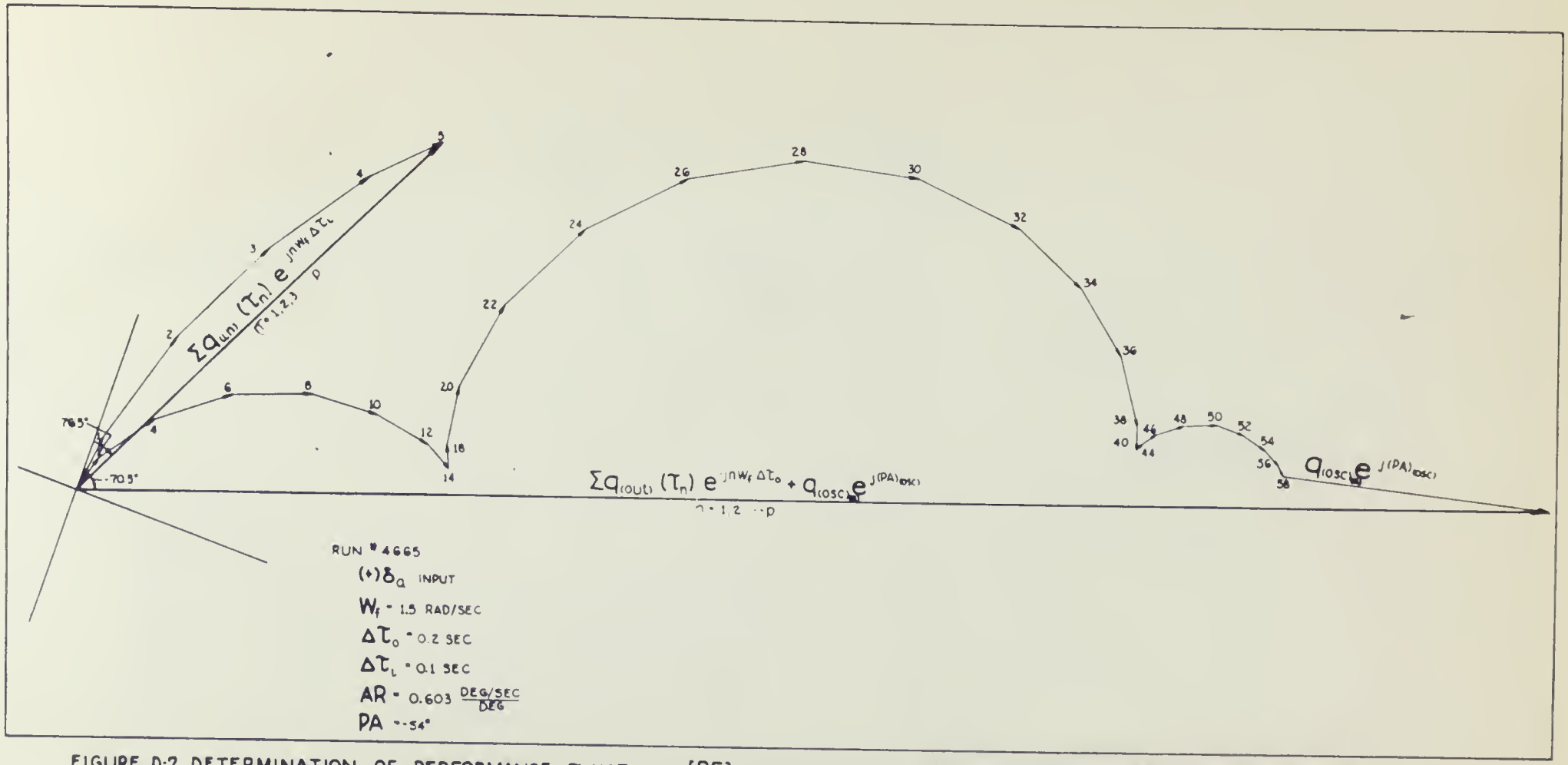

FIGURE D-7 DETERMINATION OF PERFORMANCE FUNCTION, $[PF]_{(\delta_a; W_z)}$ AT THE RESONANT FREQUENCY BY METHOD NO. 2

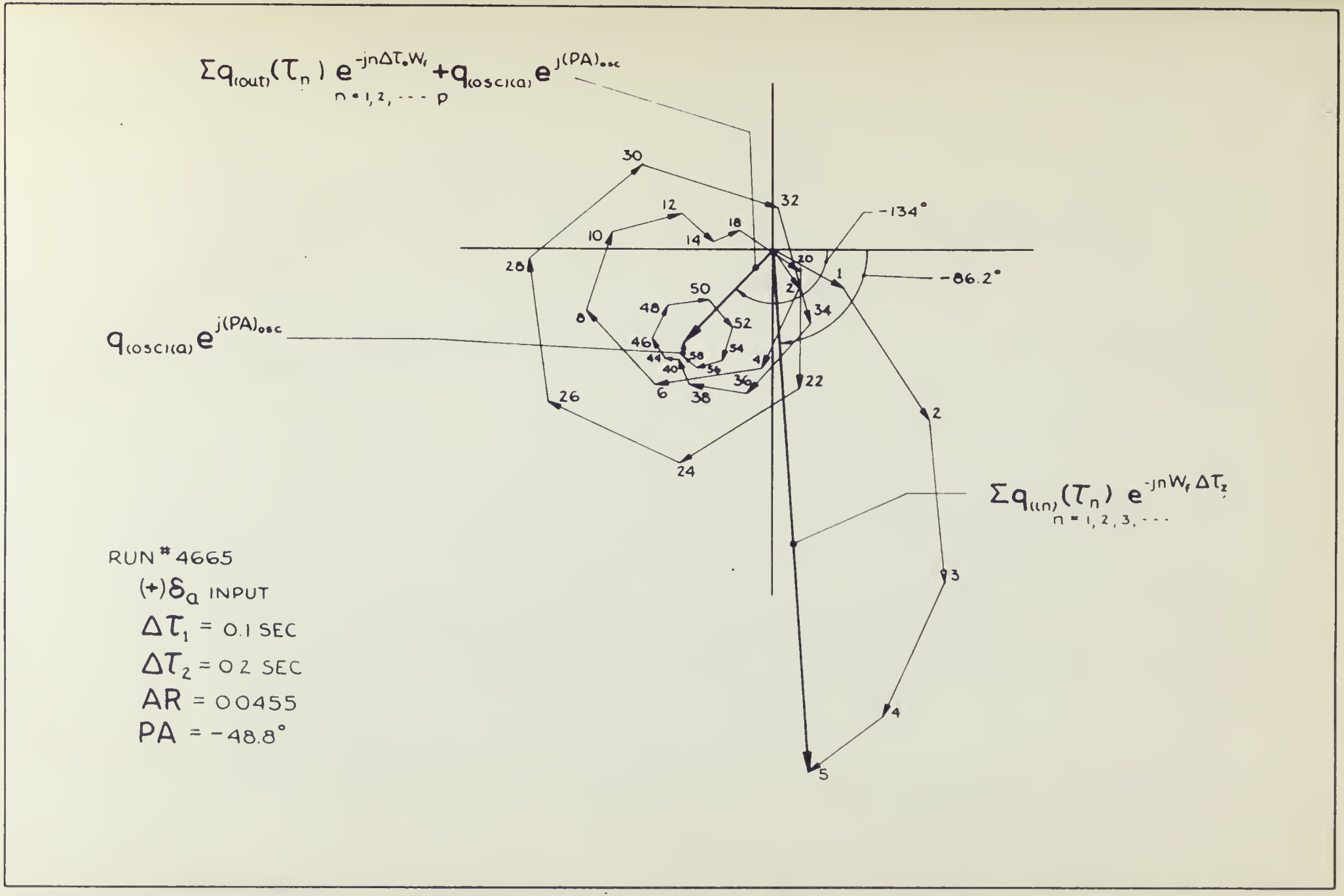

FIGURE D-8. DETERMINATION OF PERFORMANCE FUNCTION, $[PF]_{(A)(\delta_a W_z)}$, AT W_f = 5 RAD/SEC BY METHOD OF ANALYSIS (2) OF TABLE 2.

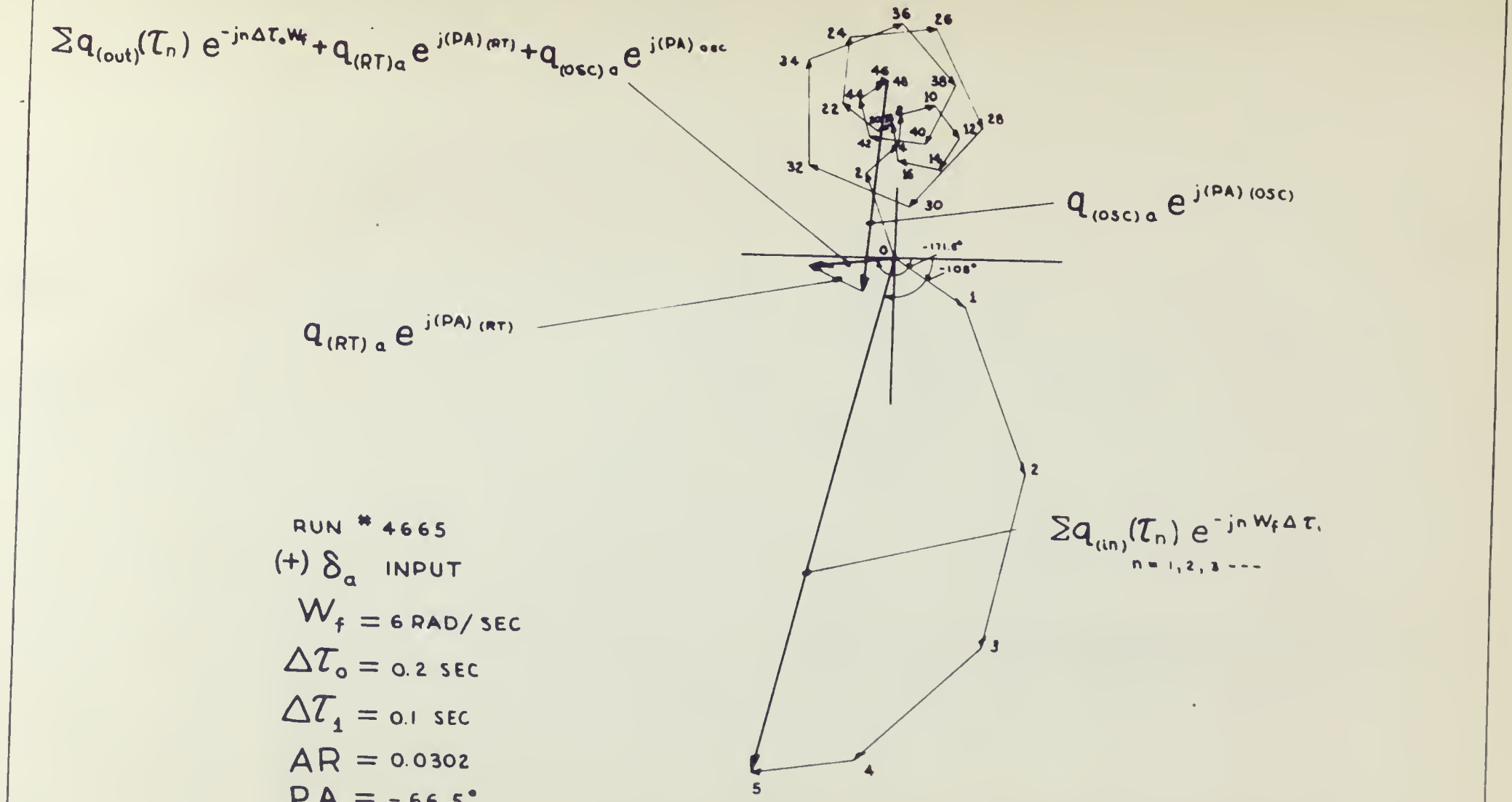

FIGURE D-9. DETERMINATION OF PERFORMANCE FUNCTION, $[PF]_{(A)(\delta_a, W_z)}$, AT $W_f = 6$ RAD/SEC BY METHOD (3) OF TABLE 2

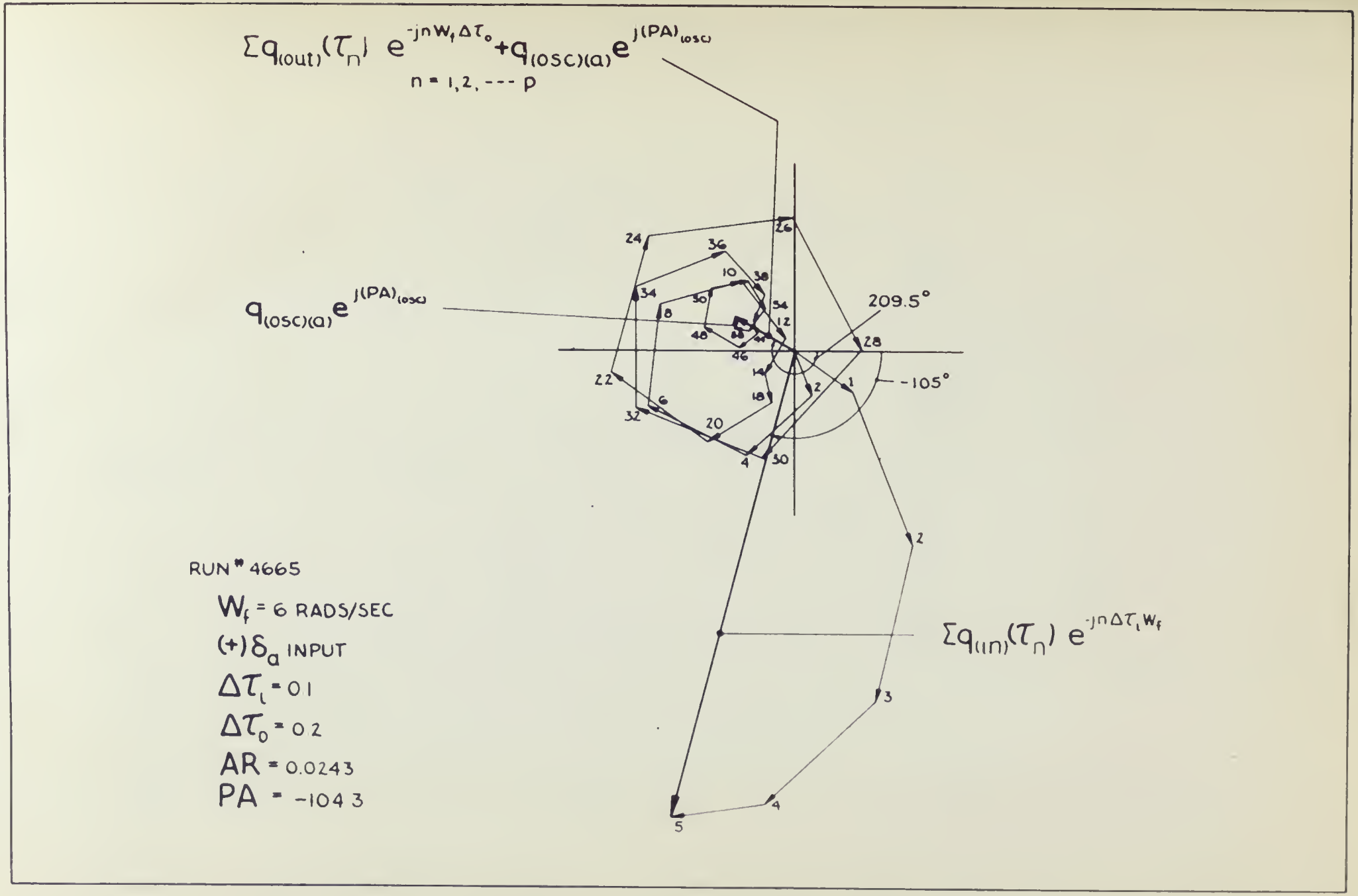

FIGURE D-10. DETERMINATION OF PERFORMANCE FUNCTION, $[PF]_{(A)(\delta_a W_z)}$ AT W_f = 6 RADS/SEC BY METHOD OF ANALYSIS (2) OF TABLE 2.

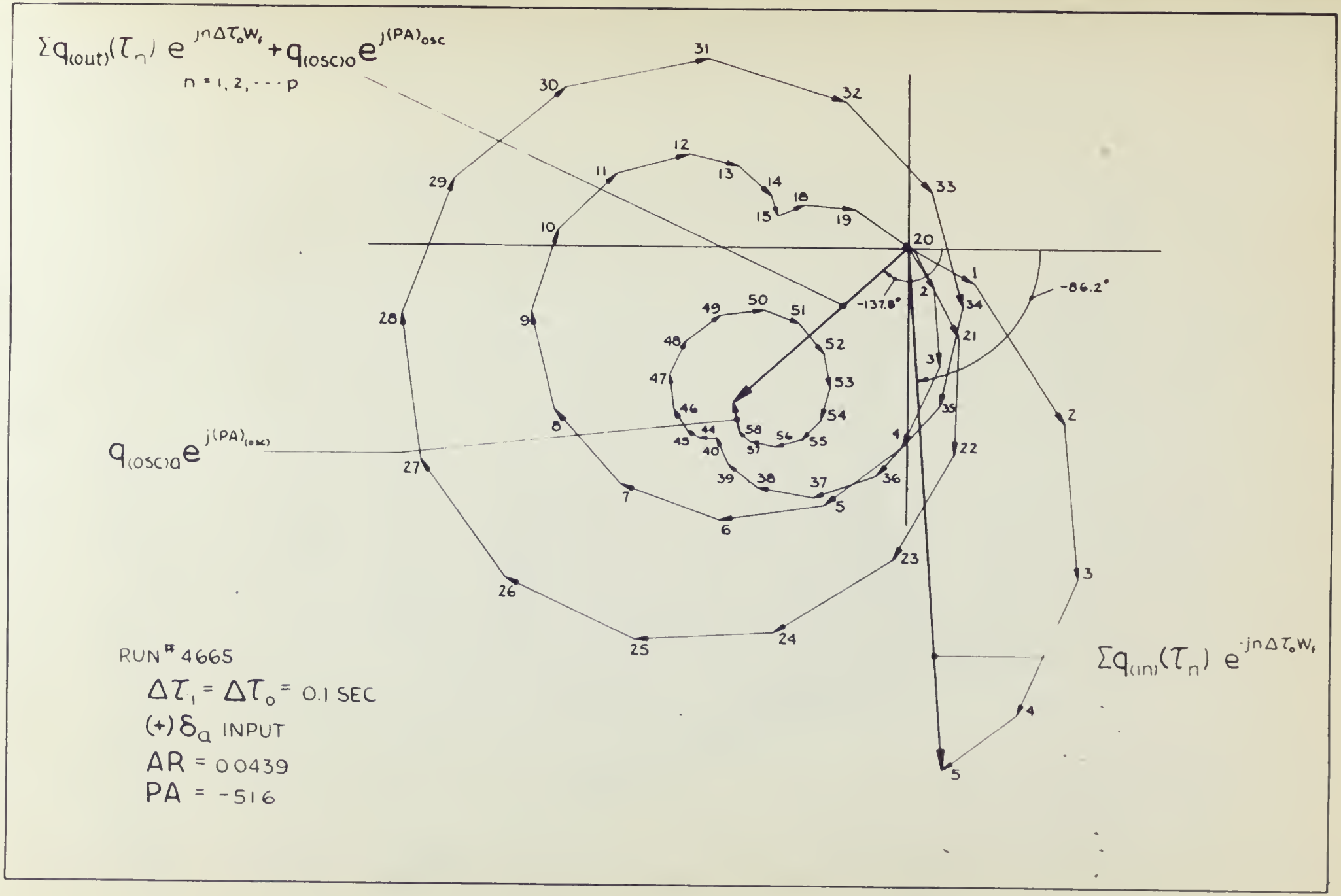

FIGURE D-11. DETERMINATION OF THE PERFORMANCE FUNCTION, $[PF]_{(A)(\delta_a W_z)}$, FOR W_t = 5 RADS/SEC

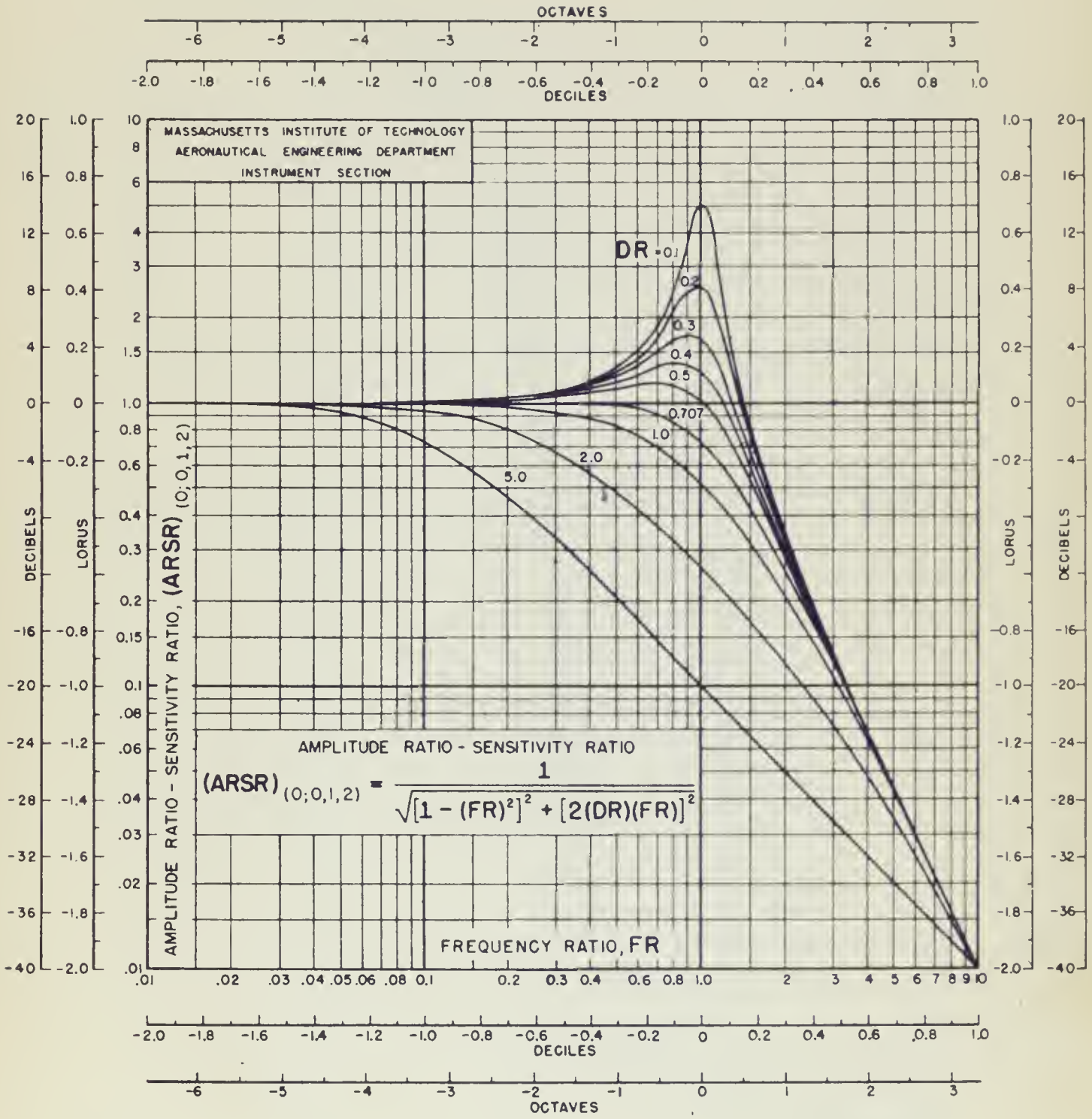

FIG. D-12. LOG - LOG PLOT OF STEADY-STATE SINUSOIDAL RESPONSE CHARACTERISTICS ASSOCIATED WITH THE DIFFERENTIAL EQUATION $\ddot{q}_{(dep)} + 2(DR)W_n \dot{q}_{(dep)} + W_n^2 q_{(dep)} = W_n^2 S_{(q_{ref} q_{dep})} q_{(ref)}$.

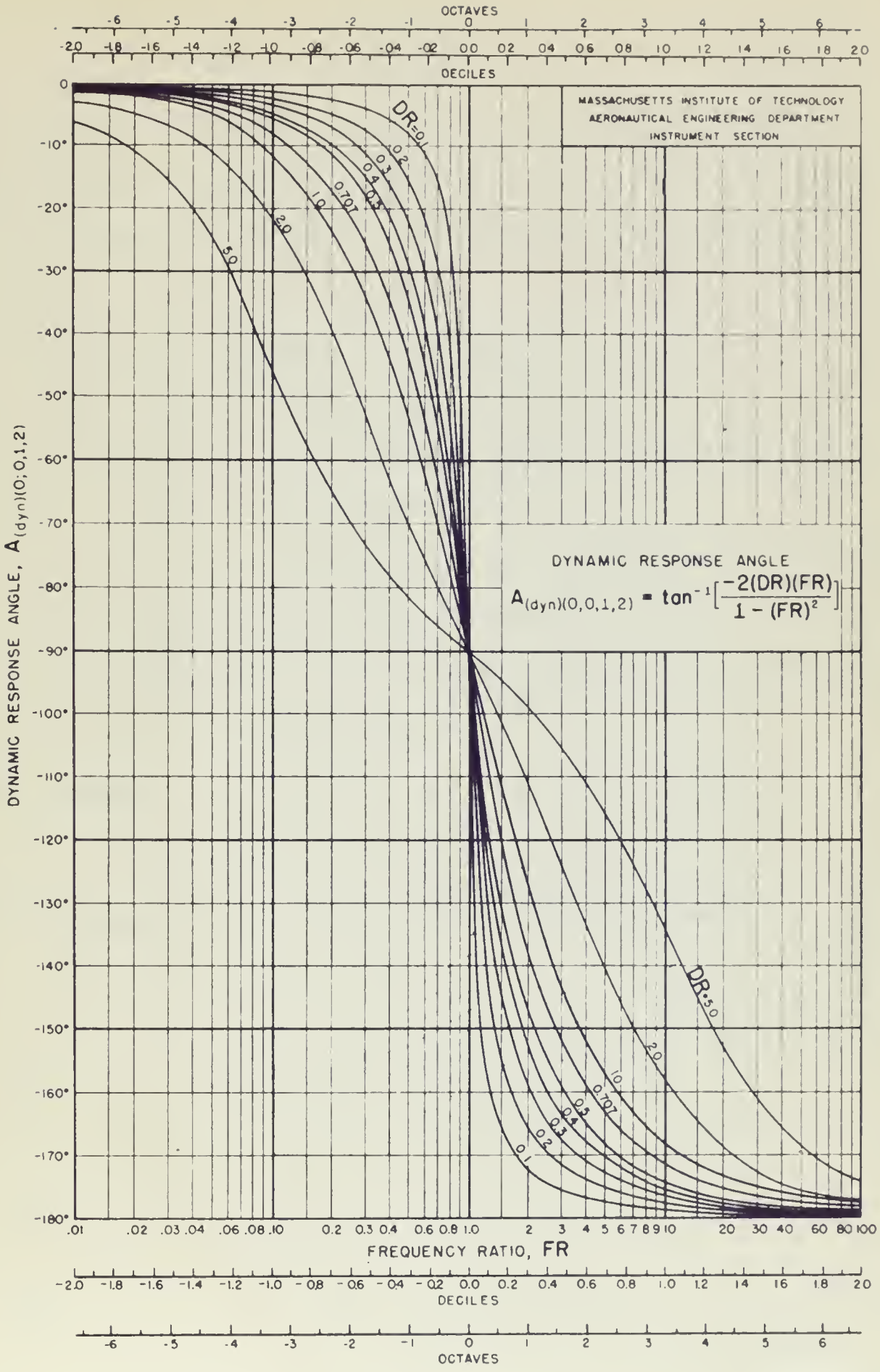

FIG D-13. SEMI-LOG PLOT OF STEADY-STATE SINUSOIDAL RESPONSE CHARACTERISTICS ASSOCIATED WITH THE DIFFERENTIAL EQUATION $\ddot{q}_{(dep)} + 2(DR)W_n\dot{q}_{(dep)} + W_n^2 q_{(dep)} = W_n^2 S_{(q_{ref}\, q_{dep})} q_{(ref)}$.

APPENDIX E

GLOSSARY

The system of notation adopted for use in this thesis has been selected because of its peculiar usefulness in representing operating system performance. In particular, it has the following specific advantages:

1. It is easily learned.

2. It is adopted to a wide range of situations.

3. It is built up almost exclusively of characters found on the keyboard of a standard American typewriter.

4. Any one of the compound symbols of the system is readily interpreted without recourse to an extensive glossary.

A representative list of the primary symbols and those used as subscripts is given in the following table.

Primary Symbols

A	Angle
$(AR)_{(\ )(q_{in}\ q_{out})}$	Input - output amplitude ratio for a given operating component = $\frac{q_{(out)a}}{q_{(in)a}}$
c	Linear viscous damping coefficient
(CT)	Characteristic time
(DR)	Damping ratio = $\frac{c}{2\sqrt{S_{(er)}\ m}}$
(FR)	Frequency ratio = $\frac{W_f}{W_n}$
(FT)	Fourier transform
g	Force of gravity/unit of mass
I_{XX}	Moment of inertia of airplane about X axis
I_{XZ}	Product of inertia

I_{ZZ}	Moment of inertia of airplane about Z axis
L	Rolling moment
L_p	Rolling moment due to rolling velocity
L_r	Rolling moment due to yawing velocity
$L_{\delta a}$	Rolling moment due to aileron displacement
L_v	Rolling moment due to side slip velocity
$(LT)[q(t)]$	Direct Laplace transform of $q(t) = Q(S)$
m	Mass
N	Yawing moment
N_p	Yawing moment due to rolling velocity
N_r	Yawing moment due to yawing velocity
N_v	Yawing moment due to side slip velocity
$N_{\delta a}$	Yawing moment due to aileron deflection
$N_{\delta r}$	Yawing moment due to rudder deflection
$\{P\}_{(\ )}(q_{in}\ q_{out})$	Input - output performance operator for a given operating component
$(PA)_{(\ )}(q_{in}\ q_{out})$	Input - output dynamic phase angle for a given operating component
$(PF)_{(\ )}(q_{in}\ q_{out})$	Input - output performance function for a given operating component, where $q_{(in)} = q_{(in)a}\, e^{j[W_f t + (PA)_{(in)}]}$ $q_{(out)} = q_{(out)a}\, e^{j[W_n t + (PA)_{(out)}]}$
$q_{(in)}$	Input quantity
$q_{(out)}$	Output quantity
$q(t)$	A quantity which is a function of the real variable, time
RT	Right triangle
s	Complex variable used in Laplace transform theory
$S_{(\ )}(q_{in}\ q_{out})$	Static sensitivity for a given operating component

t_d	Time delay
Δt	Finite increment of time
U	Airplane forward velocity
(UT)	Unit triangle
(URT)	Unit right triangle
$\dot{v}$	Acceleration along Y axis
$W_{(\ )}$	Airplane angular velocity about axis ( )
W_f	Angular forcing frequency
W_n	Natural frequency
Y	Side force
Y_v	Side force due to side slip velocity

A dot over a variable represents its derivative with respect to time (e.g. $\dot{(\ )} = \frac{d(\ )}{dt}$).

Two dots over a variable represents a second derivative with respect to time (e.g. $\ddot{(\ )} = \frac{d^2(\ )}{dt^2}$).

The following Greek letter symbols are retained because their meanings have become thoroughly identified with these symbols in the aeronautical engineering field.

δ_a	Total aileron deflection (sum of left and right aileron deflection) (positive deflection of right aileron is downward)
δ_r	Rudder deflection (left rudder deflection is positive)
ϕ	Angle of bank
β	Angle of yaw
ω	Angular forcing frequency

Modifying symbols (subscripts)

a	Aileron
(a)	Amplitude
A	Airplane
(div)	Divergent
(in)	Input
(ind sys)	Indicating system
M	Measuring
o	Output
(out)	Output
(osc)	Oscillating
p	Rate of change of bank angle = W_X
(rem)	Remainder
r	Rate of change of heading = W_Z
v	Side slip velocity

APPENDIX F

BIBLIOGRAPHY

1. ''Dynamic Lateral Stability Flight Tests of a B-25J Airplane by the Forced Oscillation Methods,'' Cornell Aeronautical Laboratory Report TB-405-F-7.

2. ''Investigation of the Response of an Aircraft to a Finite Pulse Input,'' M.I.T. Master's Thesis by Gerhardt C. Clementson, 1948.

3. ''The Pulse Method for Determining Aircraft Dynamic Performance,'' Paper by Seamans, Blasingame, Clementson (First version) April, 1949.

4. ''Stability and Control Flight Tests of the B-25J,'' AAF Technical Report 5413.

5. ''Preliminary Lateral Response Data to Step Deflections of the Ailerons and Rudder for A-26C Airplane, V_e = 180, 240, and 270 mph,'' Cornell Aeronautical Laboratory Report.

6. ''Handbook Structural Repair Instructions, USAF B-25 Navy Model PBJ-1 Series Aircraft,'' 20 July 1944, Revised 26 May 1948. Published under authority of the Air Force and the Chief of the Bureau of Aeronautics.

7. ''Correlation Between Flight Test Lateral Performance Function Data and Wind Tunnel Data for the B-26 Airplane,'' Engineering Memorandum No. 6445-E-22, Instrumentation Laboratory, M.I.T. 15 December 1948 by Homer Eckhardt.

8. ''Transients in Linear Systems,'' by Gardner and Barnes, published by John Wiley and Sons, New York, Fourth Printing, 1947.

9. ''Calculated Airplane Moments of Inertia, Model XA-26 Airplane, Contract W535-AC-17946 of June 1942,'' Report No. ES-1230, M.I.T.

10. ''Application of the Performance Operator to Aircraft Automatic Control,'' by Seamans, R.C., Bromberg, B.G., and Payne, L.E., - Journal of the Aeronautical Sciences, Vol. 15, No. 9, p 535, September 1948.

11. ''Aerodynamic Theory,'' Vol. V, Durand, W.F. (Editor), Durand Reprinting Committee, California Institute of Technology, 1943.

12. ''Determination of Lateral Dynamic Stability Characteristics of an A-26C Airplane by the Methods of Forced Oscillations and Step Function,'' Cornell Aeronautical Laboratory Report UB-418-F-3.

DATE DUE			

11500
Thesis
B14 Bain
Investigation of aircraft lateral motion performance function by pulse technique.

Thesis 11500
B14 Bain
Investigation of aircraft lateral motion performance function by pulse technique.

thesB14
Investigation of aircraft lateral motion
3 2768 001 91179 5
DUDLEY KNOX LIBRARY